Gametogenesis and Neuropeptide APGWamide Distribution in TBT-Induced Imposex Spotted Babylon, *Babylonia areolata* (Link, 1807)

Chutchawan Muenpo

A Thesis Submitted in Partial Fulfillment of the Requirements
for the Degree of Doctor of Philosophy in Biology
Prince of Songkla University
2010

Thesis Title	Gametogenesis and Neuropeptide APGWamide Distribution in TBT-Induced Imposex Spotted Babylon, *Babylonia areolata* (Link, 1807)
Author	Mr. Chutchawan Muenpo
Major Program	Biology

Major Advisor:

……

(Assoc. Prof. Jintamas Suwanjarat)

Co-advisors:

……....

(Prof. Dr. Jan van Minnen)

……..

(Assist. Prof. Dr. Uraporn Vongvatcharanon)

Examining Committee:

…….Chairperson

(Assist. Prof. Dr. Nisaudah Radenahmad)

…….....

(Assoc. Prof. Jintamas Suwanjarat)

…….

(Assoc. Prof. Dr. Prapee Sretarugsa)

The Graduate School, Prince of Songkla University, has approved this thesis as partial fulfillment of the requirements for the Doctor of Philosophy Degree in Biology

……..……..

(Assoc. Prof. Dr. Krerkchai Thongnoo)

Dean of Graduate School

ชื่อวิทยานิพนธ์ กระบวนการสร้างเซลล์สืบพันธุ์และการกระจายของฮอร์โมน APGWamide ในหอยหวานแปลงเพศ (imposex) *Babylonia areolata* (Link, 1807) ที่ถูกชักนำด้วยสาร TBT

ผู้เขียน นายชัชวาล หมื่นโพธิ์

สาขาวิชา ชีววิทยา

ปีการศึกษา 2552

บทคัดย่อ

ศึกษากระบวนการสร้างเซลล์สืบพันธุ์และการกระจายของฮอร์โมน APGWamide ในหอยหวาน (*Babylonia areolata*) ที่ถูกชักนำให้เกิดลักษณะสองเพศ (imposex) ด้วยสาร tributyltin (TBT) ที่มีความเข้มข้นของสารแตกต่างกัน 7 ชุด (1, 10, 50, 100 และ 500 ng TBT as Sn/L) ในห้องปฏิบัติการ เป็นเวลา 6 เดือน โดยแบ่งความรุนแรงของการแปลงเพศเป็น 6 ระดับ และจากการประเมินค่าต่าง ๆ คือ เปอร์เซ็นต์ของการแปลงเพศ ค่าเฉลี่ยของระยะของการแปลงเพศ (VDSI) ค่าเฉลี่ยของความยาวเพนิสของเพศเมีย (FPL) และขนาดของเพนิสแบบสัมพัทธ์ของเพศเมีย (RPSI) พบว่าระดับของการแปลงเพศมีแนวโน้มเพิ่มขึ้นตามระยะเวลาและความเข้มข้นที่เพิ่มขึ้น นอกจากนี้ ในการทดลองยังพบการเจริญเติบโตอย่างผิดปกติของท่อนำอสุจิในหอยเพศผู้ที่ได้รับสาร TBT และพบการเจริญของเพนิส 2 อันในหอยเพศเมียแปลงเพศในระยะที่ 4 เมื่อศึกษาผลของสาร TBT ที่อาจจะมีต่อกระบวนการสร้างอสุจิในหอยเพศผู้ที่ได้รับสาร TBT ที่ความเข้มข้นสูงสุด เป็นระยะเวลา 6 เดือน พบว่า กระบวนการสร้างเซลล์สืบพันธุ์เพศผู้เหมือนกับในหอยเพศผู้ปกติและไม่มีการเปลี่ยนแปลงทางด้านเนื้อเยื่อวิทยาและโครงสร้างโดยละเอียด สำหรับผลของสาร TBT ที่มีต่อกระบวนการสร้างเซลล์ไข่ในหอยหวานเพศเมียแปลงเพศ พบว่า ลักษณะทางเนื้อเยื่อวิทยาและโครงสร้างละเอียดของกระบวนการสร้างเซลล์ไข่มีลักษณะโดยทั่วไปปกติและไม่มีการเจริญแทรกของเนื้อเยื่ออัณฑะในรังไข่ แต่พบการเสื่อมของเซลล์ไข่และการแทรกซึมของเซลล์เม็ดเลือดในปริมาณมาก (ศึกษาด้วยกล้องจุลทรรศน์ธรรมดา) นอกจากนี้ยังพบหยดของไลปิดขนาดใหญ่จำนวนมากในไซโตปลาสซึมของเซลล์ไข่ในเกือบทุกระยะของการพัฒนา โดยเฉพาะเซลล์ไข่ที่อยู่ในระยะของการสร้างไข่แดง รวมทั้งยังพบหยดของไลปิดในไซโตปลาสซึมของเซลล์ฟอลลิเคิลด้วย (ศึกษาด้วยกล้องจุลทรรศน์อิเล็กตรอนแบบส่องผ่าน) ผลการศึกษาดังกล่าวยืนยันถึงการเสื่อมของเซลล์ไข่ในเนื้อเยื่อรังไข่ของหอยเพศเมียแปลงเพศ

การศึกษาการกระจายของฮอร์โมน APGWamide ในหอยเพศเมียแปลงเพศโดยใช้วิธีอิมมิวโนฮิสโตเคมมิสตรี้ (immunohistochemistry) พบว่า หอยเพศเมียแปลงเพศในระยะที่

1 - 4 มีจำนวนของเซลล์ประสาทที่มี APGWamide ในปมประสาทหลัก (เซรีบรัล พลูรัล และพาไรเอทัล) เท่ากับหอยเพศเมียปกติ ($p > 0.05$) ในขณะที่หอยเพศเมียแปลงเพศในระยะที่ 5 มีจำนวนของเซลล์ประสาทที่มี APGWamide ไม่แตกต่างจากหอยเพศผู้ปกติ ($p > 0.05$) และสูงกว่าในหอยเพศเมียปกติและหอยเพศเมียแปลงเพศในระยะอื่น ๆ อย่างมีนัยสำคัญ ($p < 0.05$) ส่วนในปมประสาทพีดัลและบัคเคิล พบว่า จำนวนของเซลล์ประสาทที่มี APGWamide ไม่มีความแตกต่างกันระหว่างกลุ่ม ($p > 0.05$) นอกจากนี้ เมื่อตรวจสอบการกระจายของ APGWamide ในอวัยวะสืบพันธุ์ของหอยหวาน แสดงให้เห็นว่า มีการกระจายของ APGWamide ในแขนงประสาทที่พบในเนื้อเยื่อเกี่ยวพันของทั้งอัณฑะของหอยเพศผู้ปกติและรังไข่ของหอยเพศเมียปกติและหอยเพศเมียแปลงเพศ รวมทั้งยังพบการกระจายของ APGWamide ในแขนงประสาทที่พบในชั้นกล้ามเนื้อของเพนิสในหอยเพศผู้ปกติและหอยเพศเมียแปลงเพศ

การศึกษาครั้งนี้สรุปได้ว่า สาร TBT ซึ่งเป็นความเข้มข้นที่พบได้ในธรรมชาติ (1-500 ng TBT as Sn/L) สามารถชักนำให้เกิดการแปลงเพศในหอยหวาน *B. areolata* ที่เลี้ยงในห้องปฏิบัติการ สำหรับการศึกษาทางด้านเนื้อเยื่อวิทยาและโครงสร้างโดยละเอียดของกระบวนการสร้างเซลล์สืบพันธุ์ในหอยหวานที่ได้รับสาร TBT (เพศผู้และเพศเมียแปลงเพศ) ชี้ให้เห็นว่า สาร TBT ไม่มีผลกระทบต่อกระบวนการสร้างอสุจิในหอยเพศผู้ ส่วนในหอยเพศเมียแปลงเพศ พบว่า กระบวนการสร้างเซลล์ไข่มีลักษณะทั่วไปเหมือนกับในหอยเพศเมียปกติและไม่มีเนื้อเยื่อสืบพันธุ์เพศผู้เจริญแทรก อย่างไรก็ตามการเสื่อมของเซลล์ไข่และการแทรกซึมของเซลล์เม็ดเลือดในรังไข่ ทำให้ยืนยันถึงผลกระทบในด้านลบของสาร TBT ที่มีต่อระบบสืบพันธุ์ การศึกษาครั้งนี้เป็นการรายงานการกระจายของฮอร์โมน APGWamide ในปมประสาทเป็นครั้งแรกในหอยฝาเดียวแปลงเพศ และผลการศึกษาชี้ให้เห็นว่าจำนวนของเซลล์ประสาทที่มี APGWamide ในปมประสาทหลักที่เพิ่มขึ้นมีบทบาทสำคัญเกี่ยวข้องกับการชักนำให้เกิดการแปลงเพศในหอยหวาน

Thesis Title	Gametogenesis and Neuropeptide APGWamide Distribution in TBT-Induced Imposex Spotted Babylon, *Babylonia areolata* (Link, 1807)
Author	Mr. Chutchawan Muenpo
Major Program	Biology
Academic Year	2009

ABSTRACT

This study examined the gametogenesis and distribution of APGWamide in the imposex females of the spotted babylon, *Babylonia areolata* induced by 5 different nominal aqueous TBT concentrations (1, 10, 50, 100, and 500 ng as Sn/L) for a period of 6 months in laboratory, and the imposex intensity or degree of imposex was divided into six stages. The estimation of the imposex incidence (%), VDSI (vas deferens sequence index), average FPL (female penis length) and RPSI (relative penis size index), showed that the imposex intensity tended to be increased in a concentration-and time-dependent pattern. In addition, this experiment found two malformations: an excrescence on vas deferens in a TBT-treated male, and the development of a double penis in imposex 4. The possible effect of TBT on the spermatogenesis was determined in the male *B. areolata* exposed to the highest TBT concentration for a period of 6 months and the results clearly showed that the spermatogenesis was similar to that of the normal male with no evidence of histological and ultrastructural changes. For the effect of TBT on oogenesis in imposex females, it was shown that oogenesis was generally normal and showed no development of male testicular tissue in the ovaries; however, an oocyte degeneration and diffused heamocytic infiltrations were occasionally observed in the ovarian tissue. Furthermore, ultrastructural features of oogenesis in imposex females exhibited similarity with those of normal females except the finding of numerous, large lipid droplets in the cytoplasm at almost all stages of the oocyte development (especially in the vitellogenic oocytes) and of the follicle cells, implying a sign of oocyte degeneration in the ovarian tissue of imposex females.

The investigation of the distribution of APGWamide in imposex female *B. areolata* showed that in the main ganglia (cerebral, pleural, and parietal), the imposex 1 - 4 had the numbers of APGWamide immunoreactive neurons similar to normal females ($p > 0.05$), while imposex 5 had the numbers of APGWamide immunoreactive neurons close to those of normal males ($p > 0.05$) and significantly higher than those of normal females and other lower stages of imposex ($P < 0.05$). In contrast to the main ganglia, the numbers of APGWamide immunoreactive neurons in the pedal and buccal ganglia were not different between groups of *B. areolata* ($p > 0.05$). The examination of the APGWamide distribution in the peripheral reproductive organs showed that the distribution of APGWamide immunoreactivity in nerve processes were detected in the connective tissue of the testes of normal males as well as the ovaries of normal females and imposex 5, while in the penis, the distribution was confined to the muscle layers surrounding the penis ducts of normal males and imposex 5.

In conclusion, this study confirms the ability of TBT at a range of environmentally relevant concentrations (1-500 ng TBT as Sn/L) to induce imposex in laboratory reared *B. areolata*. The histological and ultrastructural investigations of gametogenesis in TBT-exposed *B. areolata* (males and imposex females) suggest that TBT does not affect on spermatogenesis in TBT-treated males, and in imposex females, although the oogenesis is generally similar to that of a normal female and does not exhibit male testicular tissue, but the findings of the histopathologies (oocyte degeneration and heamocytic infiltration) support the negative impact of TBT on reproductive system. This study is the first report that determines the distribution of APGWamide in ganglia of gastropod imposex and it is suggested that an increase in APGWamide immunoreactive neurons in the main ganglia caused by TBT appeared to play an important role involving in imposex induction in *B. areolata*.

ACKNOWLEDGEMENTS

I would like to take this opportunity to sincerely thank Assoc. Prof. Jintamas Suwanjarat who is my advisor, for her guidance, advice, outstanding supervision, and kindness. I am deeply indebted to my co-advisors: Assist. Prof. Dr. Uraporn Vongvatcharanon for her help and advice and Prof. Dr. Jan van Minnen for his advice and recommendation. I would like to express my deeply gratitude to the Thesis Examination Committees, including Assist. Prof. Dr. Nisaudah Radenahmad and Assoc. Prof. Dr. Prapee Sretarugsa for their correction and valuable suggestion.

My grateful thanks are due to the Royal Golden Jubilee Ph.D. Program (Grant no. PHD/0076/2547) under Thailand Research Fund (TRF) and the Graduate School, Prince of Songkla University (PSU), Thailand for their financial support throughout this project.

I am extremely thankful to Prof. Dr. Waltraud Klepal, Department of Cell Imaging and Ultrastructure Research, Faculty of Life Science, University of Vienna, Austria for her valuable expertise, guidance and encouragement throughout this study and her TEM staff for their assistance in electron microscopic techniques. I also thank Prof. Dr. Naweed Syed, the head of Department of Cell Biology and Anatomy, Faculty of Medicine, University of Calgary, Canada, for his advice and kindness and his staff for their assistance in the immunohistochemical techniques.

Thanks are also due to the Electron Microscopy Unit, Faculty of Medicine, PSU, for the assistance in electron microscopic techniques and the Aquatic Animal Hatchery Research Unit, Faculty of Science and Technology, PSU, Pattani campus, for providing the specimens. Thanks to the students of the Histology Research Unit, Department of Biology, PSU, for their help and Ms. Lamai Thoungboon for her technical assistance. Finally, I would like to thank my parents, my sisters and brothers as well as my friends for their support and encouragement.

Chutchawan Muenpo

CONTENTS

CONTENTS (Continued)

LIST OF TABLES

LIST OF FIGURES

LIST OF FIGURES (Continued)

LIST OF FIGURES (Continued)

LIST OF FIGURES (Continued)

LIST OF ABBREVIATIONS AND SYMBOLS

A	=	Acrosomal complex
ab	=	Apical bleb
ac	=	Acrosome
am	=	Accessory membrane
AN	=	Amphinucleolus
an	=	Annulus
ANOVA	=	Analysis of variance
APGWa-lir	=	APGWamide-like immunoreactivity
APGWamide	=	Ala-Pro-Gly-Trp-NH2
ar	=	Axial rod
ASO	=	Accessory Sex Organs
av	=	Acrosomal vescicle
ax	=	Axoneme
bp	=	Basal plate
C	=	Cerebral ganglia
CG	=	Cortical granule
ch	=	Chromatin
DAB	=	Diaminobenzidine
db	=	Dense body
E	=	Esophagus
ea	=	Egg atrophy
E2	=	Estradiol
EDCs	=	Endocrine disrupting chemicals
eg	=	Electron-dense granule
EN	=	Eunucleolus
ep	=	End piece
ES	=	Electron-lucent space
et al.	=	Et. Ali (Latin), and others
EVO	=	Early vitellogenic oocyte

LIST OF ABBREVIATIONS AND SYMBOLS (Continued)

ex	=	Excrescence
FC	=	Follicle cell
FPL	=	Female penis length
Fyo	=	First yolk globule-accumulating oocyte
G	=	Golgi body
gp	=	Glycogen piece
GV	=	Golgi vesicle
hc	=	Heterochromatin
Ie	=	Inner epithelium layer
l	=	Lumen
L	=	Lipid droplet
LBG	=	Left buccal ganglion
LCG	=	Left cerebral ganglion
LM	=	Light microscope
LPaG	=	Left parietal ganglion
LPeG	=	Left pedal ganglia
LPlG	=	Left pleural ganglion
LS	=	Longitudinal section
LVO	=	Late vitellogenic oocytes
M, m	=	Mitochondria
ml	=	muscle layer
Mo	=	Mature oocyte
Mp	=	Midpiece
MPL	=	Male penis length
N	=	Nucleus
nd	=	Not detected
NG	=	Neuroglia
NPC	=	Neurons per cluster
NR	=	Neuron

LIST OF ABBREVIATIONS AND SYMBOLS (Continued)

Nu	=	Nucleolus
oc	=	Ocular tentacle
OC	=	Oocyte
Oe	=	Outer epithelium layer
Og	=	Oogonium
Ov	=	Ovary
Ovf	=	Ovarian follicles
P	=	Penis
pa	=	Proacrosome
Pa	=	Parietal ganglia
pav	=	Proacrosomal vesicle
PBS	=	Phosphate buffered saline
Pe	=	Pedal ganglia
Pl	=	Pleural ganglia
pm	=	Plasma membrane
PMF	=	Penis Morphogenic Factor
Po	=	Primary oocyte
PVO	=	Pre-vitellogenic oocytes
RBG	=	Right buccal ganalia
RCG	=	Right cerebral ganglion
RER	=	Rough endoplasmic reticulum
RPeG	=	Right pedal gangion
RPlG	=	Right pleural ganglion
RPSI	=	Relative penis size index
S	=	Stomach
Sc	=	Spermatocytes
Sg	=	Spermatogonia
St	=	Spermatid
ST	=	Seminiferous tubules

LIST OF ABBREVIATIONS AND SYMBOLS (Continued)

Syo	=	Second yolk globule-accumulating oocyte
Sz	=	Spermatozoa
T	=	Testosterone
TBT	=	Tributyltin
Te	=	Testis
TEM	=	Transmission electron microscope
TPT	=	Triphenyltin
TS	=	Transverse section
U	=	U-shaped
V	=	Electron-lucent vesicle
vd	=	Vas deferens
VDSI	=	Vas deferens sequence index
Vo	=	Vaginal opening
Y	=	Yolk body

CHAPTER 1
INTRODUCTION

In recent years, global concerns have been raised over the adverse effects of various substance groups such as organometallic compounds including organotins, heavy metals, herbicides, and xenoestrogenic compounds to many groups of aquatic invertebrates. Particular attention has focused on endocrine disrupting chemicals (EDCs) that have the potential to interfere with the synthesis, secretion, transport, binding, action, or elimination of natural hormones in the body. These processes are responsible for the maintenance of homeostasis, reproduction, development, and/or behavior (WHO, 2002). One of the most important groups of animals used to quantify the exposure to and effects of EDCs in the environment are the molluscs. This is because of the high sensitivity of the prosobranch gastropods to EDCs, in comparison to other invertebrate groups (Legierse *et al*., 1988). Hence pollutants might exhibit negative impacts on snails at lower environmental concentrations than other animals. Today, imposex, a well-known and well-documented effect of tributyltin (TBT) compounds on marine prosobranchs, is the clearest example of EDCs affecting reproduction and endocrine systems in invertebrates. This phenomenon is described as a development of male sexual organs (penis and vas deferens) in females (Smith, 1971).

TBT has been defined as one of the most toxic agents ever to be intentionally introduced into the marine environment (Goldberg, 1986). Since the late 1960s, the presence of this chemical in seawater is mainly due to its massive worldwide use as a biocide in the antifouling paints used on boats and ship hulls to prevent the colonization of the small marine invertebrates (i.e. bivalves, algae, bacteria etc.) that attach to underwater surfaces (Evans *et al*., 1991). The negative impacts of TBT have been reported on various groups of aquatic organisms such as bivalves, gastropods, crustaceans, algae, sea grasses, and fish (Evans *et al.*, 1995). However, the two well-known effects are shell deformation in oysters (Waldock and Thain, 1983) and imposex in gastropods (Gibbs *et al*., 1987). Under field conditions,

imposex is a specific response to TBT, and it is known to occur in more than 160 species belonging to more than 60 genera (deFur *et al*., 1999). At present, many lines of evidence have confirmed that TBT has been implicated in the development of imposex. Firstly, it has been shown that the intensity of imposex or the degree of imposex correlates to the proximity of harbors and marinas where high TBT concentrations have been detected (Swennen *et al*., 1997; Blackmore, 2000; Ramon and Amor, 2000; Pellizzato *et al*., 2004; Leung *et al*., 2006). Secondly, in a given species, the degree of imposex also increases consistently with the tissue concentrations of TBT (Pellizzato *et al*., 2004; Leung *et al*., 2006). Thirdly, gastropods transplanted from clean areas to harbour sites or areas with high shipping activities accumulate TBT and develop imposex (Quintela *et al*., 2000). Fourthly, following restrictions on the use of TBT there have been reductions in the levels or degree of imposex (Smith, 1996).

For reproduction, TBT can impact different levels of biological integration from molecular to communities. At a high degree of imposex, TBT commonly causes the imposex females to have reproductive failure (Barroso *et al*., 2002; Axiak *et al*., 2003) that can finally lead to a population decline in some gastropod species (Barroso and Moreira, 2002; Horiguchi *et al*., 2006). A local extinction caused by TBT induced female sterilization has also been previously reported in several regions (Barroso and Moreira, 2002). Histologically, previous reports have revealed an occurrence of spermatogenesis in the ovarian tissues of imposex females (Mensink *et al*., 2002; Horiguchi *et al*., 2006). In addition to the induction of spermatogenesis in the ovaries, some studies have shown that TBT also has negative effects on oogenesis of imposex females (Horiguchi *et al*., 2002). However, there have been no reports that TBT has possible effects on spermatogenesis in males exposed to TBT. In some cases, Triphenyltin (TPT) but not TBT, can effect on spermatogenesis in male gastropods (Schulte-Oehlmann *et al*., 2000). At present, information on the effects of TBT on ovarian spermatogenesis, oogenesis and male spermatogenesis, at the ultrastructural level, is scanty. Only ovarian spermatogenesis in *Hexaplex trunculus* has been investigated (Axiak *et al*., 2003). For oogenesis, TBT has been shown to cause extensive oocyte degeneration in *H. trunculus* and a high degree of imposex (Axiak *et al*., 2003).

In order to understand how TBT can induce the female gastropods to develop imposex we probably need to understand the action of normal male hormones in controlling male sexual differentiation and reproduction. Ala-Pro-Gly-Trp-NH2 (APGWamide) is a neuropeptide localized in the cerebral ganglia and the pedal ganglia, and in the male reproductive organs in a variety of mollusc species, especially gastropods. It is known to be largely, but not entirely, associated with the control of male sexual behavior (De Lange *et al*., 1998; De Lange and Van Minnen, 1998; Koene *et al*., 2000). Previous investigations have shown an involvement of neurohormones in the development of imposex (Feral and Le Gall, 1983). Administration of APGwamide significantly induced imposex in *Ilyanassa obsoleta* (Oberdoster and McClellan-Green, 2000). Oberdoster and McClellan-Green (2000) have proposed that APGWamide could represent the Penis Morphogenic Factor (PMF) in this species, and that it may play a role in imposex induction. Recent results showed that all TBT-treated animals (male, female, and imposex) of *I. obsoleta* had APGWamide levels similar to normal males and significantly higher than normal females (Oberdoster *et al*., 2005).

Babylonia areolata, an economically important marine gastropod for human consumption in Thailand, has a broad geographic range. It is a common tropical species distributed along the coastal areas from south to north of the Gulf of Thailand and inhabits shallow waters between 5 and 20 m depth on sandy and muddy sea bottoms. The first reports on high TBT concentrations in sediments from Thailand from many regions including the coastal areas along the Gulf of Thailand were observed in about 1996 (Kan-atireklap *et al*., 1997). Swennen *et al*. (1997) recorded a high imposex occurrence in various kinds of meso- and neogastropods including *Murex* spp., *Nassarius* spp. and *B. areolata* in the northern part of the Gulf of Thailand and in the southern part around Pattani, Thailand. Recently, a survey of levels of TBT in sediments and mussel tissues (*Perna viridis*) from coastal areas of Thailand revealed some high levels (Harino *et al*., 2006). In spite of these facts and according to the finding that TBT induces imposex at different levels for different gastropods, and that only about 15 of the mentioned 160 species from the list have been subjected to TBT laboratory experiments (Oehlmann *et al*., 2000), therefore, in this thesis, TBT-exposure experiments were designed to assess any chronic effects of

TBT on the incidence of imposex in *B. areolata* in the laboratory. Ultrastructurally, it is necessary to determine not only the effect of TBT on spermatogenesis in males, but also the spermatogenesis and oogenesis in the ovaries of imposex females to significantly achieve our understanding of these processes at the levels of cells and organelles. In this thesis, therefore, a whole gametogenetic sequence was characterized in TBT-exposed *B. areolata* (male and imposex) and comparisons were made on the gametogenesis in the normal snails of this species. Furthermore, from the information above there is a suggestion that a possible mode of action of TBT to induce imposex occurs via an abnormal release of APGWamide, so it was also necessary to further investigate the distribution of APGWamide in the TBT-induced imposex females to ensure that there is a correlation between the neurohormone release and development of imposex. Therefore, the direct effects of TBT on the distribution of APGWamide in the neural ganglia and the reproductive structures of the snails exposed to TBT were also examined using an immunohistochemical technique.

Literature review

1. Biology of the spotted babylon, *Babylonia areolata*

1.1 Taxonomy

Babylonia areolata (Link, 1807) has been placed in a subclass Prosobranchia. This snail has then been classified as follows:

Phylum Mollusca

Class Gastropoda

Subclass Prosobranchia

Order Neogastropoda

Family Buccinidae

Genus *Babylonia*

Species *Babylonia areolata*

1.2 General characters, distribution, feeding

The shell of *B. areolata* has the stepstair tower shape. The exterior surface of the shell has a white color on which there are brown violet or brown pink rectangular vein webs. The shell size of big individuals is more or less 80 mm high and 45 mm wide (http://www.fistenet.gov.vn.). In Thailand, *B. areolata*, is an economically important marine gastropod for human consumption, and has a broad geographic range. It is the common tropical species distributed along the coastal areas from south to north of the Gulf of Thailand and inhabits shallow waters between 5 and 20 m depth on sandy and muddy sea bottoms. During its planktonic larval stage of development this snail is a filter feeder using its velum and feeds on phytoplankton.

From juveniles to adults, it is a carnivorous feeder that inhabits sandy bottoms and its main foods are organic detritus.

1.3 Reproductive system

Like most neogastropods, *B. areolata* is dioecious. There is copulation and internal fertilization with a correspondingly complex reproductive system. In males, the single testis is located in the spirals of the visceral mass near the digestive gland. The entire gonoduct consists of a coiled tube (vas deferens) leading from the testis and functions in sperm storage and transport. The pallial vas deferens, containing a prostate gland, runs in the floor of the mantle cavity and out to a tentacle-like penis located behind the right cephalic tentacle (Fig. 1-A2). In the female the pallial section of the oviduct is modified to form both an albumen gland and a large jelly gland or capsule gland (Fig. 1-A1). The eggs are enclosed in a capsule as observed in many of the higher prosobranchs. In addition, there is a seminal receptacle or bursa or both for the storage of sperm (Ruppert *et al*., 2004).

1.4 Nervous system

The nervous system of gastropod is similar to that of molluscs, but some key differences are noted. In gastropods, it is affected by a torsion which commonly occurs in the gastropods within subclass Prosobranchia. Before the evolution to have torsion, the nervous system of prosobranchs is bilateral symmetry, containing six pairs of ganglia-cerebral, buccal, plural, visceral, pedal and parietal ganglia. After torsion has evolved, this leads to a change in the nervous system and affects the ganglia that run from the head to visceral mass. The anterior nervous system including cerebral, buccal, plural, and pedal ganglia are still at the same position but the posterior nervous system containing visceral and parietal ganglia as well as visceral nerve or cord are twisted to resemble a figure 8 (Fig. 1B) (Ruppert *et al*., 2004).

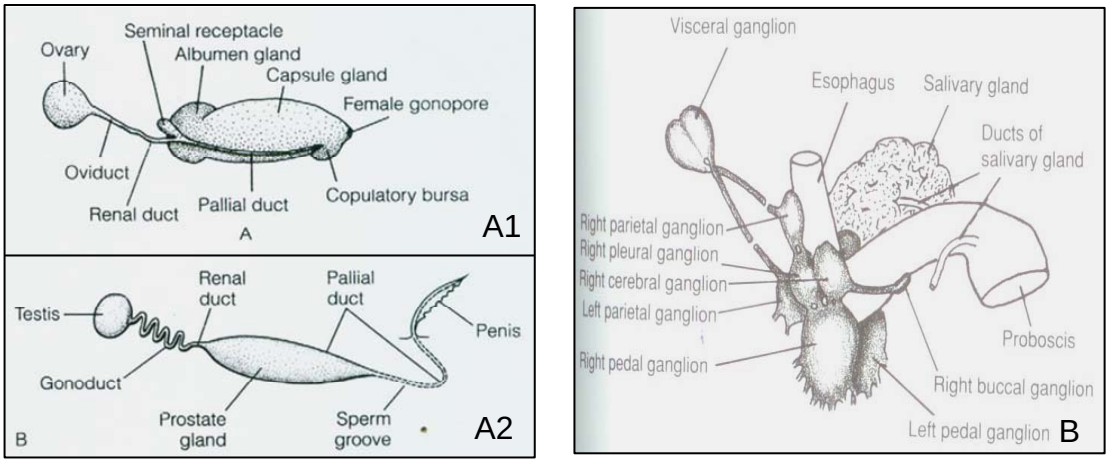

Figure 1. Diagrams of the reproductive system and concentrated nervous system. **A**: Reproductive system of *Littorina* (A1 = female; A2 = male). **B:** Nervous system in *Busycon* (Ruppert *et al*., 2004).

2. Ecotoxicological effects of TBT on aquatic organisms

TBT is known to be harmful to a range of aquatic organisms such as fish, bivalves, gastropods, and algae by inducing a number of physiological, morphological and toxicological effects. The known effects of TBT in fish include inhibition of spawning, development, growth and behaviour (Holm *et al*., 1991; Fent and Meire, 1992; Triebskorn *et al*., 1994; all cited in Jamari, 2001). The first adverse effect of TBT on molluscs was observed in the adult oyster, *Crassostrea gigas*, with shell thickening at the centers of oyster agriculture in France (Waldock and Thain, 1983). Other reported impacts of TBT on bivalves, include decreased oxygen consumption (Sujatha *et al*., 1996) and growth (Coelho *et al*., 2001) by the clams as well as modulations of the internal immune systems, genotoxic effects, and cytogenetic damage in the mussels (Jha *et al*., 2000). For marine algae, TBT exposures lead to increased respiration, and decreased growth (Moore *et al*., 1992). In gastropods, TBT in particular, at an ambient concentration of just a few nanograms per litre, has the potential to induce a genital disorder, termed imposex, in females of different species. Such imposex was first noticed in *Nucella lapillus* in 1969 when penis-like outgrowths were observed behind the right cephalic tentacle of females (Blaber, 1970). It consists of the superimposition of male sexual characteristics (penis and vas deferens) onto females (Smith, 1971). Today, many lines of evidence have

confirmed that imposex development has been induced by TBT (Smith, 1996; Pellizzato *et al*., 2004; Leung *et al*., 2006).

TBT is very toxic to aquatic life as demonstrated by numerous acute and chronic toxicity studies in a variety of marine and freshwater organisms. According to the available literature and Table 1 that compiles some selected toxicity data, the acute toxicity of fish lies in the range of a few µg/L, whereas, the most sensitive algae and invertebrates are affected at a few 100 ng/L or less. It is interesting to note that gastropod imposex in the *N. lapillus* can occur at the very low concentration of TBT (2 ng/L).

3. Reproductive effects of imposex

The effects of TBT on imposex can vary, depending on the species. In some cases, this phenomenon does not impair reproduction. But in some others, it can lead to population decline and local extinction, which are a consequence of reproductive failure due to female sterilization. The effects of TBT without impairment on reproduction are commonly found in the imposex female in the VDSI (vas deferens sequence index) of 1-4. In *Bolinus brandaris*, all imposex females were in stage 4 which showed no serious consequences on female reproduction (Ramon and Amore, 2001). Similarly, *Buccinum undatum* was induced by TBT to become imposex but no sterilized females were observed in the samples (Mensink *et al*., 2002).

In the case of impairment to reproduction, TBT causes imposex female in the stages 5 and 6 to be effectively sterilized by two mechanisms. The first mode of functional sterilization is the blockage of the pallial oviduct by the vas deferens and/or prostate gland developed in the imposex. This prevents the release of egg capsules, resulting in an accumulation of abortive capsular material in the pallial oviduct. The second mechanism is a split of the bursa copulatrix and capsule gland leading to prevention of copulation and capsule formation. To date, the reproductive failure in imposex as a consequence of the sterilization has been observed in many

Table 1. Toxicity of TBT to selected sensitive aquatic biota. Data was extracted from Fent (2006)[1].

Organism		Toxicity TBT	($\mu g\ L^{-1}$)	Refs.
Acute toxicity				
Algae	Diatoms	$EC_{50,}$ 72 h	0.3-0.4	[1]
Zooplankton	*Arcartia tonsa*	LC_{50}, 6 d	0.4	[2]
Amphipod	Gammarus	LC_{50}, 96 h	1.3	[3]
Molluscs	*Oyster C. virginica*	LC_{50}, 48 h	1.3	[4]
Crustaceae	Mysid shrimp	LC_{50}, 96 h	0.3	[5]
Fish	Minnows *P. phoxinus*	LC_{100}, 8 d	3.5	[6]
Chronic toxicity				
Algae	Diatoms	growth	0.1	[7]
Zooplankton	*Arcartia tonsa*	death, 144 h	0.3	[8]
Amphipod	Gammarus	24 d	0.53	[9]
Molluscs	Oyster *C. virginica*	LC_{100}, 12 d	0.18	[10]
	Spat	growth	0.01	[11]
Gastropods	*Nucella lapillus*	imposex	0.002	[12]
Fish	Minnows *P. phoxinus*	histology	0.7	[13]

[1] References (all cited by Fent, 2006): [1] Wash *et al*. (1985); [2] Sidharthan *et al*. (2002); [3, 9] Bushong *et al*. (1998); [4] Roberts (1987); [5] Valkirs *et al*. (1987); [6, 13] Fent and Meir (1992); [7] Beaumont and Newnan (1986); [8] U'ren (1983); [10] His and Robert (1985); [11] Lawler and Aldrich (1987); [12] Gibbs and Bryan (1986).

gastropod species such as *Nassarius reticulatus* (Barroso *et al*., 2002) and *Hexaplex trunculus* (Axiak *et al*., 2003). This can finally lead to a population decline in some species as reported in *Ocinebrina aciculata* (Oehlmann *et al*., 1996), *N. lapillus* (Barroso and Moreira, 2002) and *Babylonia japonica* (Horiguchi *et al*., 2006). Furthermore, local extinction due to female sterilization by TBT has been reported previously in some species i.e. *N. lapillus* (Barroso and Moreira, 2002). Most importantly, TBT also seems to disturb the reproductive cycle in *Haliotis madaka*

(Horiguchi *et al*., 2005) and *B. japonica* (Horiguchi *et al*., 2006), that live in an area with high TBT contamination.

4. Effects of TBT on ovarian spermatogenesis and oogenesis.

Unlike most of the toxins, previous available investigations have shown that TBT, at environmentally relevant concentrations, has no toxic effects on spermatogenesis in the male, but it induces female caenogastropods to become imposex and develop spermatogenesis in the ovary, termed ovarian spermatogenesis, and it also has an effect on oogenesis of the imposex females. This ovarian spermatogensis has been observed in neogastropods such as *N. lapillus* (Gibbs *et al*., 1988), *O. aciculata* (Oehlmann *et al*., 1996), *H. trunculus* (Axiak *et al*., 2003) and *B. japonica* (Horiguchi *et al*., 2006), and in archeaogastropods such as *H. madaka* (Horiguchi *et al*., 2005) and *H. gigantea* (Horiguchi *et al*., 2002).

Light microscopy (LM) is commonly used to observe the effects of TBT on the ovarian tissues of the imposex females. In the exposed females of *H. madaka* (Horiguchi *et al*., 20005), *H. gigantea* (Horiguchi *et al*., 2002) and *B. japonica* (Horiguchi *et al*., 2006), most of the gonadal tissues were ovaries with a small amount of testis tissue and either spermatogenesis or seminiferous tubule-like structural forms were observed, but there was no significant histological changes observed in the testis of exposed males. At the ultrastructural level, there is limited information on the alterations or the developments of ovarian spermatogenesis in imposex females. Only one study by Axiak *et al*. (2003) is available for some ultrastructural details of this process in the ovarian tissues of *H. trunculus*. In their study, transmission electron microscopy (TEM) was used to clarify the response of this snail to TBT from the field collections. For stages 1 to 4.7 of VDSI, females were found to retain normal histology as in normal females. At VDSI 5, however, sperm-like structures were found in the ovaries. These were complete with acrosomes and characteristics axonemes (9 + 2 microtubular structures). Several studies have shown that TBT also affects the oogenesis of imposex females that are in a high stage of imposex. In *H. gigantea*, there were significantly more contracted primary oocytes in females exposed to TBT than in the controls (Horiguchi *et al*., 2002). In *H. trunculus*

(VDSI stages 1 to 4.7), oogenesis proceeded normally (Axiak *et al*., 2003). Similarly, in *B. brandaris* all the females examined were affected by the imposex in degree 4 (Ramon and Amor, 2001), but oogenesis alterations at the ultrastrutural level were not found (Amor *et al*., 2004). At VDSI 5, however, oocytes of *H. trunculus* females had degenerating yolk platelets, with ooplasm consisting of a mixture of lipid droplets, vitelline and fluid vesicles, aberrant membranes and crystalline inclusions (Axiak *et al*., 2003). One part of this thesis, thus, was to characterize the ultrastructures during gametogenesis in males and females affected by TBT by comparing them to gametogenesis in the normal snails of this species.

5. Involvement of the APGWamide in imposex induction

In invertebrate species, the endocrinology associated with reproductive functions is not well understood. However, peptide hormones have been proposed to control the normal sexual differentiation and reproduction of molluscs. APGWamide is a neuropeptide found in a variety of molluscs species, especially gastropods. By using immunohistochemistry and in situ hybridization, it is known to be secreted by the central nervous system (ganglia), the copulatory duct and the penial complex of male gastropods. The expression or localization of APGWamide has been mainly studied in gastropods of the subclass Pulmonata and Opisthobranchia. In pulmonate *Lymnaea* (Croll and Van Minnen, 1992) and *Helix* (Li and Chase, 1995) as well as in the opisthobranch *Aplysia* (Fan *et al*., 1997), the populations of APGWamide-like immunoreactive cell were localized not only in the anteriomedial region of the right cerebral ganglion, but also in the male accessory sex organs, including the prostate gland, the vas deferens, the preputium, the penis, and the penis retractor muscle. In addition, a cluster of APGWamide expressing neurons has also been isolated from the ganglia of the prosobranchs such as *Fusinus ferrugineus* (Kuroki *et al*., 1990) and *Littorina littorea* (De Lange and Van Minnen, 1998).

Evidence to date thus indicates that APGWamide is largely, but not entirely, associated with the control of male reproduction in gastropods. Neurons, containing APGWamide, in the right cerebral ganglia of *Helix* are involved in the control of male copulation and/or courtship (Chase, 1986). Similarly, APGWamide

plays a key role (Van Golen *et al*., 1995) in the regulation of male copulatory behavior in *Lymnaea stagnalis*. This behavior is mainly controlled by the five clusters of neurons in the ganglia, which innervate the penial complex via the penis nerve. The detection of APGWamide-like immunoreactivity in the male reproductive organs of *Aplysia* and *Bulinus* (Fan *et al*., 1997; De Lange and Van Minnen, 1998) indicates that APGWamide may play a role in regulating the male reproductive function in these two species, as it does in other gastropods.

In the case of imposex, which is a highly specific response to TBT, females develop male sexual characteristics, especially a penis and vas deferens. As mentioned earlier, the peptide, APGWamide has been largely reported to act as a sex hormone in gastropods, especially in the control of male sexual development. TBT possibly targets this hormone that is a critical component of the sex differentiation pathways in gastropods. This thesis, thus, is mainly focused on the involvement of APGWamide in the development of imposex in gastropods caused by TBT. Previous investigations have shown the possibilities of the involvement of neuropeptides in the development of imposex. Feral and Le Gall (1983) showed that TBT exposure led to an increase of an unidentified neurohormone termed Penis Morphogenic Factor (PMF) in the cerebroplural and pedal ganglia of juvenile and female *O. erinacea* after 24 h. From that observation, it is implied that PMF was first identified as a neurohormone involved in imposex induction. In male *I. obsoleta* , the PMF is thought to control the development of the male Accessory Sex Organs (ASO) that include the sperm duct, seminal vesicle, external sperm groove and the penis prior to the mating season (Joosse, 1988). PMF has been identified in several species affected by imposex or intersex, including *Littorina* and *Buccinum* (Bauer *et al*., 1995; Deutsch and Fioroni, 1996), but it has not been chemically characterized.

A model of imposex induction based on the change in peptide hormones and steroid hormones has been proposed (Fig. 2) (Oberdoster and McClellan-Green, 2000). Many lines of evidences are needed before this model can be accepted, and neuropeptides that may function as the candidate PMF must be first identified.

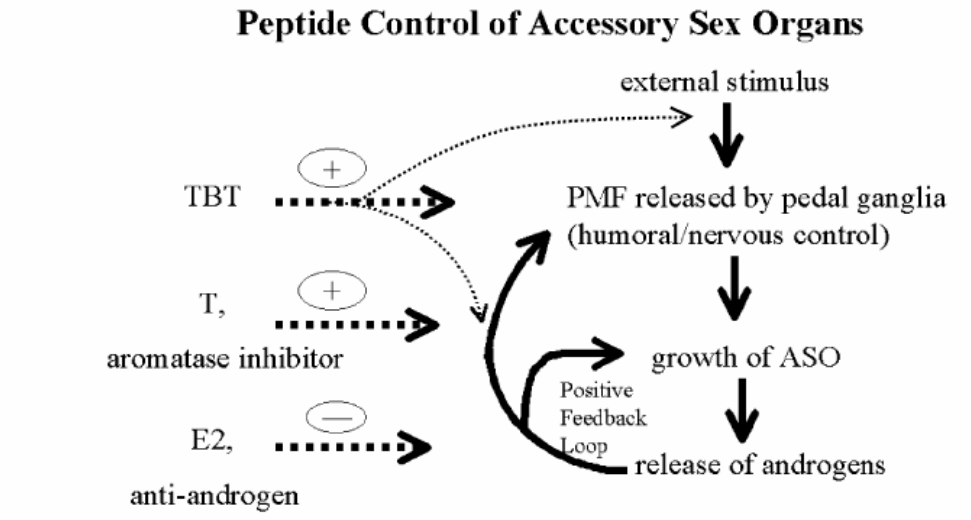

Figure 2. The hypothetical mechanism for imposex induction by TBT and steroids. TBT acts on the nervous system, while steroids (T = testosterone; E2 = estradiol) act on the positive feedback loop that maintains the Accessory Sex Organs (ASO). + indicates induction of imposex while - indicates inhibition of imposex (modified from Oberdorster and McClellan-Green, 2000).

At present there are several neuropeptide candidates for PMF. To investigate whether neuropeptides that regulate sexual differentiation in molluscs can induce imposex-a condition where female snails grow male accessory sex organs, Oberdoster and McClellan-Green (2000) dosed the mud snails, *I. obsoleta*, with one of four neuropeptides that have been identified in gastropods: APGWamide, conopressin, LSSFVRIamide, or FMRFamide. APGWamide regulates male sexual behavior and is localized in the cerebral ganglion near the penis and vas deferens in gastropods (De Lange and Van Minnen, 1998; Koene *et al*., 2000). Conopressin, an antagonist of APGWamide, is co-localized in the pedal ganglia with APGWamide (van Golen *et al*., 1995). Two other neuropeptides, FMRFamide and LSSFVRIamide have both found in several species of molluscs, and are considered to be cardioexcitatory and inhibitory/excitatory of various muscles (Kobayashi and Moneoka, 1990; De Lange *et al*., 1998). The study of Oberdoster and McClellan-Green (2000) found that APGwamide resulted in an even higher percent of imposex induction after injection. None of the other peptides tested exhibited any effect on imposex induction. From this, Oberdoster and McClellan-Green (2000) suggested that APGWamide may indeed be a candidate for PMF, and that it may play a role in

imposex induction in gastropod molluscs. Recently, APGWamide also induced vas deferens growth in the rock shell, *T. clavigera* (Horiguchi *et al*., 2003). According to the data above and the model of imposex induction (Fig. 2), it indicates that TBT possibly causes the abnormal release of APGWamide, leading to ASO growth in female snails. From this point of view, it can be hypothesized that if TBT acts as a neurotoxin to induce imposex via this process, then the change in distribution of APGWamide in an imposex female that has been externally stimulated by TBT could be detected. Therefore, one part of this thesis was to examine the direct effects of TBT on the distribution of APGWamide in the neural ganglia of the snails during imposex induction by TBT in the laboratory.

Hypotheses

1. TBT directly induces imposex in *B. areolata* at a certain concentration.
2. The ultrastructures of germ cells of TBT-exposed *B. areolata* would be different from those of normal snails.
3. If TBT acts as neurotoxin to induce imposex in *B. areolata* via abnormal release of the APGWamide, so the distribution of APGWamide in neural ganglia and male sexual organs of imposex females could be detected and imposex females should show an increase in APGWamide containing neurons.

Objectives

1. To assess the chronic effects of TBT on the incidence of imposex in *B. areolata* in the laboratory.
2. To investigate the ultrastructural changes of germ cells in both male and female *B. areolata* affected by TBT.
3. To determine the role of APGWamide in the induction of imposex in *B. areolata*.

CHAPTER 2
MATERIALS AND METHODS

1. Acute toxicity test

An acute toxicity test was carried out on the adults of *B. areolata* in order to estimate a possible effect of TBT on a mortality of this species and to find an appropriate range of TBT concentrations for performing the chronic experimental study.

1.1 Experimental snails

The reared mature specimens of *B. areolata* for both sexes were obtained from the marine laboratory breeding stock at the Aquatic Animal Hatchery and Research Unit, Prince of Songkla University, Pattani campus and the size larger than 30 mm in shell length were used. They were acclimatized in a plastic tank containing 100 L of natural seawater with aeration for a period of 72 h before starting the test and were not fed from this acclimation period until the test ended.

1.2 Test chemicals

TBT chloride of > 96% purity was from Aldrich Chemical Co. Stock solutions of TBTCl were made by dissolving TBTCl into glacial acetic acid. The test solutions of TBTCl used in the experiment were prepared through a serial dilution with a freshly prepared stock solution in seawater, and renewed every 24 h. The final carrier solvent concentration was never higher than 0.001% in all treatments.

1.3 Toxicity experiment

A 96-h static-renewal acute toxicity test was conducted for TBT and divided into 7 treatments based on the concentration series of TBTCl: 0, 0.001, 0.01, 0.1, 1, 10 and 100 μg TBT as Sn/L. The bioassay experiment was started by transferring a total of 420 acclimatized snails from stock tanks and distributing them into 21 small aquaria under the following conditions: 20 adult *B. areolata* per

replicate: 3 replicates for each tested concentration. The behavior and general condition of the snails as well as their mortality at each tested concentration were recorded once every 12 h. The snails were considered dead if they did not respond to gentle prodding. The toxicity end point (LC_{50}) was determined as the concentration required to kill 50% of the snails after 24, 48, 72 and 96 h exposure using Probit analysis (Finney, 1971). Water quality conditions, including pH, temperature and salinty were measured daily.

2. Chronic TBT- exposure experiment

2.1 Experimental design

For this experiment, almost 1,260 females and 270 males of adult *B. areolata* (size larger than 30 mm in shell length) were obtained from the marine laboratory breeding stock at the Aquatic Animal Hatchery and Research Unit, Prince of Songkla University, Pattani campus. Snails were allowed to acclimatize for two months prior to the onset of the experiment by maintaining them in 100 L aquaria provided with a 48 h static renewal system, an air filter, and natural seawater. After this period, three replicate groups of 70 sexually mature females and 15 males were each exposed to five different nominal aqueous concentrations of TBT as follows:

Treatment 1: 1 ng TBT as Sn/L
Treatment 2: 10 ng TBT as Sn/L
Treatment 3: 50 ng TBT as Sn/L
Treatment 4: 100 ng TBT as Sn/L
Treatment 5: 500 ng TBT as Sn/L

They were treated with TBT for at least 6 months and kept in the same manner as the holding conditions described above. TBT exposure solutions were replaced once every 48 h and snails were regularly fed with fish. Stock solutions of TBT chloride were prepared by dissolving TBTCl into glacial acetic acid. Additionally, two control groups were run in parallel (water only and glacial acetic acid in water). The concentration of glacial acetic acid in all treatments (except control with water only) was never higher than 0.001%. Water parameters, including pH, temperature, and salinity were measured once every two weeks for each replicate.

2.2 Morphometry and imposex assessments

30 females and 5 males from each treatment were analyzed at monthly intervals. For morphological analyses, snails were relaxed for 2 h using 7% $MgCl_2$ in distilled water; shell length and shell width were then measured to the nearest 0.1 mm. After crushing the shell with a vice to remove the soft tissue, total weight and soft body weight were recorded, and the specimens were sexed. The males were recognized by the presence of a penis and a prostate gland, while the females were defined by the presence of a vagina and the capsule gland. The imposex females characterized by the development of additional male parts (penis and vas deferens)(see Fig. 3B-C) were divided into 6 stages according to criteria as shown in Table 2 and their numbers were recorded for each treatment. Penis length in males and imposex females was measured to the nearest 0.1 mm under a stereo-dissecting microscope using an eyepiece.

For the measurement of the intensity of imposex in each treatment, the following indices were calculated. (1) % imposex incidence was computed as (number of imposex females found/number of total females examined) x 100. (2) VDSI (vas deferens sequence index) was calculated as the mean of the imposex stages that occurred in the sample. (3) RPSI (relative penis size index) was defined as (mean length of female penis^3)/ (mean length of male penis^3) x 100 (Bryan *et al*., 1986). (4) The mean of the female penis length (FPL) of a sample was determined. Additionally, a percentage of imposex female in each stage of VDSI (1-6) in the sample was also calculated as (number of imposex females for each stage/number of total imposex females examined) x 100.

3. Gametogenesis

3.1 Histological investigation

30 ovaries of either imposex females in each stage (1 to 5) or normal females (Fig. 3A) as well as 30 testes of both TBT-treated males (exposed to the 500 ng TBT as Sn/L for a period of 6 months) and normal males (Fig. 3B) were dissected and fixed in Bouin's fluid for about 18-24 h. They were then processed by using standard histological techniques (Bancrof and Gamble, 2002). The paraffin

embedding of ovarian and testicular tissues were sectioned at 6 μm thickness and stained with Harris's haematoxylin and Eosin. In the imposex and normal females, the ovarian sections were observed using a light microscope for determining the presence of spermatogenesis in the ovaries and any histopathological disorders. Testicular sections from both TBT-treated-and normal males were histologically compared.

Table 2. Criteria for the imposex stages determined according to VDSI (Stroben *et al.*, 1992).

Stage	Description
0	Female are normal without any penis or vas deferens
1	A tiny penis appearing behind the right ocular tentacle
2	Penis with penis duct and a vas deferens which runs continuously from the right ocular tentacle
3	Development of a penis and vas deferens which reaches up to the vaginal opening
4	Presence of penis and vas deferens which passes through the vaginal opening
5	Penis and vas deferens which passes through the vaginal opening and reaches up to the capsule gland
6	Penis and vas deferens which penetrates the capsule gland and the capsule material is black in colour

3.2 Ultrastructural investigation

Ovaries of imposex females (stage 5) and normal females as well as testes of TBT-treated males and normal males were removed, cut into small pieces and prefixed in cold (4 °C) 2.5% glutaraldehyde in 0.1 M phosphate buffer, pH 7.4 for 24 h. They were rinsed for 10 min in 3 changes of buffer, and postfixed in 1% OsO_4 in 0.1 M phosphate buffer, pH 7.4 for 1 h at room temperature. After fixation, the tissue was dehydrated in a graded series of ethanol up to 100% and with the intermedium propylene oxide. The samples were embedded in Epon 812. Semi-thin and ultrathin sections were cut with glass knives on a Reichert-Jung Ultracut E ultramicrotome at the Department of Cell Imaging and Ultrastructure Research, Faculty of Life Sciences, University of Vienna, Austria. Semi-thin sections were

stained in 0.1% toluidene blue and observed with a light microscope. Ultrathin sections were stained in 2% uranyle acetate (30 min) and 0.5% lead citrate (5 min) and viewed with a Zeiss EM 902.

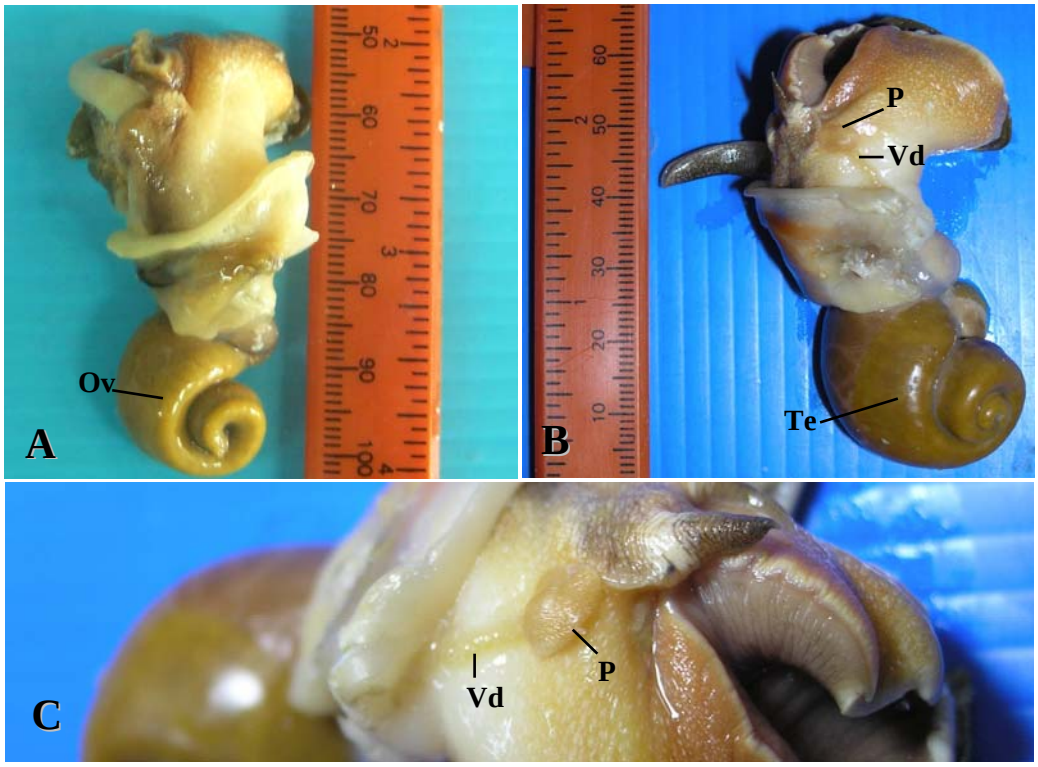

Figure 3. The morphology of reproductive organs of *B. areolata*. **A**: Normal female. **B-C**: Normal male. Ov-ovary; P-penis; Te-testis; Vd-vas deferens.

4. Neuropeptide APGWamide distribution

Neural ganglia (Fig. 4-6) and selected reproductive organs (penis and gonads) (Fig. 3A-C) were quickly dissected from five groups of the imposex females (stages 1 to 5) and two groups of the normal snails (male and female) (n = 5 for each group), fixed in Bouin's fluid for 16–24 h at 4°C, and then processed for histology with procedures previously described to selectively label APGWamide-like immunoreactivity (APGWa-lir) in *Lymnaea* (Croll and Van Minnen, 1992). The fixed tissues were dehydrated in a graded series of ethanol, cleared in xylene, and embedded in paraffin. Serial sections (7 μm) were cut and placed on coated slides. The sections were deparaffinized, rehydrated and washed in phosphate buffered saline

(PBS: 50 mM Na_2HPO_4 $7H_2O$, 140 mM NaCl, pH 7.4). After a 10-min incubation with normal goat serum, the adjacent sections were next incubated overnight at 4 °C with the primary rabbit anti-APGWamide serum (kindly provide by Prof. Dr. Jan van Minnen) (1: 500 in 10% normal goat serum, 1% Triton X-100 in PBS). Afterwards, the sections were washed twice in PBS and incubated with the secondary antibody peroxidase-conjugated swine antirabbit (Dako, Danmark; 1:100) for 1 h followed by visualization by staining with 3,3 - diaminobenzidine (DAB). All sections were next dehydrated in an ascending alcohol series, cleared in xylene and mounted in Entellan (Merck). Tissues were examined with a light microscope and digitally photographed with an Olympus DP12. Sections serving as negative controls were treated similarly except that normal rabbit serum were used instead of the anti-APGWamide serum. No staining was observed in these preparations.

In imposex and normal snails, the distribution or localization of APGwamide-like immunoreactivity in central nervous system including buccal (Fig. 4), cerebral (Fig. 4-6), pleural (Fig. 5), parietal (Fig. 5), and pedal ganglia (Fig. 4, 6), and in the reproductive tracts (penis and gonad) of *B. areolata* was described. In each group of snails, the number of immunoreactive neurons per cluster (NPC) was counted for all clusters of neurons detected in each side (left and right) of the ganglion and the values were averaged (n = 5) in order to compare them between groups of *B. areolata*. In addition the average number of total immunoreactive neurons was calculated for each side and both sides of ganglia and compared between groups of *B. areolata*.

5. Data analyses

The data were statistically analyzed using SPSS program version 11.5 for Windows and the differences were considered significant when $p < 0.05$. Either a One-way analysis of variance (ANOVA) when an equal variance was assumed or a Brown-Forsythe of Robust test for non-equal variances was used to evaluate the differences in the mean values of the following parameters: (1) water parameters including pH, temperature and salinity between exposure times during the acute and chronic toxicity studies, (2) indices (VDSI and FPL) used to compare the imposex

intensity between TBT concentrations, and (3) the number of immunoreactive neurons per clusters (NPC) as well as the number of total immunoreactive neurons between groups of *B. areolata* (imposex 1-5, normal male, and normal female).

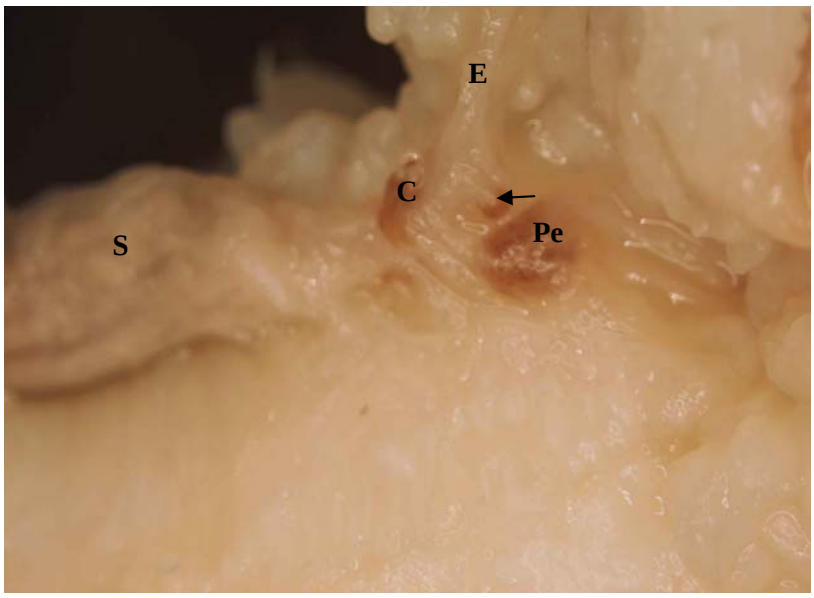

Figure 4. Ganglia of *B. areolata*. Note buccal ganglia (arrow). C-cerebral ganglia; E-esophagus; Pe-pedal ganglia; S-stomach (Magnification = x70) (from Thaweethamsewee *et al*., 2010).

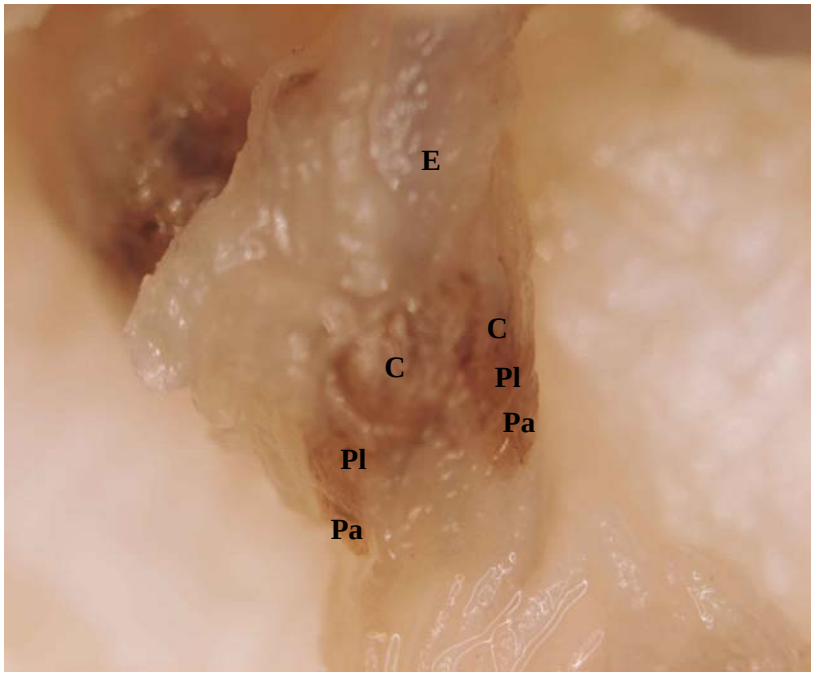

Figure 5. Ganglia of *B. areolata*. C-cerebral ganglia; E-esophagus; Pa-parietal ganglia; Pl-pleural ganglia; (Magnification = x160) (from Thaweethamsewee *et al*., 2010).

Figure 6. Ganglia of *B. areolata*. C-cerebral ganglia; E-esophagus; Pe-pedal ganglia. (Magnification = x70) (from Thaweethamsewee *et al*., 2010).

CHAPTER 3
RESULTS

1. Acute toxicity test

1.1 Water quality conditions

The mean values of all water parameters during the acute toxicity test were constant and did not vary between exposure times except for some slight differences in the salinity (Table 3).

Table 3. The water quality conditions (mean ± S.E.) during the test periods.

Times	N	Temperature (^{0}C)	pH	Salinity (ppt)
24 h	36	26.81 ± 0.13	7.81 ± 0.05	36.81 ± 0.19^{c}
48 h	36	26.91 ± 0.16	7.81 ± 0.06	36.72 ± 0.15^{bc}
72 h	36	27.03 ± 0.17	7.69 ± 0.09	36.19 ± 0.14^{ab}
96 h	36	27.21 ± 0.19	7.73 ± 0.05	36.03 ± 0.17^{a}
Total	**144**	**26.99 ± 0.08**	**7.76 ± 0.03**	**36.44 ± 0.09**

Within each column, means sharing the same superscript letter are not significantly different from each other; means with different superscript letters are significantly different (one-way ANOVA, $p < 0.05$).

1.2 General symptoms and behaviors (Visual observations)

In the TBT acute tests, no mortality (dead snails) was observed at the concentrations of 0.001, 0.01, 0.1, 1 and 10 µg TBT as Sn/L as well as at the control group (0 µg TBT as Sn/L). In addition, all snails from those groups except from 10 µg TBT as Sn/L appeared to be normal from the start until the test ended. The sequence of toxicological symptoms, which were the results from the negative effect of TBT, such as the production of a very large amount of mucus along the periphery of the mantle edges, the closing of opercula, and the silt accumulation were found in the snails exposed to 10 and 100 µg TBT as Sn/L. However, the mortality of the snails was significantly affected only by a concentration of 100 µg TBT as Sn/L.

1.3 Acute toxicity study

At the 100 µg TBT as Sn/L, the test organisms died after 72 h (2%), 84 h (22%) and 96 h (100%) (Fig. 7). The 96-h LC_{100} value (based on the nominal concentration) was 100 µg TBT as Sn/L.

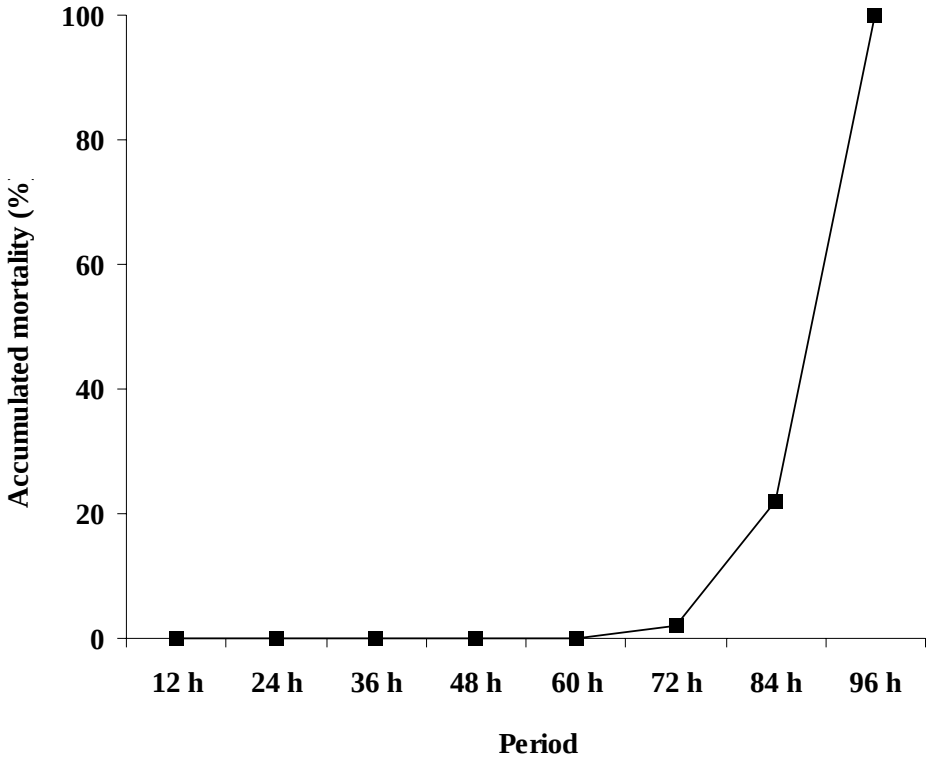

Figure 7. Percentage mortality of *B. areolata* after 96-h exposure to nominal concentration of 100 µg TBT as Sn/L during the standard acute toxicity test.

2. Chronic effect of TBT on imposex induction in *B. areolata*

2.1 Water parameters

The water quality parameters including temperature (Table 4), pH (Table 5) and salinity (Table 6) were generally consistent within a test. The overall mean values (± S.E.) (n = 252) of water temperature, pH and salinity were 27.01± 0.62 ^{0}C, 7.78 ± 0.02 and 36.56 ± 0.07 ppt, respectively. It was shown that the total mean values of temperature and pH were not different when comparing between treatments ($p > 0.05$). The difference between maximum and minimum values of the total mean temperature was never greater than 0.49 ^{0}C (Table 4) while the pH was always within 0.12 (Table 5). In contrast, at least one pair of the total mean salinity values showed a significant difference between TBT concentrations ($p < 0.05$). The difference between the highest and the lowest values of the total mean salinity did not vary by more than 1.19 ppt (Table 6).

Table 4. Temperature (^{0}C) of seawater (mean ± S.E.) during the 6 months of TBT-exposure experiment (n = 6 in each column).

Exposure time	TBT concentrations (ng TBT as Sn/L)					
(months)	0	1	10	50	100	500
1	26.37 ± 0.08^{b}	27.50 ± 0.19	26.78 ± 0.02^{b}	27.13 ± 0.07^{b}	27.03 ± 0.35^{bc}	26.18 ± 0.05^{a}
2	27.13 ± 0.04^{d}	26.25 ± 0.10	28.13 ± 0.13^{c}	27.67 ± 0.13^{b}	28.00 ± 0.07^{cd}	27.25 ± 0.34^{abc}
3	28.17 ± 0.10^{e}	26.47 ± 0.05	26.73 ± 0.09^{b}	28.45 ± 0.15^{c}	27.95 ± 0.06^{cd}	28.47 ± 0.28^{c}
4	26.83 ± 0.06^{c}	26.83 ± 0.07	26.77 ± 0.06^{b}	27.17 ± 0.03^{b}	28.25 ± 0.10^{d}	28.00 ± 0.03^{bc}
5	28.00 ± 0.07^{e}	26.92 ± 0.71	25.43 ± 0.04^{a}	25.53 ± 0.04^{a}	25.63 ± 0.11^{a}	27.12 ± 0.43^{abc}
6	25.60 ± 0.05^{a}	26.90 ± 0.11	27.60 ± 0.50^{bc}	26.20 ± 0.38^{a}	26.42 ± 0.47^{ab}	26.77 ± 0.48^{ab}
Total	**27.02 ± 0.15**	**26.81 ± 0.13**	**26.91 ± 0.16**	**27.03 ± 0.17**	**27.21 ± 0.19**	**27.30 ± 0.18**

Within each column, means sharing the same superscript letter are not significantly different from each other; means with different superscript letters are significantly different (one-way ANOVA, $p < 0.05$).

Table 5. pH of seawater (mean ± S.E.) during the 6 months of TBT-exposure experiment.

Exposure time (months)	TBT concentrations (ng TBT as Sn/L)					
	0	**1**	**10**	**50**	**100**	**500**
1	7.87 ± 0.21	7.93 ± 0.02	7.97 ± 0.28	7.88 ± 0.04	7.87 ± 0.21	7.92 ± 0.02^{c}
2	7.63 ± 0.07	7.87 ± 0.20	7.82 ± 0.09	7.18 ± 0.45	7.63 ± 0.07	7.48 ± 0.15^{ab}
3	7.65 ± 0.10	7.70 ± 0.12	7.68 ± 0.12	7.72 ± 0.08	7.65 ± 0.10	7.88 ± 0.02^{bc}
4	7.85 ± 0.07	7.87 ± 0.08	7.76 ± 0.08	7.67 ± 0.11	7.85 ± 0.07	7.38 ± 0.14^{a}
5	7.60 ± 0.15	7.63 ± 0.14	7.90 ± 0.03	7.77 ± 0.09	7.60 ± 0.15	7.83 ± 0.07^{bc}
6	7.80 ± 0.08	7.85 ± 0.07	7.73 ± 0.11	7.93 ± 0.03	7.80 ± 0.08	7.82 ± 0.09^{bc}
Total	**7.73 ± 0.05**	**7.81 ± 0.05**	**7.81 ± 0.06**	**7.69 ± 0.09**	**7.73 ± 0.05**	**7.72 ± 0.05**

Within each column, means sharing the same superscript letter are not significantly different from each other; means with different superscript letters are significantly different (one-way ANOVA, $p < 0.05$).

Table 6. Salinity (ppt) of seawater (mean ± S.E.) during the 6 months of TBT-exposure experiment.

Exposure time (months)	TBT concentrations (ng as Sn/L)					
	0	**1**	**10**	**50**	**100**	**500**
1	37.50 ± 0.22^{ab}	35.33 ± 0.42^{a}	36.33 ± 0.21^{ab}	35.83 ± 0.17^{ab}	36.83 ± 0.31^{b}	38.00 ± 0.00^{c}
2	37.50 ± 0.22^{ab}	37.17 ± 0.17^{c}	36.17 ± 0.31^{a}	36.00 ± 0.26^{ab}	35.50 ± 0.22^{a}	36.00 ± 0.26^{ab}
3	36.83 ± 0.17^{a}	38.00 ± 0.00^{c}	37.67 ± 0.21^{b}	35.33 ± 0.21^{a}	35.00 ± 0.00^{a}	35.17 ± 0.17^{a}
4	36.50 ± 0.22^{a}	37.50 ± 0.22^{c}	36.83 ± 0.17^{ab}	36.50 ± 0.22^{ab}	35.00 ± 0.00^{a}	34.83 ± 0.17^{a}
5	37.00 ± 0.45^{ab}	35.83 ± 0.40^{ab}	36.67 ± 0.21^{ab}	36.83 ± 0.17^{b}	36.83 ± 0.17^{b}	36.67 ± 0.61^{bc}
6	38.00 ± 0.00^{b}	37.00 ± 0.37^{bc}	36.67 ± 0.61^{ab}	36.67 ± 0.56^{b}	37.00 ± 0.26^{a}	37.00 ± 0.37^{bc}
Total	**37.22 ± 0.13**	**36.81 ± 0.19**	**36.72 ± 0.15**	**36.19 ± 0.14**	**36.03 ± 0.17**	**36.28 ± 0.22**

Within each column, means sharing the same superscript letter are not significantly different from each other; means with different superscript letters are significantly different (one-way ANOVA, $p < 0.05$).

2.2 Imposex assessments

2.2.1 Imposex development

The imposex phenomenon was characterized by a superimposition of additional male parts i.e. a penis and/or vas deferens (as shown in Fig. 8A for normal male), on females. The imposex development was generally described by an evolutionary scheme with six stages (1-6) most of which could be multiple types (a-c) (Stroben *et al*., 1992, Oehlmann *et al*., 1996). Five stages of imposex development in *B. areolata* induced by TBT during the exposure experiment were observed with two different types (a and c) in stage 1, three types (a, b and c) in stages 2 and 3, and only one type in stages 4 and 5; however stage 6, a final point of imposex, did not occur in

this species. According to their external morphology, the females at different imposex stages were described as follows (Table 7):

Table 7. Descriptions of each imposex stage in *B. areolata*.

Imposex stages	Types	Descriptions
0	-	Normal female without any male characteristics (Fig. 8B).
1	a	Tiny penis with no penis duct behind the right ocular tentacle (Fig. 8C).
	c	No penis but a short, proximal vas deferens tract beginning at a vaginal opening (Fig. 8D).
2	a	Penis with a closed penis duct behind the right ocular tentacle (Fig. 8E).
	b	Distal vas deferens tract behind the right ocular tentacle and proximal vas deferens tract beginning at a vaginal opening (Fig. 8F).
	c	Penis without penis duct and proximal vas deferens tract beginning at a vaginal opening (Fig. 8G).
3	a	Penis with a penis duct continuing along a short distal tract of the vas deferens (Fig. 8H).
	b	Vas deferens running continuously from the right ocular tentacle up to the vaginal opening (Fig. 8I).
	c	Penis with a penis duct continuing to a distal portion of the vas deferens; additionally a short proximal vas deferens portion arising from the vaginal opening (Fig. 8J).
4	-	Penis with a penis duct and a continuous vas deferens from the penis up to the vaginal opening (Fig. 8K).
5	b	Penis length is extended and the complete vas deferens passes through the vaginal opening (Fig. 8L).

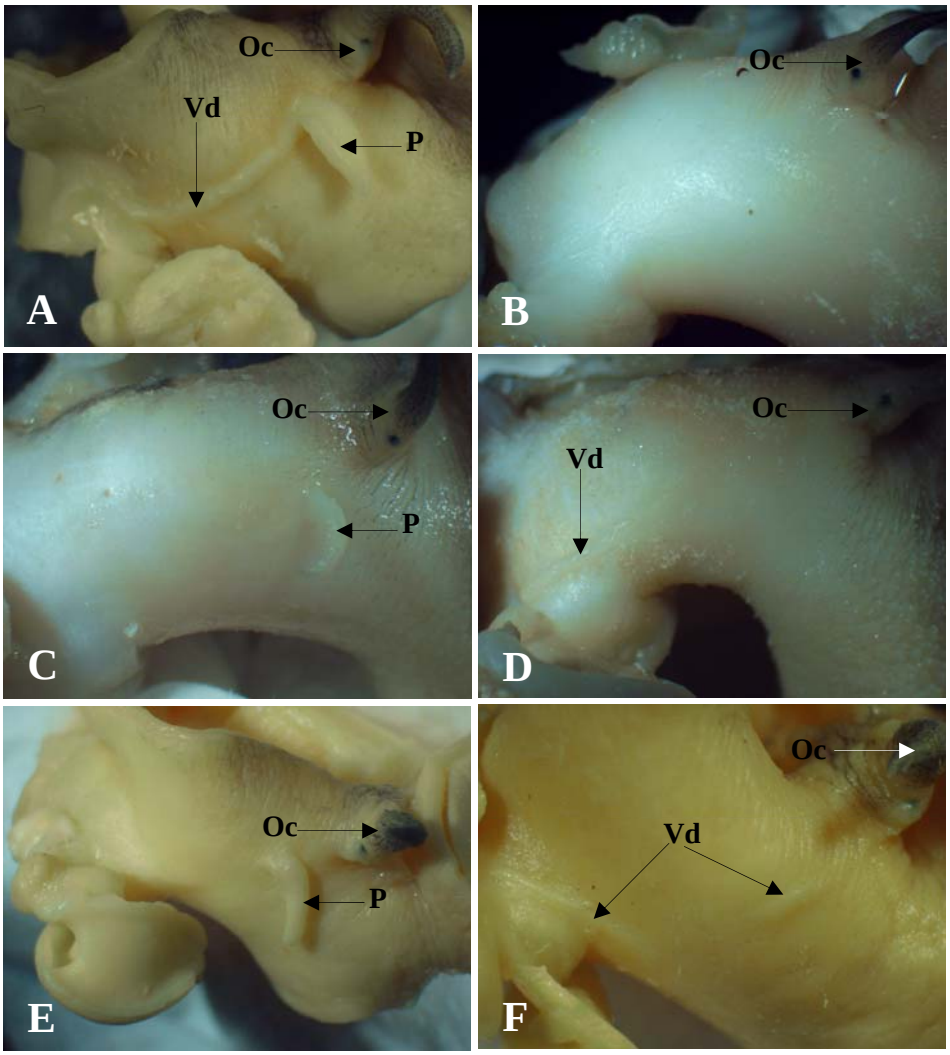

Figure 8. External morphology of imposex progression in female *B. areolata*. **A**: Normal male. **B**: Stage 0 (normal female). **C**: Stage 1a. **D**: Stage 1c. **E**: Stage 2a. **F**: Stage 2b. **G**: Stage 2c. **H**: Stage 3a. **I**: Stage 3b. **J**: Stage 3c. **K**: Stage 4. **L**: Stage 5b. Oc-ocular tentacle; P-penis; Vd-vas deferens; Vo-vaginal opening.

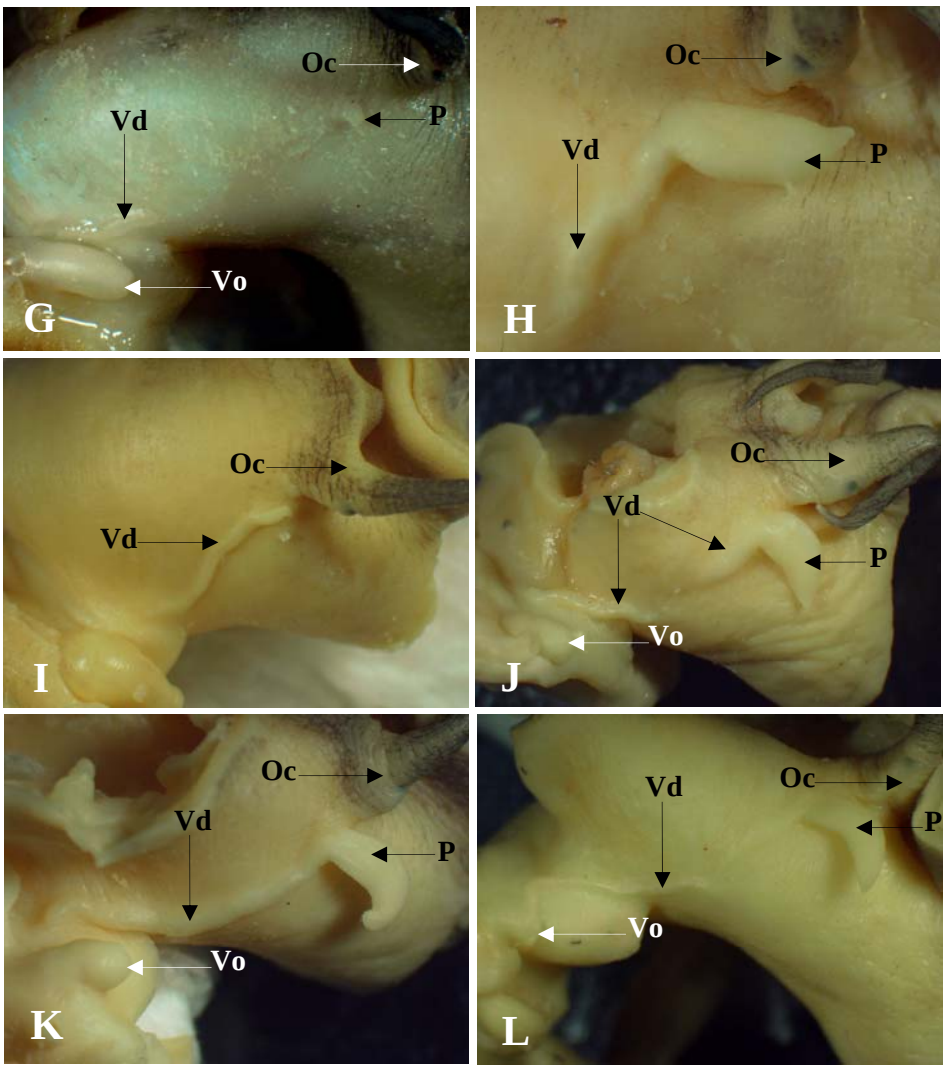

Figure 8. (Continued)

2.2.2 Imposex incidence

The study clearly showed that all TBT concentrations (1, 10, 50, 100, and 500 ng TBT as Sn/L) had the potential to induce imposex in female *B. areolata*, whereas no imposex was observed during all exposure times in the control group. Table 8 showed the imposex incidence that was variable and fluctuated among TBT concentrations and exposure times. After the 1st month of exposure, the highest percentage of imposex females (48.15%) was recorded at the concentration of 100 ng TBT as Sn/L, whereas the lowest value (6.90%) was found at the concentration of 1 ng TBT as Sn/L. In the 2nd month, the percentage of imposex females increased at all concentrations and ranged from 35.00% (50 ng TBT as Sn/L) to 75.86% (500 ng TBT

as Sn/L). In the females after the 3rd month of TBT exposure, the highest (86.67%) and lowest (38.46%) percentages of imposex incidence were at the concentration of 50 and 1 ng TBT as Sn/L, respectively. During the 4th, 5th and 6th months of the experiment, the highest concentration (500 ng TBT as Sn/L) induced the highest imposex incidence of 64.52%, 85.71% and 92.31%, respectively, compared to other lower TBT concentrations in which the percentages of imposex incidence ranged from 12.50% - 64.29% (Table 8).

Table 8 The percentage of imposex incidence in female *B. areolata* during the 6 months of exposure to different nominal TBT concentrations**.**

TBT concentrations (ng TBT as Sn/L)	**% imposex female**					
	Exposure time (months)					
	1	**2**	**3**	**4**	**5**	**6**
0	0.00(30)	0.00(29)	0.00(28)	0.00(30)	0.00(30)	0.00(25)
1	6.90(29)	51.72(29)	38.46(26)	23.08(26)	12.50(24)	20.00(20)
10	27.59(29)	40.00(20)	50.00(20)	50.00(20)	33.33(18)	61.11(18)
50	26.67(30)	35.00(20)	86.67(15)	50.00(28)	62.50(16)	47.06(17)
100	48.15(27)	57.89(19)	64.29(28)	64.29(28)	55.17(29)	62.07(29)
500	31.03(29)	75.86(29)	65.52(29)	64.52(30)	85.71(28)	92.31(26)

(n) = the total number of females examined

2.2.3 Vas deferens sequence index (VDSI)

The various frequencies of each imposex stage in *B. areolata* were given in the Fig. 9 during exposure to a range of TBT concentrations for a period of 6 months. The stages of imposex observed ranged from 1 to 4 for the 1 and 50 ng TBT as Sn/L as well as from 1 to 5 for the 10, 100 and 500 ng TBT as Sn/L (Fig. 9). The results clearly showed that at all concentration most of the imposex females found with high percentages were in stage 1 in all experimental months (Fig. 9). Although the 10, 100 and 500 ng TBT as Sn/L could induce imposex of stage 5, the highest number of imposex snails at this stage was observed in the 500 ng TBT as Sn/L. The monthly average of VDSI in *B. areolata* showed that the values were not significantly

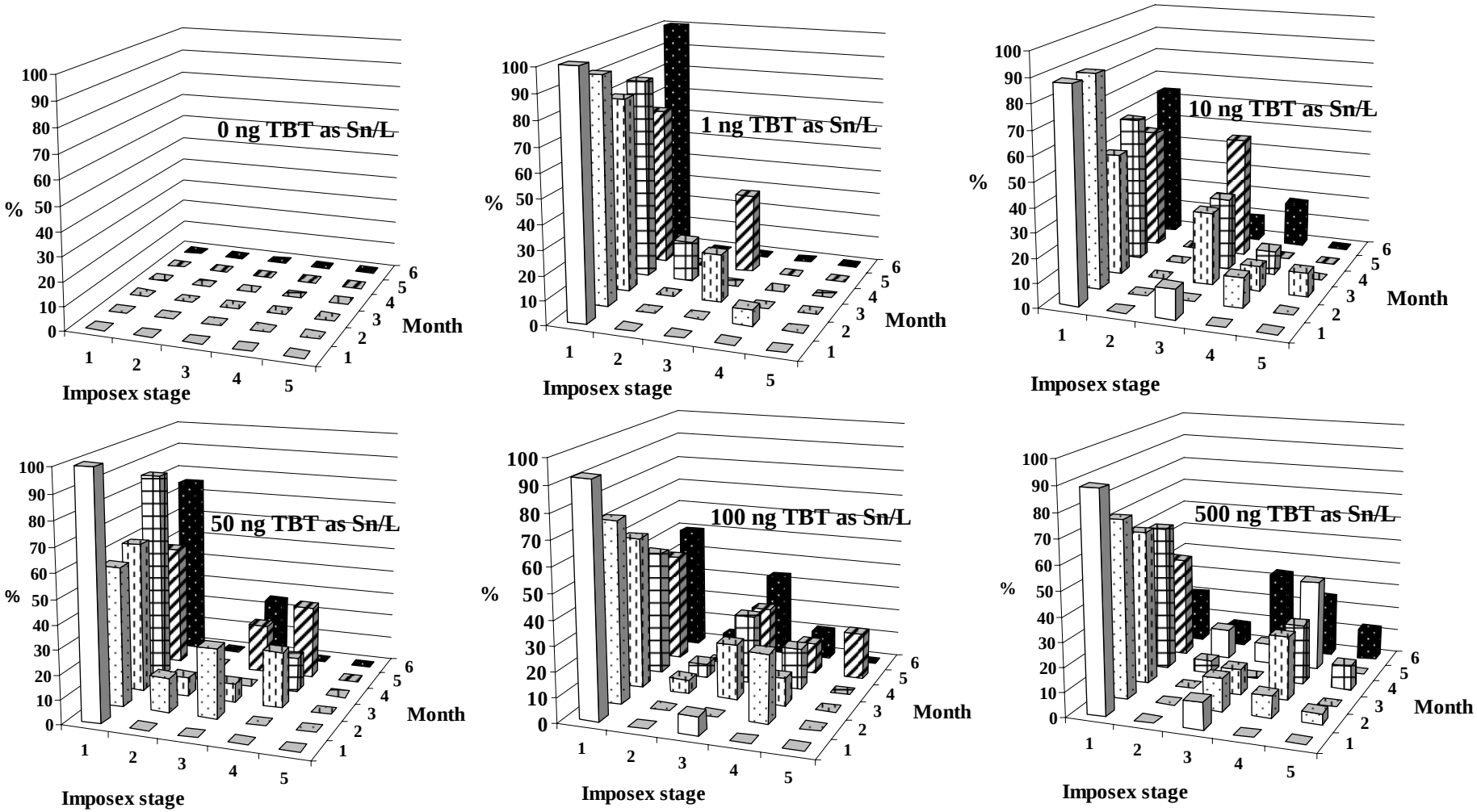

Figure 9. Percentage of imposex stages in *B. areolata* for the different TBT concentrations (ng TBT as Sn/L).

different between each treatment in all experimental months ($p > 0.05$) (except for the 6th month). However, at the concentrations of 1, 10 and 50 ng TBT as Sn/L, almost all VDSI values were lower than those of the higher concentrations (100 and 500 ng TBT as Sn/L). The VDSI values of snails at the 1 ng TBT as Sn/L, ranged from 1.00-1.67, were lowest in all six months compared to those of others, while the VDSI values for the 10 and 50 ng TBT as Sn/L ranged from 1.25-2.30 and 1.00-2.30 respectively (Fig.10). At the concentrations of 100 ng TBT as Sn/L, the mean VDSI rose from a minimum value (1.15) in the 1st month to a maximum value (2.63) in the 5th month. For the highest concentration (500 ng TBT as Sn/L), the mean VDSI increased from the 1st month with a value of 1.22 to the end of the experiment with a value of 3.00 which was significantly higher than those found in all other concentrations ($p < 0.05$). For the pooled data, the VDSI values for *B. areolata* were never higher than 3.

2.2.4 Female penis length (FPL)

A penis length of the imposex females varied from a small protuberance (1.50 mm in imposex stage 1) up to 8.67 mm (in imposex stage 4) while the values in the TBT-treated males and normal males ranged from 1.00 to 8.00 mm. Overall, the mean penis lengths of imposex females in stages 2 – 5 were similar to those of the normal males ($p > 0.05$) and significantly higher than those of the imposex females in stage 1 ($p < 0.05$), whereas the mean penis length of TBT-treated males were significantly greater than those of all the other groups ($p < 0.05$) (Fig. 11). For the pooled data, the mean penis length of the imposex females for all imposex stages was 4.19 ± 0.16 (S.E.) mm ($n = 81$) which was close to that of the normal males (3.77 ± 0.24 mm) ($n = 39$) ($p > 0.05$). These values were significantly lower than that of the TBT-treated males (4.94 ± 0.12 mm) ($n = 39$) ($p < 0.05$).

In all TBT concentration treatments, imposex females started to develop their penis in the 2nd – 3rd month (except that of the 1 ng TBT as Sn/L in which the penis was not formed) (Fig. 12). Comparing the mean female penis length (FPL) between the TBT concentrations, the results showed that almost all the FPL values for the 10, 50 and 100 ng TBT as Sn/L were below 4.00 mm and ranged from

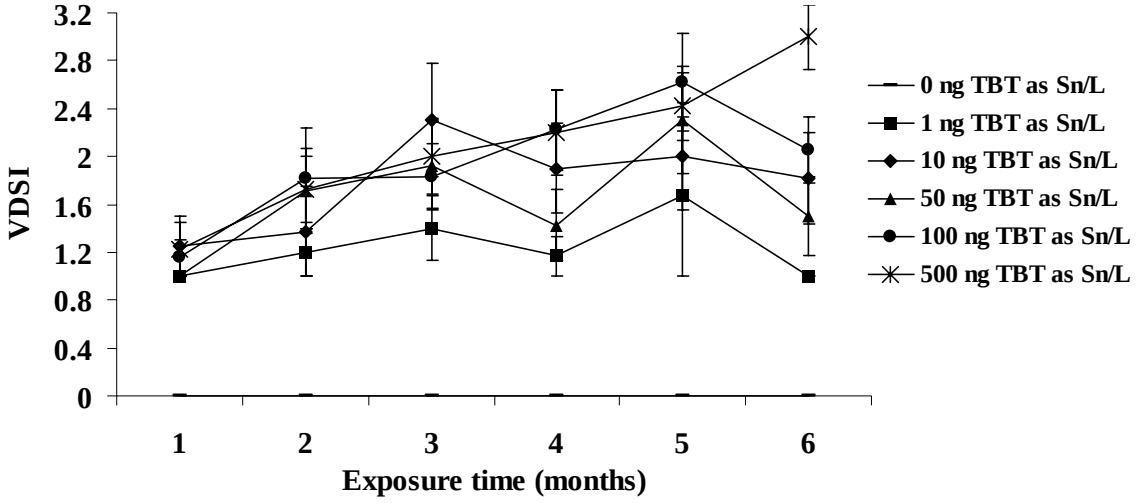

Figure 10. The vas deferens sequence index (VDSI) (mean ± S.E.) in female *B. areolata* during the 6 months of exposure to different nominal TBT concentrations.

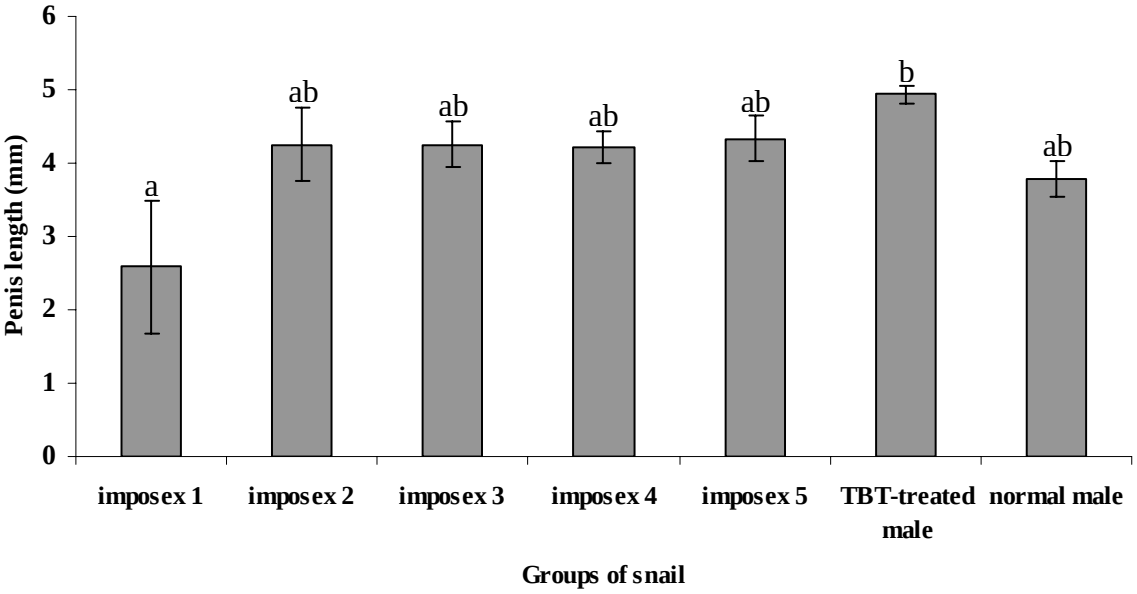

Figure 11. The penis length (mean ± S.E.) between groups of *B. areolata*, including imposex females (stages 1 to 5), TBT-treated males, and normal males during TBT-exposure experiment. Bars not sharing the same superscript are significantly different (one-way ANOVA, $p < 0.05$)

1.67 - 3.75, 2.67 – 4.06 and 2.17 - 4.13 mm, respectively. These were lower than those of the mean male penis length (MPL) in which almost all values were above 4.00 mm with the maximum value of 6.42 mm (Fig. 13). The FPL values for imposex females at a concentration of 500 ng TBT as Sn/L, were higher than 4.00 mm and ranged from 4.22 mm (2^{nd} month) – 6.05 mm (3^{rd} month). These were significantly higher ($P < 0.05$) than those found at all lower concentrations during the same period of exposure (Fig. 12); this was the only concentration that could result in the closure of the FPL to the MPL. Furthermore, this experiment found two interesting morphological malformations. The first one was observed in an imposex female in stage 4 which exhibited a double penis (Fig. 14A), while the second one was an excrescence on the vas deferens in a TBT-treated male (Fig. 14B).

2.2.5 Relative penis size index (RPSI)

At concentrations of 10, 50 and 100 ng TBT as Sn/L, most RPSI values were below 60 with a wide range from 4.35 – 55.89, 12.22 – 49.34, and 9.49 – 58.55, respectively (Fig. 15). In contrast, all RPSI values at the highest concentration (500 ng TBT as Sn/L) were above 60 with a minimum value in the 6^{th} month (64.11) and higher than that of all other TBT concentrations during all the exposure times. RPSI values of 234.76 and 128.31, were also found after 3 and 4 months exposure to the concentration of 500 ng TBT as Sn/L.

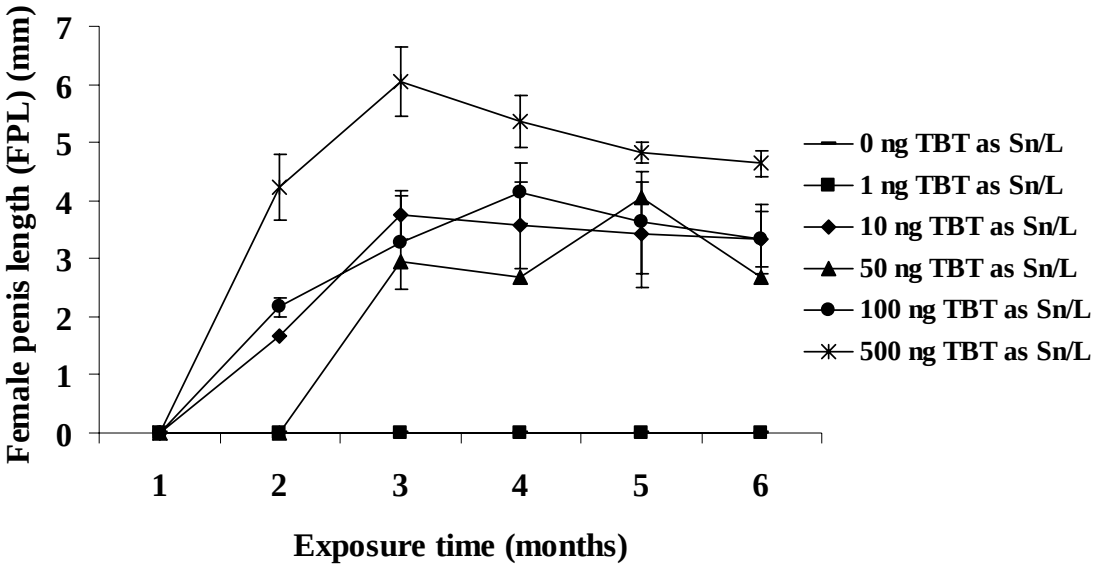

Figure 12. The female penis length (FPL) (mean ± S.E.) in female *B. areolata* during the 6 months of exposure to different nominal TBT concentrations.

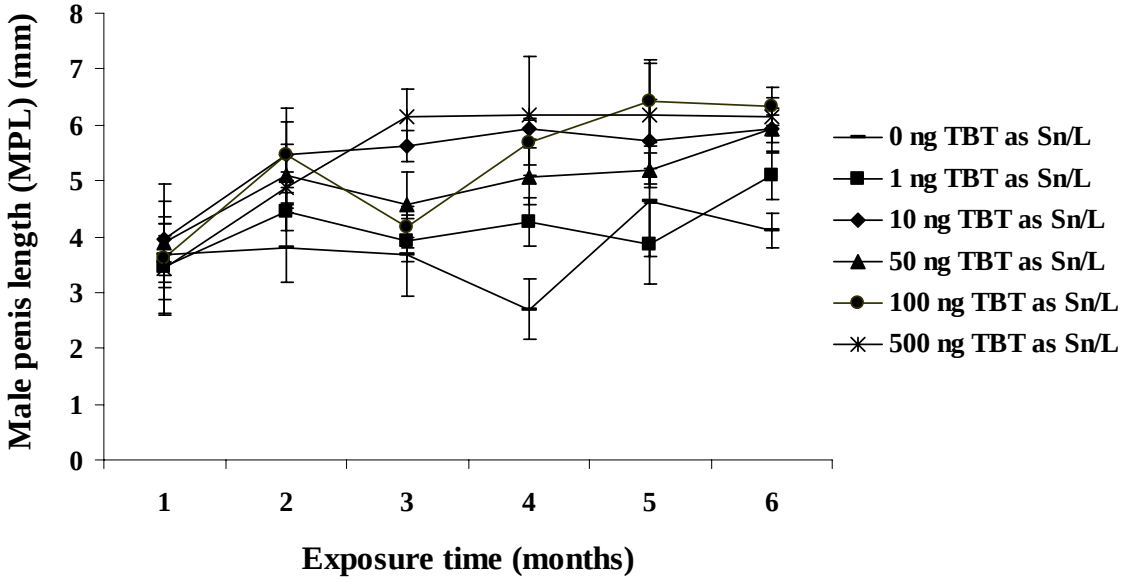

Figure 13. The male penis length (MPL) (mean ± S.E.) in the normal male from the control (0 ng TBT as Sn/L) and TBT-treated male from the exposure groups in *B. areolata* during the 6 months of exposure to different nominal TBT concentrations.

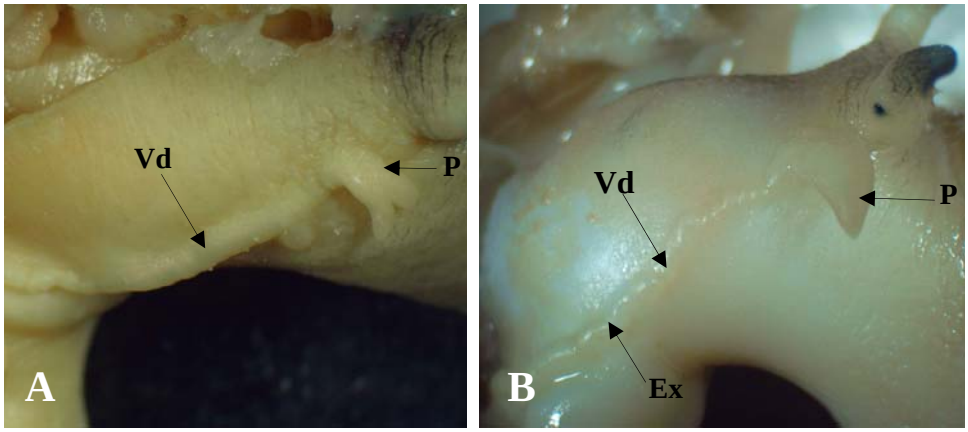

Figure 14. Malformations in imposex female *B. areolata*. **A**: A double penis in the imposex female in stage 4. **B**: The excrescence on the vas deferens in the TBT-treated male. Ex-excrescence; P-penis; Vd-vas deferens.

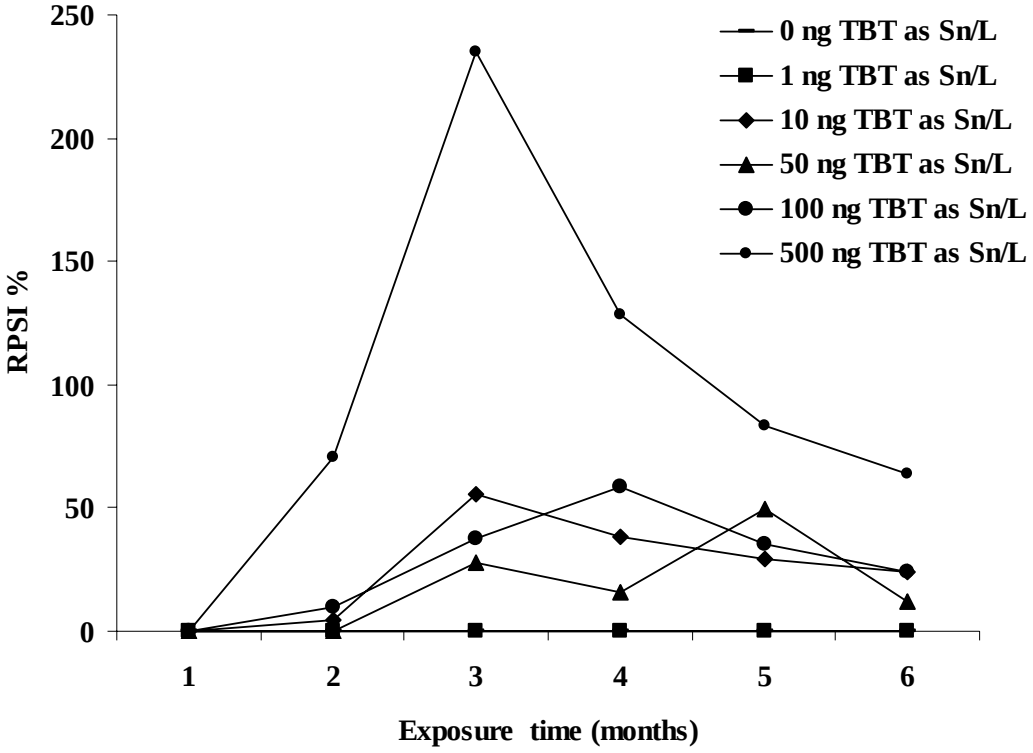

Figure 15. The relative penis size index (RPSI) (%) in female *B. areolata* during the 6 months of exposure to different nominal TBT concentrations.

3. Gametogenesis in TBT-exposed *B. areolata*

3.1 Spermatogenesis in TBT-treated male *B. areolata*

3.1.1 Histological investigation

Testis of the normal male *B. areolata* was located in the visceral coil and attached to the digestive gland. From a total of 30 individuals of TBT-treated males analyzed, it was obvious that their testes had similar histological structures to those of the untreated males (n = 30). In both groups of snails, the testes were surrounded by a layer of loose connective tissue at their outermost position and had a many seminiferous tubules (Fig. 16A-B) where spermatogenesis occurred. Male reproductive cells were categorized into four developmental stages: spermatogonia, spermatocytes, spermatids, and spermatozoa. The spermatogonia were located in the basal compartment of the seminiferous tubules and were oval cells having nuclei with small granules that stained with hematoxylin; the nuclei also had a few nucleoli that were stained by eosin (Fig. 16C). In the first phase (spermatocytogenesis) of spermatogenesis, spermatogonia underwent mitotic division to form more spermatogonia as well as primary spermatocytes. The round primary spermatocytes were the largest cells of the seminiferous tubules and had nuclei with granules that stained intensively with hematoxylin; the shape of the nucleus varied (Fig. 16D). In the second phase (meiosis) of spermatogenesis, primary spermatocytes entered the first meiotic division to form secondary spermatocytes that were relatively small and underwent a second meiotic division to form the haploid cells known as spermatids. The spermatids were crescent-shaped cells whose nuclei were located at one pole of the cells and stained intensively with hematoxylin; the shape of some spermatids resembled an oval or rod, with a reduced volume of cytoplasm (Fig. 16E). In the last phase (spermiogenesis) of spermatogenesis, spermatids discarded much of their cytoplasm, rearranged their organelles, and formed a flagellum to become transformed into spermatozoa. The spermatozoa were thread shaped cells, that stained intensively with hematoxylin (Fig. 16F).

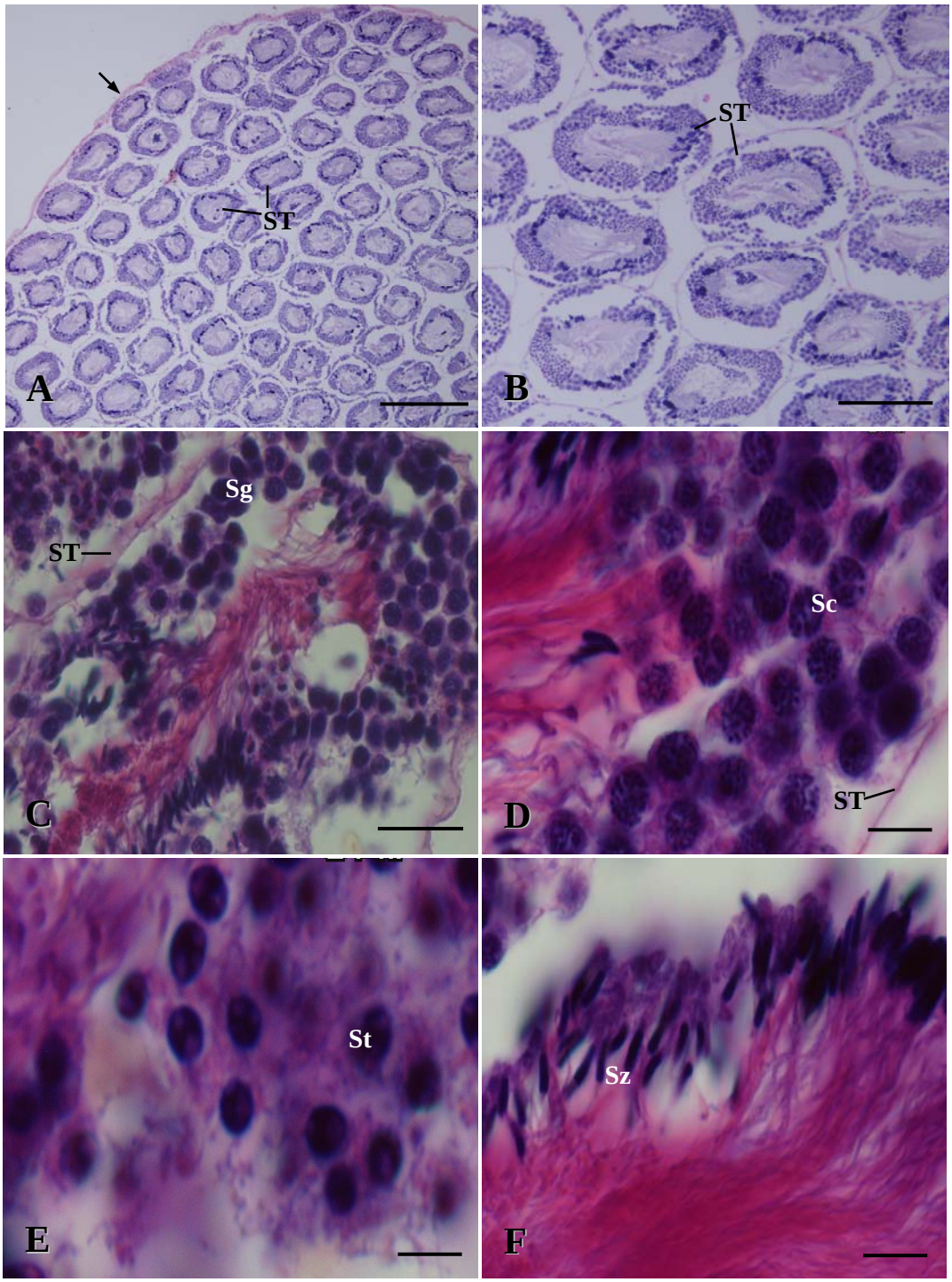

Figure 16. Reproductive cells in the testes of *B. areolata* (H&E). **A-B**: Testicular sections of normal males showing seminiferous tubules (ST). Note. A layer of loose connective tissue (arrow). **C-F**: Testicular sections of the TBT-treated males with spermatogonia (Sg) (C), spermatocytes (Sc) (D), spermatid (St) (E) and spermatozoa (Sz) (F). Scale bars = 6 µm (D-F), 20 µm (C), 100 µm (B) and 250 µm (A).

3.3.2 Ultrastructural investigation

The TEM study clearly showed that TBT-treated male *B. areolata* had a mostly identical ultrastructure of spermatogenesis to that of an untreated male from the control group. Their testes showed various stages of germ cells during spermatogenesis. Spermatogonia, spermatocytes, spermatids (spermiogenesis) and mature spermatozoa are described at the ultrastructural level as follows:

Spermatogonia*:* Spermatogonia lying within the epithelium of the seminiferous tubules of the testis. These cells were spherical or oval with a diameter of approximately 7.5 µm. The large nucleus (6 µm in diameter) was round or slightly oval and contained only one prominent nucleolus (0.7 µm in diameter). Small clumps of electron-dense euchromatin were loosely distributed throughout a transparent nucleoplasm (Fig. 17A). The narrow rim of cytoplasm contained a few small mitochondria, and a Golgi body.

Primary spermatocytes: Four stages of the primary spermatocytes were observed in *B. areolata* including leptotene, zygotene, pachytene, and diplotene. (1) Leptotene spermatocytes were round, approximately 8.7 µm in diameter. The chromatin, which had started to condense into small blocks of heterochromatin, was scattered evenly throughout the nucleoplasm. The spherical nucleus (6.3 µm in diameter) had a nucleolus (0.7 µm in diameter) but not as prominent as that of the spermatogonium. The cytoplasm exhibited a few mitochondria and a Golgi body (Fig. 17B). (2) Zygotene spermatocytes were oval, approximately 8.3 µm in diameter. The round nucleus (6.0 µm in diameter) had no nucleolus in the nucleoplasm. The heterochromatin blocks were denser than those of the leptotene spermatocytes. The cytoplasm contained numerous mitochondria identified mainly at one cell pole (Fig. 17C). (3) Pachytene spermatocytes were round to oval, approximately 8.0 µm in diameter. The nucleus (6.3 µm in diameter) was irregular in shape. The heterochromatin appeared as long threads and thick fibres that were entwined into a bouquet pattern, and were obvious throughout the nucleoplasm. The cytoplasm contained a few mitochondria (Fig. 17D). (4) Diplotene spermatocytes had an irregular shape approximately 8.0 in diameter. The nucleus (4.7 µm in diameter) was oval to irregular in shape. Their heterochromatin had begun to condense into dark

blocks, with intervening light areas of nucleoplasm. The cytoplasm contained a few mitochondria, a Golgi body, and a proacrosomal vesicle (Fig. 17E).

Secondary spermatocytes: These cells (6.4 µm in diameter) were round and smaller than the primary spermatocytes. Their nuclei (2.8 µm in diameter) were irregular in shape. The secondary spermatocytes had thick chromatin blocks composed of criss-crossing fibres, which appeared as reticulate chromatin. A few mitochondria and a Golgi body were visible in the cytoplasm (Fig. 17F).

Spermatids: During spermiogenesis, the spermatids underwent differentiation to become mature spermatozoa. The following major steps then took place: nucleus condensation, acrosome formation, and development of a midpiece and axonemal complex. These phenomena are described as follows:

Nucleus condensation: The early spermatids (5.4 µm in diameter) were irregular in shape and smaller than the spermatocytes. These cells had a spherical to an irregular, eccentric nucleus (2 µm in diameter) with no apparent nucleolus (Fig. 18A). At the beginning, their heterochromatin that appeared as homogenous distributed granules, were found as heterogeneous aggregations in the granular nucleoplasm and later progressively accumulated electron-dense chromatin. In the granular cytoplasm were a few ribosomes, a Golgi body surrounded by vesicles, some large mitochondria, and a rough endoplasmic reticulum. Another remarkable feature of the early spermatid prior to spermiogenesis was a movement of the large mitochondria, developed by fusion of the smaller ones, to the presumptive posterior pole of the nucleus (Fig. 18A). The early spermatids were connected by intercellular bridges. As spermiogenesis proceeded, the granular nuclear chromatin became condensed at the periphery of the nucleus, forming a thick layer beneath the nuclear envelope (Fig. 18B-C). They then began to accumulate at the posterior nuclear pole (Fig. 18D-F). The nucleus began to expand laterally; it was now transformed from a dispersed state to a fibrous phase with a parallel fibrillar appearance of the chromatin (Fig. 19A). During the middle stage of development of the spermatid the nuclear chromatin formed thick fibrillar threads, that became elongated and were oriented longitudinally along the nuclear vertical axis (Fig. 19B, D). The posterior nuclear pole was marked by the attachment of large spherical mitochondria and a deep invagination, the implantation fossa, with the axoneme insertion (Fig. 19A, B, D).

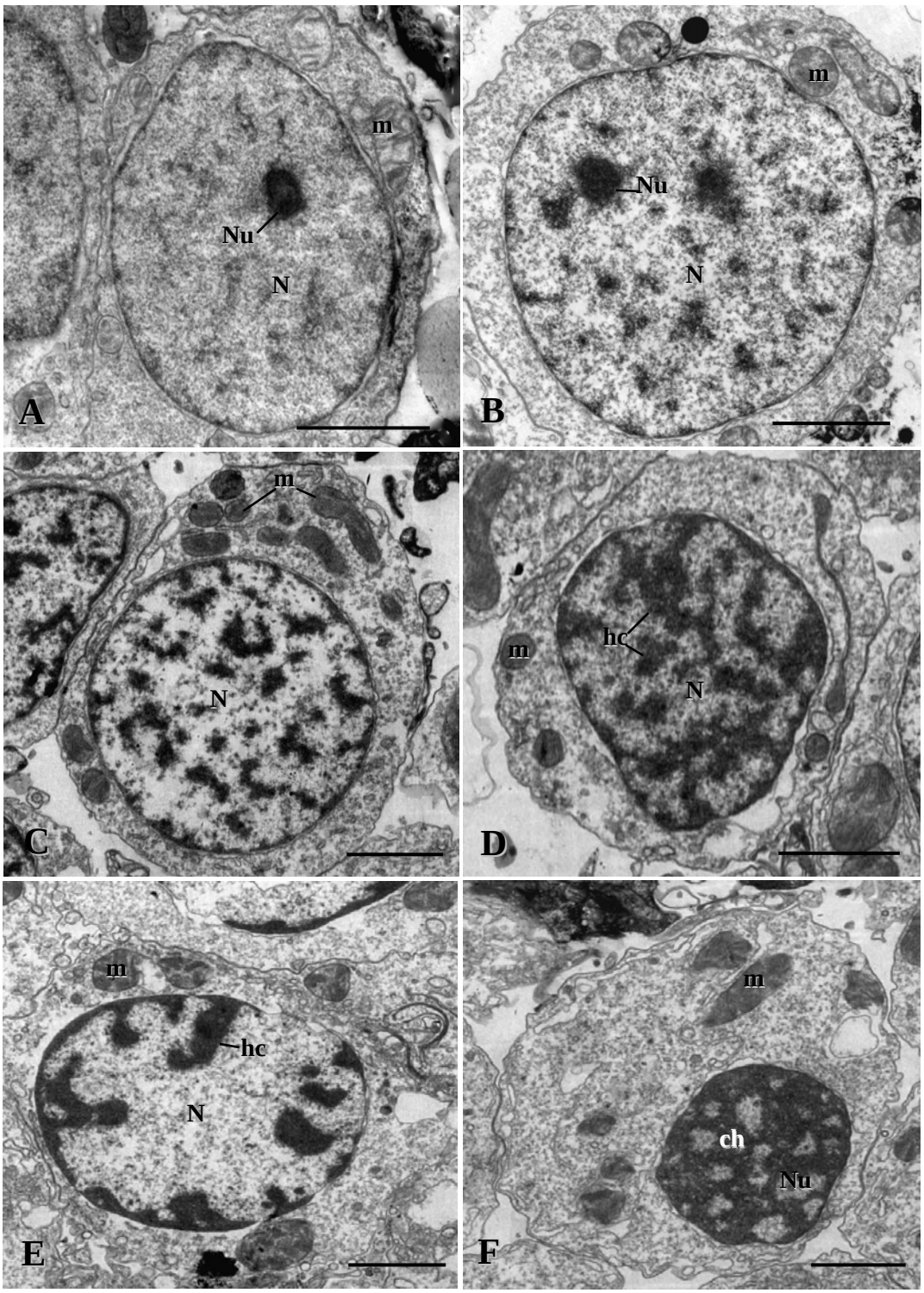

Figure 17. TEMs of various stages of the male germ cells in TBT-treated male *B. areolata*. **A**: Spermatogonia. **B**: Leptotene spermatocyte. **C**: Zygotene spermatocyte. **D**: Pachytene spermatocyte. **E**: Diplotene spermatocyte. **F**: Secondary spermatocyte. ch-chromatin; hc-heterochromatin; m-mitochondria; N-nucleus; Nu-nucleolus. Scale bars = 2 μm in all.

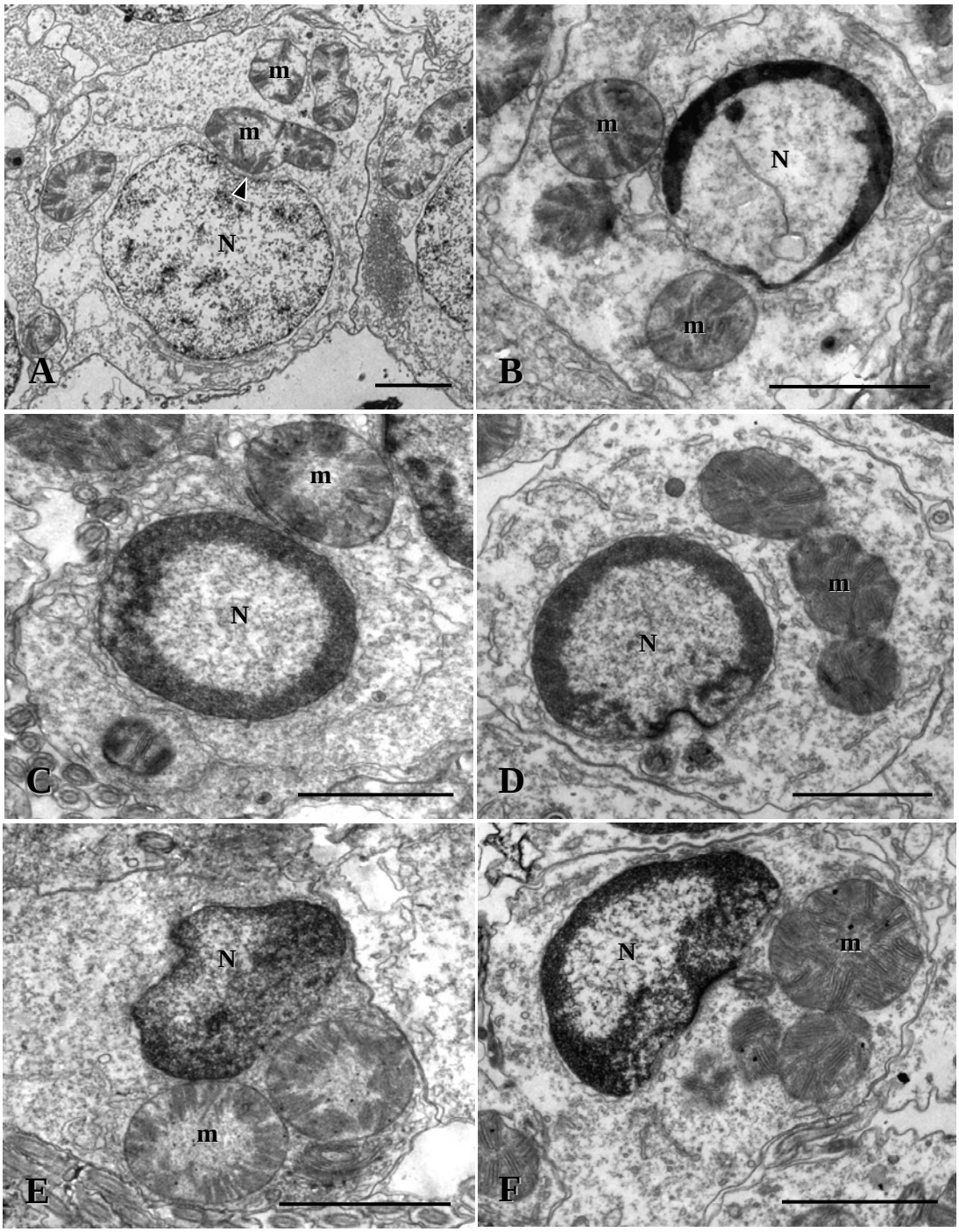

Figure 18. TEMs of early phase of nuclear condensation of spermatids in TBT-treated male *B. areolata*. **A**: Early spermatid showing the gathering enlarged mitochondria at the nuclear base (arrowhead). **B-C**: Spermatids showing beginning of chromatin condensation. **D-F**: Spermatids showing nucleus with the accumulation of granular chromatin and attachment of mitochondrial spheres. m-mitochondria; N-nucleus. Scale bars = 2 µm in all.

At the next step, the chromatin fibrils thickened to form lamellae (Fig. 19C, E). During further development the nucleus lengthened and the nuclear lamellae continued to become thicker, leaving only a few spaces between them (Fig. 19F). Extending posteriorly from the base of the nucleus was the growing axoneme. At the late stage of the spermatid, the nuclear chromatin continued to condense and the nucleus appeared homogeneous and electron dense (Fig. 19G).

Acrosome formation: In the earliest stage of acrosomal development, the Golgi body secreted numerous vesicles of varying density, some of which fused to form a proacrosomal vesicle which was visible in the cytoplasm of the early spermatid (Fig. 20A). As the proacrosomal vesicle enlarged and elongated, electron-dense material (granule) developed on its extracelluar side (Fig. 20B). The proacrosomal vesicle then differentiates to the pre-attachment acrosome which was surrounded by microtubules oriented longitudinally. This acrosome had an inner supporting structure parallel to its wall as well as an electron-dense granule in its center (Fig. 20C). The vesicle developed into the hollow acrosomal cone with the electron-dense granule fixed to its base (Fig. 20D). While the Golgi body remained basal, the maturing pre-attachment acrosome migrated along the plasma membrane to the apex of the condensing nucleus (fibrous phase), then it tilted and moved into a vertical position (Fig. 21A). At the next step, the large electron-dense granule, which was separated from the base of the acrosome cone and attached to the depression in the nuclear apex, flattened to form a basal plate (Fig. 21B). At the center of this plate, an acrosomal rod was developed (Fig. 21C). The basal plate with the acrosomal cone placed upon was set in the apical depression of the lamella phase of the nucleus (Fig. 26D-E). While the body of the acrosome underwent pronounced elongation, the acrosomal rod extended more into the subacrosomal space (Fig. 21E). In the semimature to mature sperm, the acrosomal rod was half of the acrosome's length (Fig. 21F).

Development of midpiece and axonemal complex: The development of the midpiece was closely associated with mitochondria and centrioles. In the early spermatid some mitochondria were distributed throughout the cytoplasm. They then began to aggregate at the developing posterior pole of the condensing nucleus (Fig. 18A). As the nuclear chromatin condensed, the mitochondria fused to form a ring of

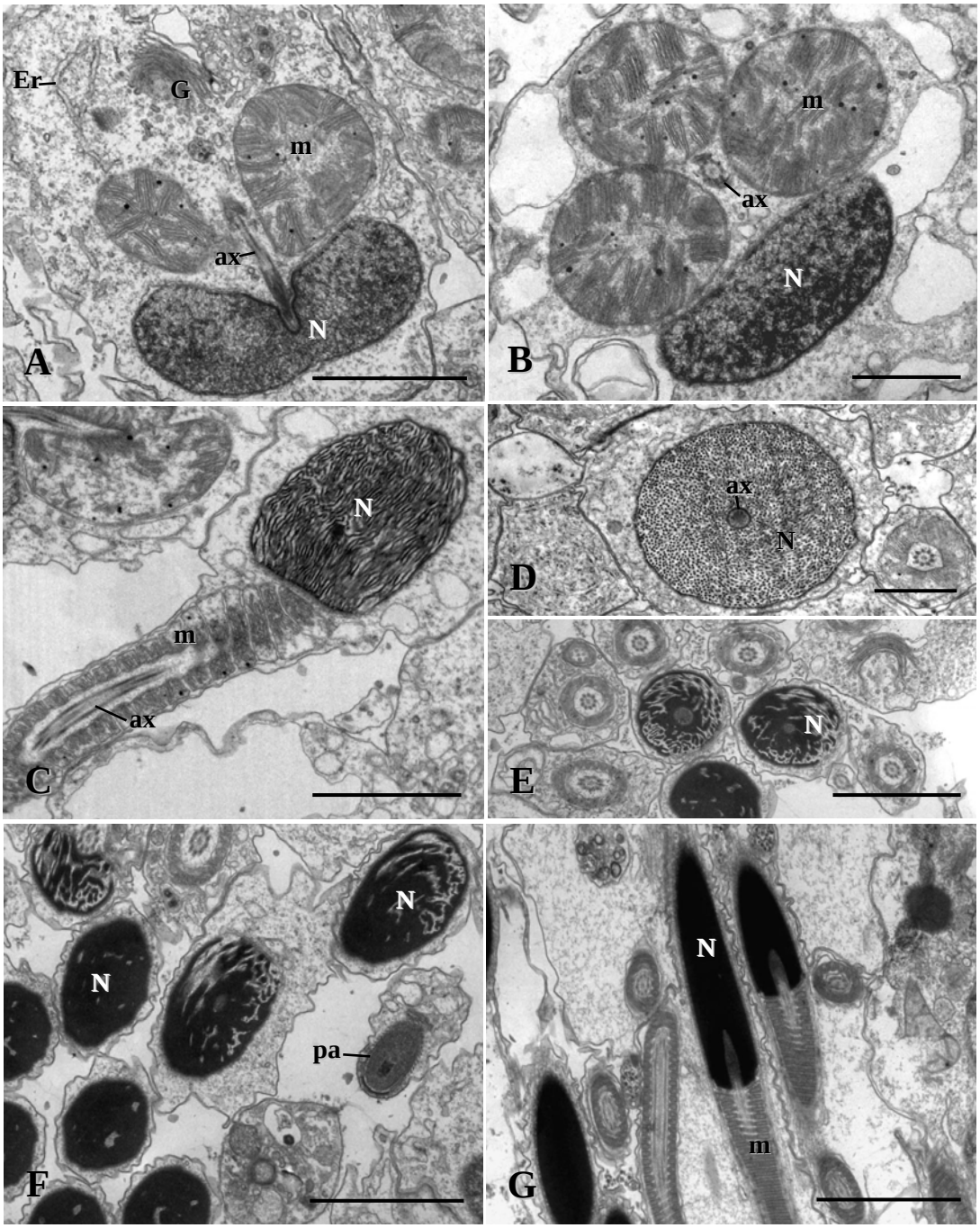

Figure 19. TEMs of late phase of nuclear condensation of spermatids in TBT-treated male *B. areolata*. **A**: Spermatid with the antero-posteriorly compressed nucleus and enlarged mitochondria. **B**: Transverse section (TS) of spermatid showing ring of three spherical mitochondria. **C**: Longitudinal section (LS) of spermatid with nucleus in the lamellar phase. **D**: TS of fibrillar nucleus of spermatid. **E**: TS of lamellar nucleus of spermatid. **F**: Spermatids showing nucleus with thick chromatin lamellae. **G**: LS of spermatid showing nucleus with homogenous and electron-dense chromatin. ax-axoneme; Er-rough endoplasmic reticulum; G-Golgi body; m-mitochondria; N-nucleus; pa-proacrosome. Scale bars = 1 µm (B, D) and 2 µm (A, C, E-G).

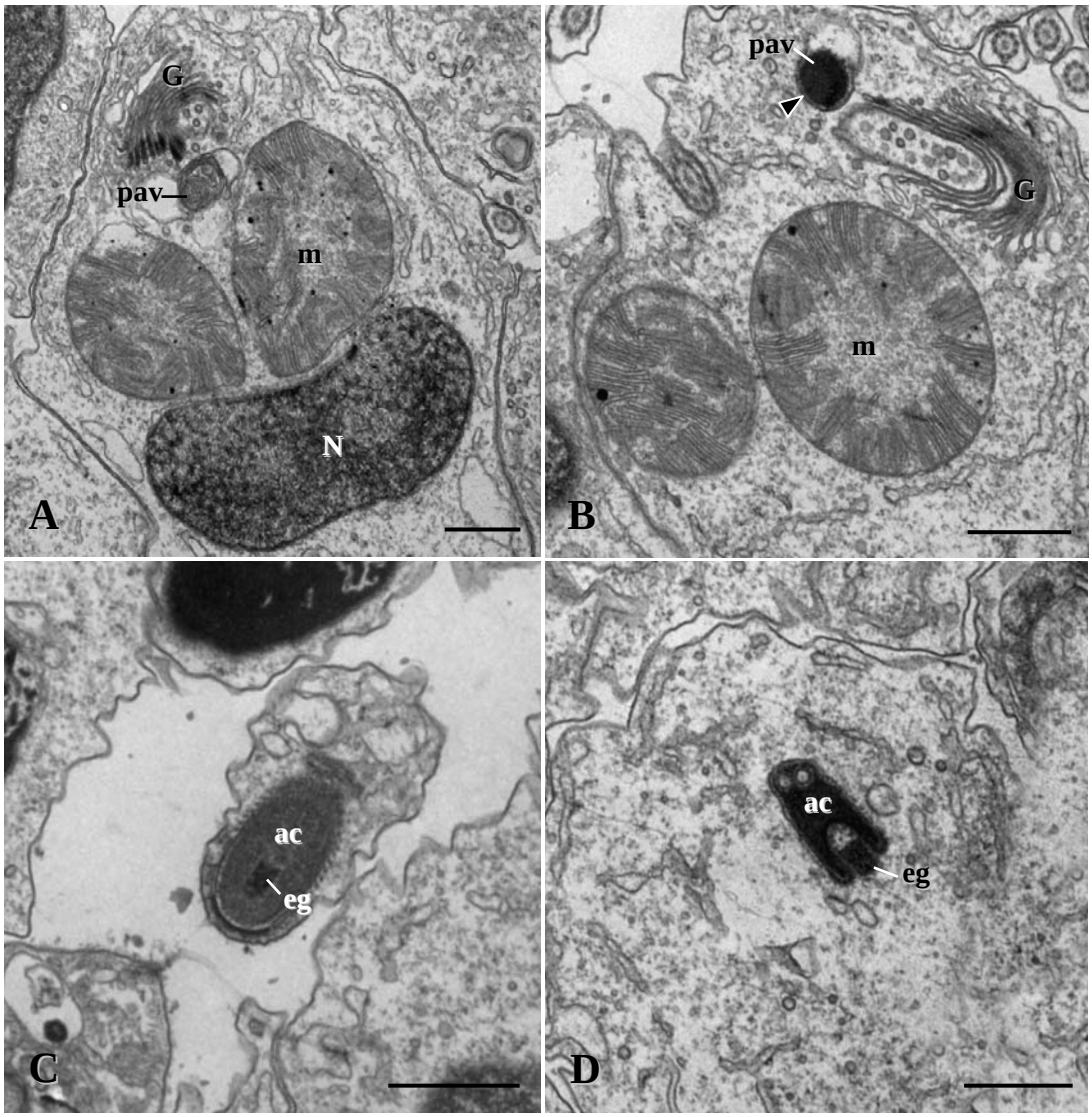

Figure 20. TEMs of early phase of acrosome formation in TBT-treated male *B. areolata*. **A**: Spermatid showing large Golgi body in close association with proacrosomal vesicle. **B**: Enlarged proacrosomal vesicle with electron-dense material on its outermost (arrowhead). **C**: Details of proacrosome. **D**: Longitudinal section showing the acrosome cone with electron-dense granule. ac-acrosome; eg-electron-dense granule; G-Golgi body; m-mitochondria; N-nucleus; pav-proacrosomal vesicle. Scale bars = 0.8 μm in all.

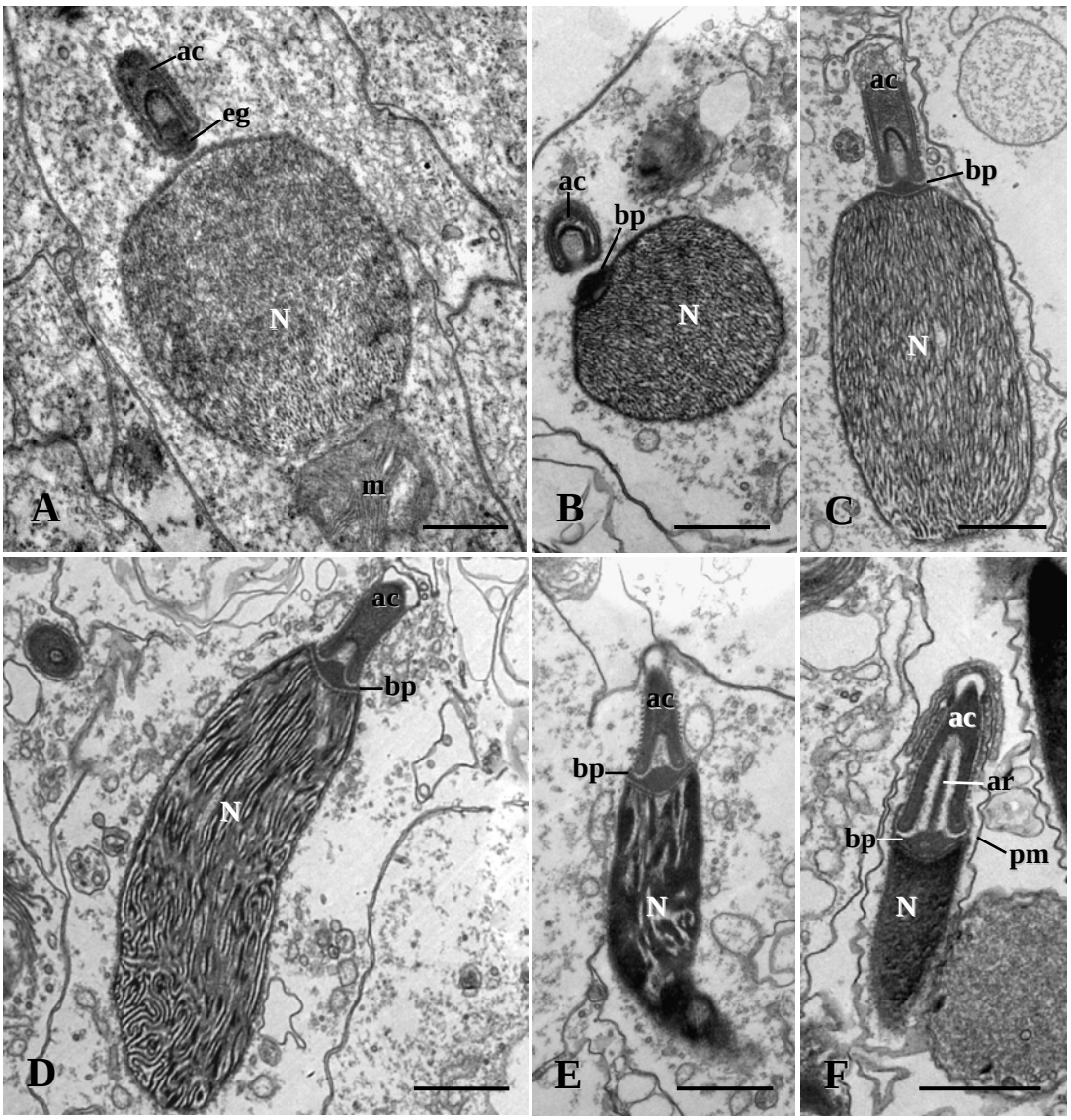

Figure 21. TEMs of late phase of acrosome formation in TBT-treated male *B. areolata*. **A**: Longitudinal section (LS) through the pre-attachment acrosome in the vertical position. **B**: Acrosome attached to the nucleus of the spermatid. **C**: Basal plate of acrosome attached to the nuclear apex. **D-E**: LS through elongated acrosome. **F**: Premature acrosome of euspermatozoon. ac-acrosome; ar-axial rod; bp-basal plate; eg-electron-dense granule; m-mitochondria; N-nucleus; pm-plasma membrane. Scale bars = 0.8 μm (A) and 1 μm (B-F).

four large, spherical mitochondria enclosing the axoneme (Fig. 19A-B). These mitochondria clustered around the proximal region of the axoneme which was associated with a single short centriole that inserted into the implantation fossa at the posterior invagination of the nucleus (Fig. 19A). For further development, the flagellum lengthened at the same time as the anterior-posterior axis of the lamellar nucleus and the four giant mitochondria elongated and finally formed helically four mature midpiece elements surrounding the axoneme (Fig. 19C).

***Mature euspermatozoa*:** All TBT-treated-and untreated male *B. areolata* examined, by light-and transmission electron microscope, contained only fertile spermatozoa or euspermatozoa which were composed of an anterior acrosomal complex followed in the anterior–posterior sequence by a rod-shaped nucleus, an elongated midpiece, a glycogen piece and an end piece. The following description outlines the fine structure of each of these euspermatozoa features.

Acrosomal complex: The anterior acrosomal complex consisted of a tall-conical acrosomal cone or vesicle, an axial rod and a basal plate (Fig. 22A-C). The acrosomal vesicle was membrane-bound, approximately 1.62 µm long, strongly compressed laterally, and its contents were moderately electron-dense. At the anterior extremity of the acrosome, the acrosomal vesicle membrane expanded away from the vesicle contents and lay close to the plasma membrane to form an electron-lucent, balloon-like space, the apical bleb. Basally, the acrosomal vesicle was surrounded by a short accessory membrane (Fig. 22B-C). The acrosomal vesicle exhibited a deep, narrow basal invagination about 0.8 µm long which was constricted anteriorly, and suited the axial rod (subacrosomal material), resting on a centrally perforate, thin basal plate that was positioned on the nuclear apex, and separated from the basal rim of the acrosomal vesicle by a subacrosomal space (Fig. 22C).

Nucleus: The eusperm nucleus is filiform (lancet or rod-shaped), 7.3 µm long, and composed of homogenous, highly electron-dense material (Fig. 22A). It exhibited a short basal invagination (0.8 µm long) that housed a centriolar derivative (modified distal centriole), and was continuous with the initial portion of a 9 + 2 microtubular pattern axoneme (Fig. 22D-E). Posteriorly the nucleus was slightly compressed laterally, giving an oval shaped transverse profile (Fig. 22H).

Midpiece: Posterior to the nucleus, the axoneme (exhibiting the typical microtubular pattern 9 + 2) was enclosed in a continuous mitochondrial sheath to form, collectively, the midpiece region of the euspermatozoon. In oblique longitudinal sections, the sheath consisted of 3-6 helically arranged, elongated mitochondrial elements around the axoneme and it was apparent that each element exhibited a, U-shaped, bilaminar, outer layer that was notably more electron-dense than the rest of the mitochondrial material. (Fig. 22D-E). In addition, each mitochondrion had a square profile in transverse section (Fig. 22G, H).

Annular complex and glycogen piece: Immediately following termination of the midpiece, the axoneme became enclosed by nine longitudinally continuous tracts of electron-dense granules and the plasma membrane to form the glycogen piece (Fig. 22F-I). In transverse sections each tract of granules was associated with each axonemal doublet, with the exception of the central pair (Fig. 22G-I).The midpiece was separated from the glycogen piece by a junction, called an annular complex, consisting of a circular, highly electron-dense band or a double ring attached to the inside of the plasma membrane (Fig. 22F).

End piece: A short end piece lacking glycogen was continuous with the glycogen piece and consisted of the continuing 9 + 2 microtubular pattern axoneme surrounded only by the plasma membrane (Fig. 22I).

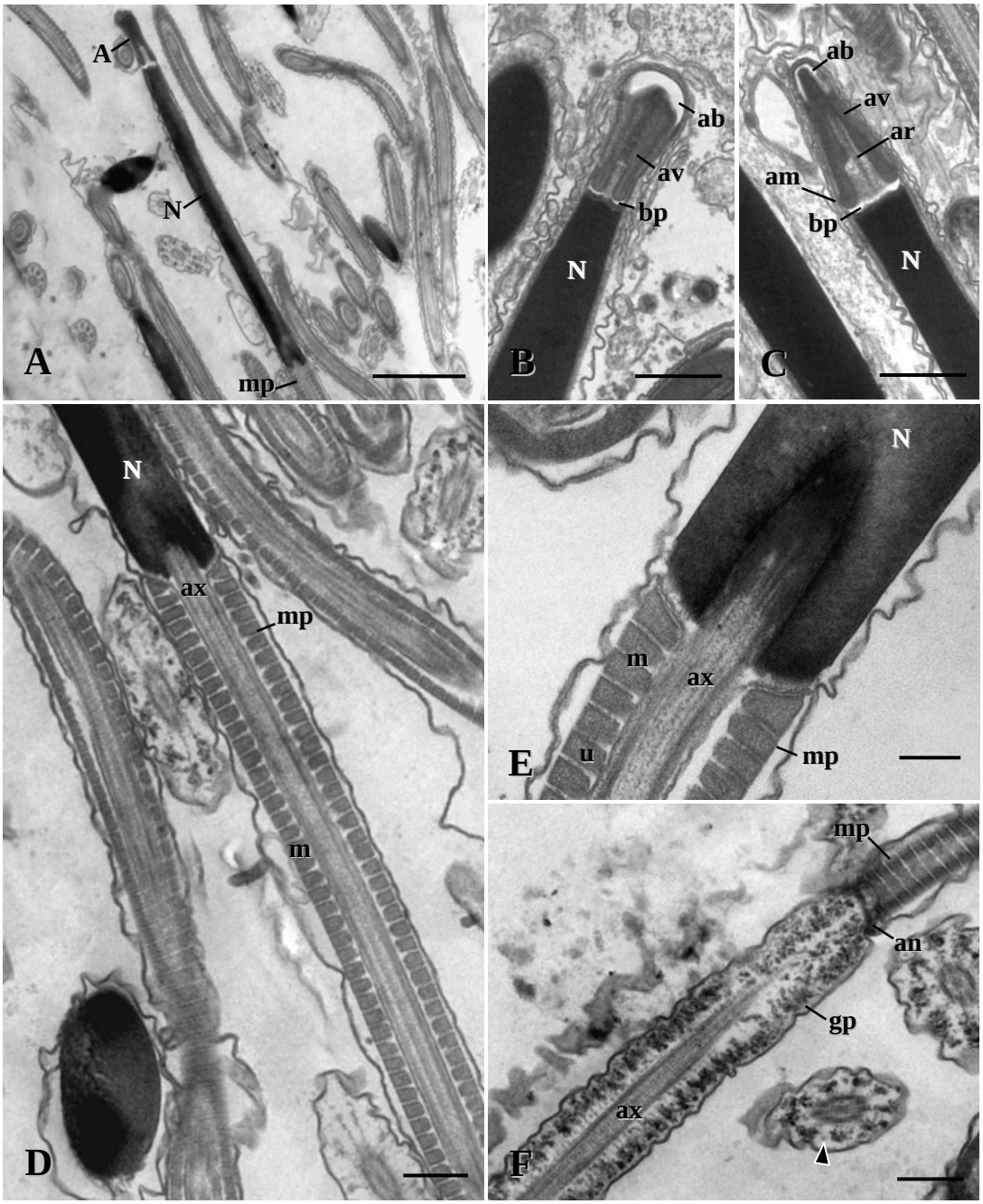

Figure 22. TEMs of mature euspermatozoa of TBT-treated male *B. areolata*. **A**: Longitudinal section (LS) through acrosomal complex, nucleus and anterior extremity of midpiece. **B-C**: LS through acrosomal complex and anterior portion of nucleus. **D-E**: LS through nucleus (showing basal invagination and centriole/axoneme insertion) - midpiece junction. **F**: LS through midpiece-glycogen piece junction. Note transverse section (TS) of glycogen piece (arrowhead). **G-I**: TS through nucleus, midpiece, glycogen piece and end piece. A-acrosomal complex; ab-apical bleb; am-accessory membrane; an-annulus; ar-axial rod; av-acrosomal vescicle; ax-axoneme; bp-basal plate; ep-end piece; gp-glycogen piece; m-mitochondria; mp-midpiece; N-nucleus; u-U-shaped defining edge of mitochondrial element. Scale bars = 0.2 µm (E, I), 0.4 µm (D, F, H), 0.8 µm (B, C), 1 µm (G) and 2 µm (A).

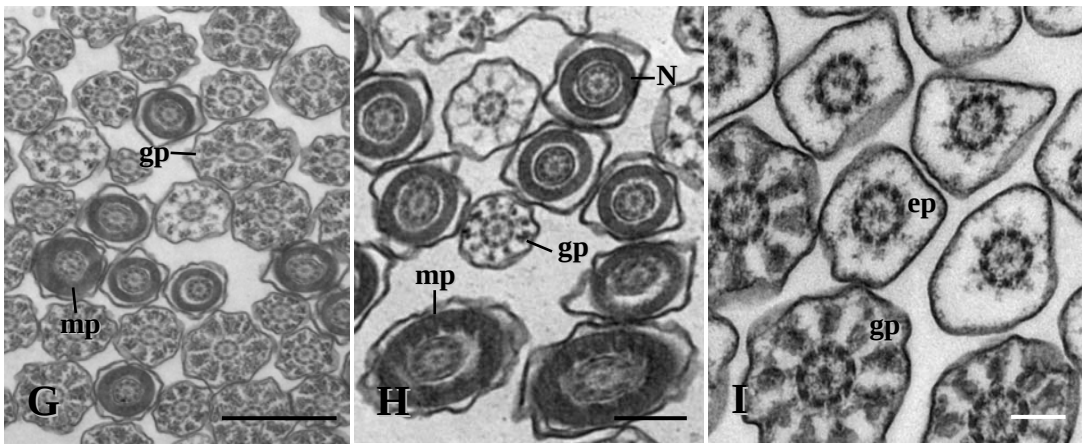

Figure 22. (Continuted).

3.2 Oogenesis in imposex female *B. areolata*

3.2.1 Histological investigation

The tubular ovary of normal female *B. areolata* was located in the visceral mass and attached to the digestive gland. Based on the light microscopic observation, the entire ovary was covered by a loose connective tissue at its outermost position and contained many ovarian follicles where germ cells were being developed (Fig. 23A). These female reproductive cells were categorized according to five developmental stages: oogonium, primary oocyte, first yolk globule-accumulating oocyte, second yolk globule-accumulating oocyte, and mature oocyte. An oogonium was an oval cell having a round nucleus with small granules that stained by hematoxylin and a less stained cytoplasm; a few nucleoli stained by eosin were visible in the nucleoplasm (Fig. 23B). A primary oocyte was larger than the oogonium, and its shape was variable, ranging from no nucleolus to a large, oval nucleolus intensively stained by eosin (Fig. 23C). In the first two stages of development, no yolk globule-accumulation was observed. A first yolk globule-accumulating oocyte was larger than the primary oocytes and its nucleus had an irregular outline and a prominent nucleolus. In this stage, a few yolk globules stained by eosin were present in the cytoplasm (Fig. 23D). A second yolk globule-accumulating oocyte was larger than the first yolk globule-accumulating oocyte and had several yolk globules observed in the cytoplasm. The edge of the second yolk globule-accumulating oocyte was adjacent to the epithelium of the ovarian follicles (Fig. 23E). A matured oocyte was a large oval cell with plentiful yolk globules and was separating from the epithelium of the ovarian lobule; its nucleus was intensively stained by hematoxylin (Fig. 23F).

In this study, 30 ovaries from each of these imposex stages (1-4) and 10 ovaries from the imposex stage 5 were histologically analyzed and compared to those of the normal females (30 ovaries). The results clearly showed that the ovaries of all the stages of imposex and normal females were similar in tissue structure. As indicated in Fig. 24, ovarian tissues taken from the spawning stage of the normal female (Fig. 24A) and imposex stages 1, 3 and 5 (Fig. 24B-D) showed normal oogenesis with well developed pre-and post-vitellogenic oocytes. In addition, the

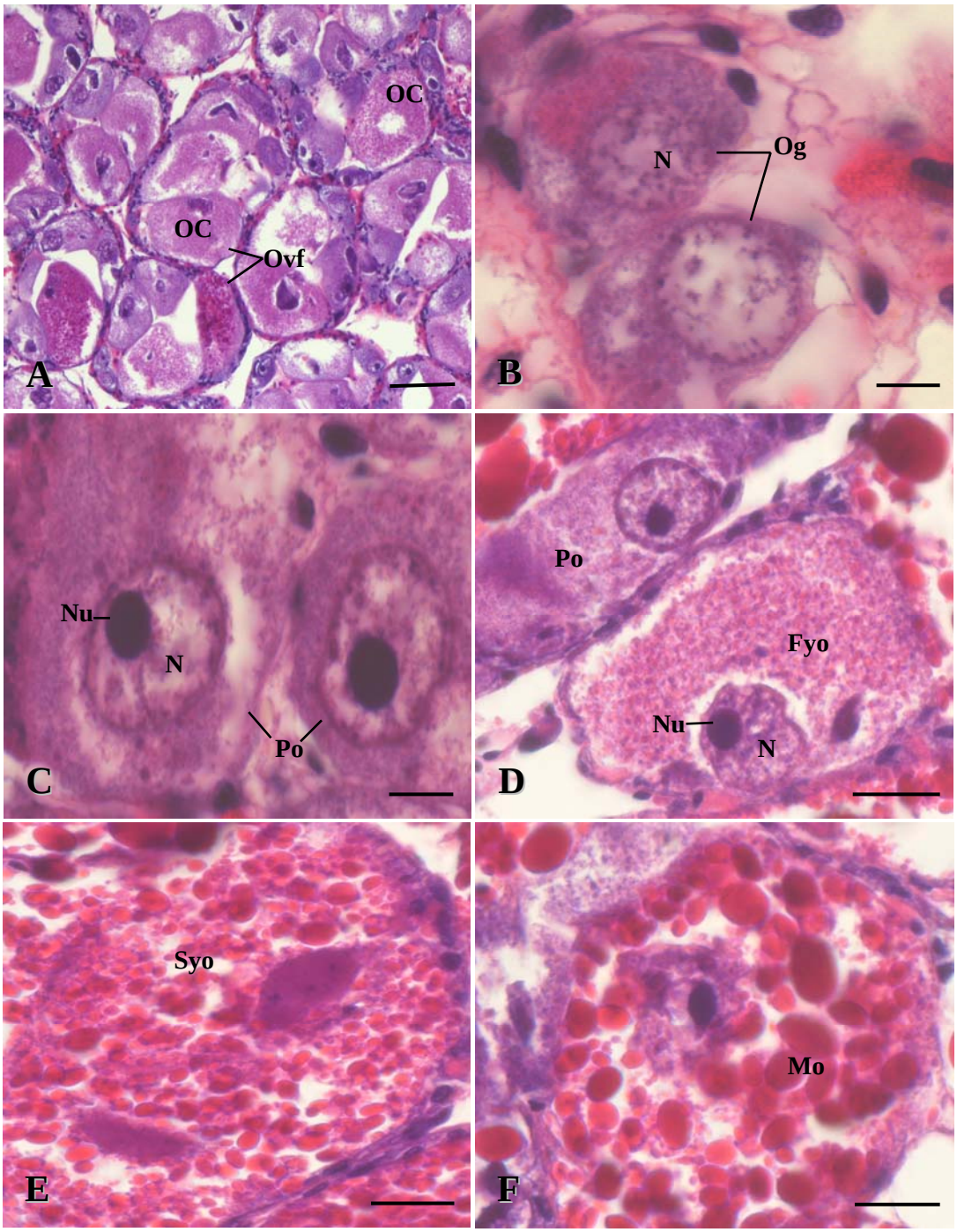

Figure 23. Reproductive cells in the ovaries of normal female *B. areolata* (H&E). **A**: Ovary in the mature stage showing various stages of germ cells developed in the ovarian follicles (Ovf). **B**: Oogonium (Og). **C**: Primary oocyte (Po). **D**: First yolk globule-accumulating oocyte (Fyo). **E**: Second yolk globule-accumulating oocyte (Syo). **F**: Mature oocyte (Mo). N-nucleus; Nu-nucleolus; OC-oocyte; Ovf-ovarian follicles. Scale bars = 6 µm (B, C), 20 µm (D, E, F) and 60 µm (A).

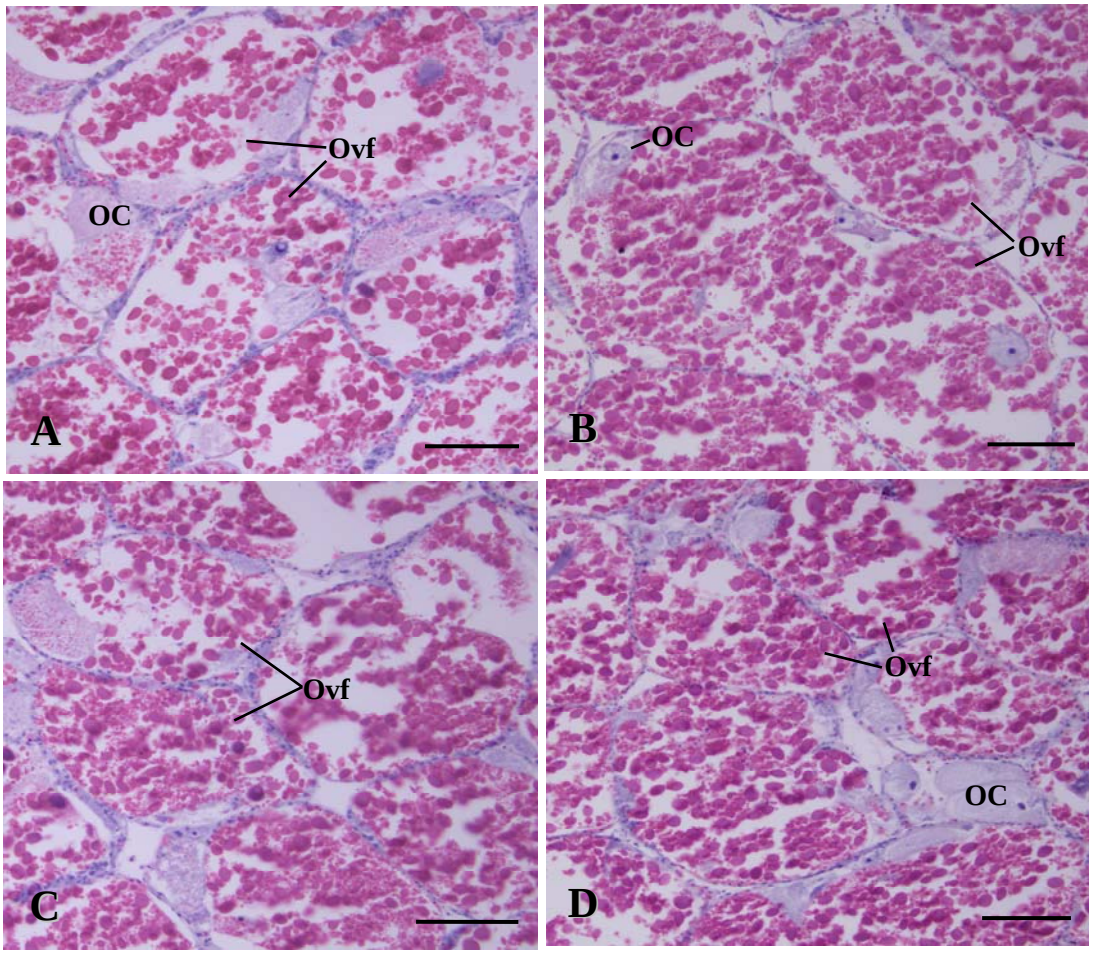

Figure 24. Histological comparisons of the ovarian tissue of normal and imposex females of *B. areolata* (H&E). **A**: Normal female. **B**: Imposex 1. **C**: Imposex 3. **D**: Imposex 5. OC-oocyte; Ovf-ovarian follicles. Scale bars = 100 µm in all.

development of testicular tissue was not observed in the ovaries at any of the stages of imposex, even with the most advanced stage (5). However, it was evident that two types of histopathological disorders were observed: a hemocytic infiltration and a sign of oocyte degeneration The former was present around the ovarian follicles in some specimens of imposex 1 (Fig. 25A), while the latter was found at the imposex stage 4 and indicated by the presence of egg atrophy and a reduction of yolk production (Fig. 25B).

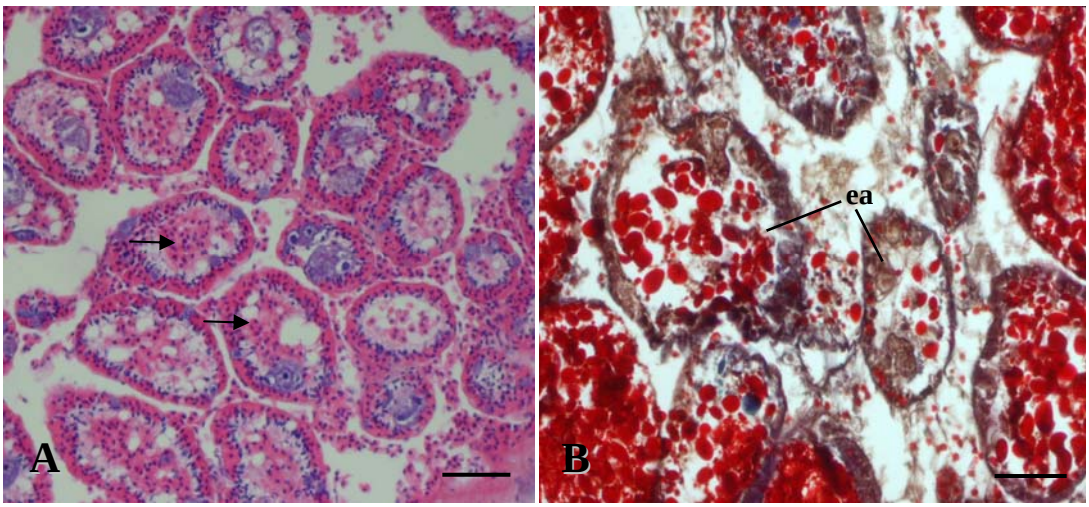

Figure 25. Ovarian tissue of imposex female *B. areolata* (H&E). **A**: Imposex 1 showing diffused hemocytic infiltrations (arrows). **B**: Imposex 4 with egg atrophy (ea). Scale bars = 60 µm in all.

3.2.2 Ultrastructural investigation

The ovaries of imposex females proceeded through various developmental stages of oocytes within each ovarian acinus in a similar way to those of normal females. Based on the changes in size and cytoplasmic contents of oocytes, the present study distinguished five stages of oocyte development in imposex females of *B. areolata*. Although the ultrastructural features of oogenesis in imposex females were generally normal, a notable histopathological disorder was present as documented in the following details:

Oogonia: Primary oogonia were groups of the smallest germinal cells and the proliferation of these cells occurred elsewhere in the ovary. In particular, they were located along the edge of the ovarian acini and had a diameter of about 24.1 µm in imposex females and 20.7 µm in normal females. The ultrastructures of the primary oogonia of imposex female were almost identical to those of the normal females. These spherical to oblong-shaped cells had a small amount of ooplasm and were dominated by a large ovoid nucleus (13 µm in diameter) where small drops of less-condensed chromatin materials were loosely distributed throughout the nucleoplasm; a nucleolus was not evident. Ooplasmic organelles were almost absent except for numerous free ribosomes and clusters of small, round mitochondria (0.6 µm in diameter) which were closely associated with the outer surface of a nuclear membrane that had few or no nuclear pores. Furthermore, patches of nuage-like material (1.2 µm in diameter) resembling fine granules appeared in the perinuclear ooplasm (Fig. 26A). At the next step, the primary oogonia divided to form the secondary oogonia which entered into the first meiotic division and became primary oocytes (pre-vitellogenic oocytes).

Pre-vitellogenic oocytes and follicle cells: No differences were observed in the ultrastructure of the pre-vitellogenic oocytes between the imposex and normal female *B. areolata*. At this stage, the oocytes were more elongated than the oogonia and were approximately 50.1 and 48.3 µm in diameter for imposex females and normal females, respectively. During the pre-vitellogenic stage, there was an increase in the size of the nucleus and in the amount of ooplasm. Early pre-vitellogenic oocytes of both groups of snails possessed a large, round nucleus (about 23 µm in diameter) with scattered heterochromatin, and a prominent electron-dense

nucleolus (6.5 µm in diameter). As the oocytes grew larger, the nucleus developed two nucleoli (Fig. 26B). At the same time, the nuclear membrane was perforated by annulated pores that increased in their numbers. In the cytoplasm adjacent to the nuclear membrane, patches of nuage-like material (12 µm in diameter), exhibiting tightly clustered fine granules and lacking a unit membrane were common in the pre-vitellogenic oocytes. These materials, possibly derived from nucleocytoplasmic transfer, were normally surrounded by small, round mitochondria (0.6 µm in diameter) with prominent cristae (Fig. 26C-D). Mitochondriogenesis commonly occurred in the pre-vitellogenic stage, with some pleomorphic mitochondria that were often concentrated in a 'mitochondrial cloud' (Fig. 26C). Aside from the nuage-like material and mitochondria, the ooplasm of the pre-vitellogenic oocytes contained numerous free ribosomes and elongate, isolated cisternae of rough endoplasmic reticulum (RER) that were scattered throughout the ooplasm (Fig. 26C).

Follicle cells were associated with all stages of oocytes particularly with the oogonia and pre-vitellogenic oocytes, and were often completely surrounded by them. These cells had a diameter of 16 µm in imposex females and 15 µm in normal females, and possessed spherical to irregularly shaped nuclei (4.6 and 6.4 µm in diameter for imposex and normal females, respectively) containing scattered patches of dense heterochromatin. A nucleolus was prominent in the nucleoplasm and measured up to 1.1 and 1.5 µm in diameter for imposex and normal females respectively (Fig. 27A-D). The cytoplasm contained a great deal of extensive, parallel arrays of RER cisternae, Golgi bodies and tubular mitochondria (Fig. 27A-F). On the whole the basic fine structures of the follicle cells were not different between imposex and normal females but a major difference was observed as indicated by the presence of considerable amount of lipid droplets (about 1.3 µm in diameter) in the cytoplasm of the imposex females (Fig. 27C-D), but not in the normal females (Fig. 27A-B). A characteristic feature of the follicle cells were the well-developed Golgi bodies that were commonly located in the perinuclear cytoplasm (Fig. 27A-B, E). Each Golgi body consisted of 7-9 cisternae and actively produced numerous small, spherical vesicles containing electron-dense material. These formed larger homogenous, electron-dense bodies (0.6 µm diameter) (Fig. 27E). At the same time, many elongated mitochondria had divided by bipartition and some lost their cristae to

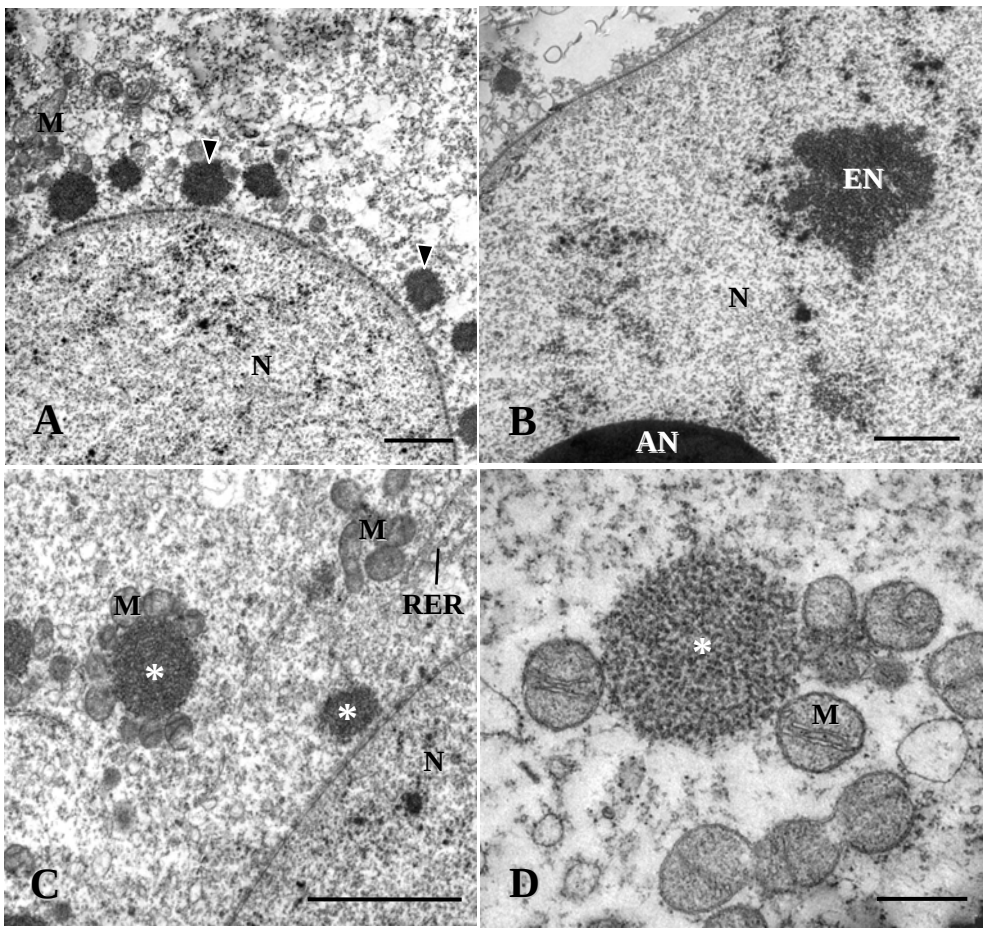

Figure 26. Primary oogonium (Og) and pre-vitellogenic oocytes (PVO) of *B. areolata*. **A**: Primary oogonium of imposex female with nuage-like materials (arrowheads). **B**: Nucleus (N) of imposex female PVO with a large amphinucleolus (AN) and a small eunucleolus (EN). **C-D**: The patches of nuage-like material (asterisks) in the perinuclear ooplasm of imposex female PVO. M-mitochondria; N-nucleus; RER-rough endoplasmic reticulum. Scale bar = 0.5 µm (D) and 2 µm (A-C).

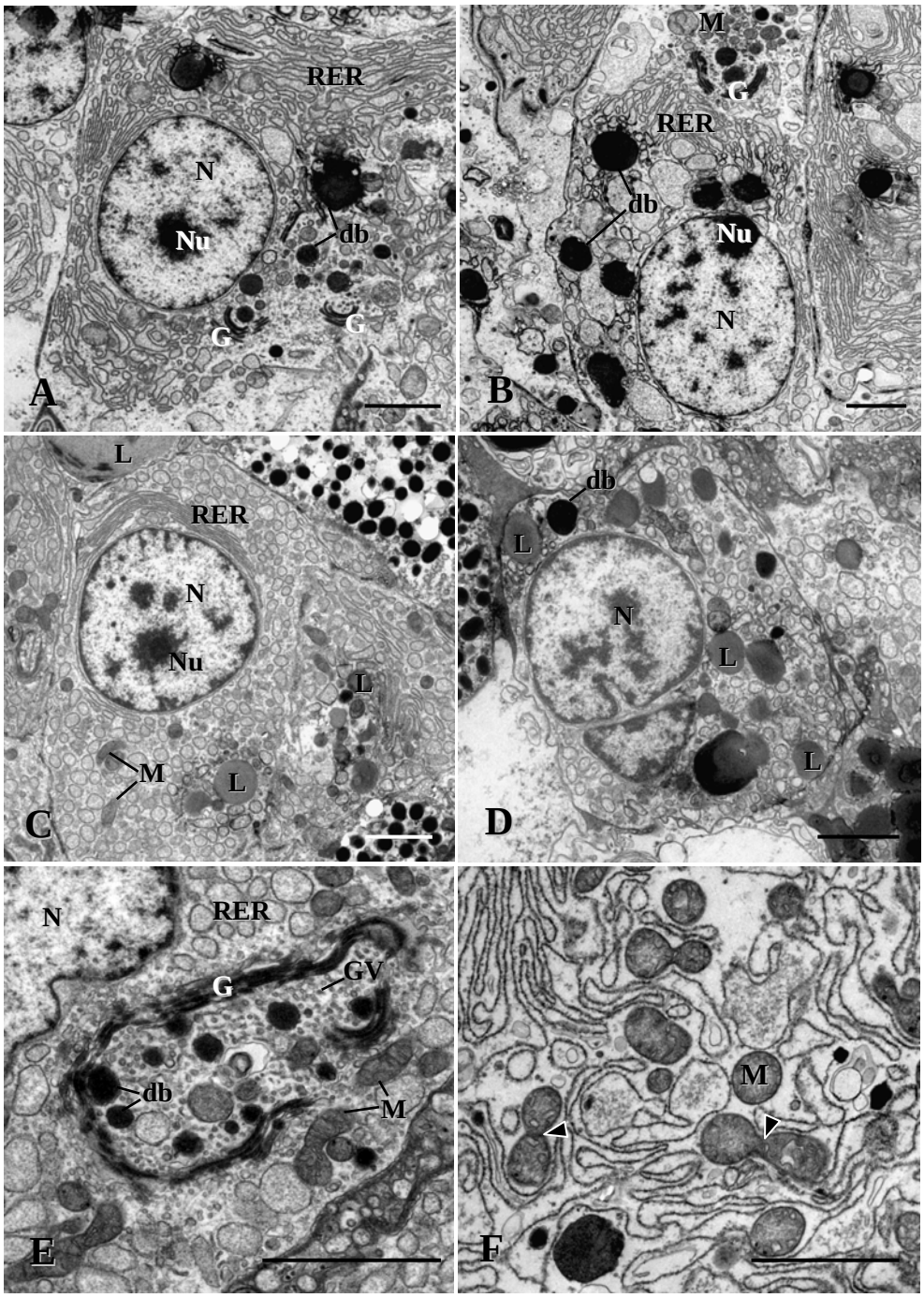

Figure 27. Follicle cells (FC) of *B. areolata*. **A-B**: FC of normal females. **C-D**: FC of imposex females with abundant lipid droplets (L). **E**: FC of imposex female showing well-developed Golgi body (G). **F**: The tubular mitochondria with bipartition (arrowheads) in the FC of normal female. db-dense body; GV-Golgi vesicle; M-mitochondria; N-nucleus; Nu-nucleolus; RER-rough endoplasmic reticulum. Scale bars = 2 µm in all.

become small, round vesicles (0.7 µm in diameter) (Fig. 27E-F).

Early vitellogenic oocytes: During this stage, the volume of the ooplasm and the germinal vesicle continued to increase. The early vitellogenic oocytes of imposex and normal females attained a size of approximately 60.2 and 65 µm in diameter, respectively. Their prominent, enlarged germinal vesicles (26 and 23.3 µm in diameter for imposex and normal females, respectively) were round to oval, contained an electron-dense nucleolus (7.4 and 8.3 µm in diameter for imposex and normal females, respectively) in which an electron-lucent space was clearly visible (Fig. 28A). Numerous well developed pores were discernable at the double-membraned nuclear envelop (Fig. 28B). In the perinuclear region, patches of nuage-like material (1.0 µm in diameter) with fine granules surrounded by small, round mitochondria (0.7 µm in diameter) were in close contact with the nuclear envelope (Fig. 28B-C). In addition to the amount of ooplasm, the number of ooplasmic organelles including the ribosomes, the mitochondria, the RER and the Golgi bodies, also increased at this stage of development (Fig. 28D-F).

The most remarkable feature of the early vitellogenic oocytes was the synthesis of at least three types of ooplasmic inclusions, including membrane-bound, electron-lucent vesicles, cortical granules and yolk bodies that were loosely dispersed throughout the ooplasm and started to increase in their numbers during this stage (Fig. 28D-F). It should, however, be noted that substantial large lipid droplets (1 µm in diameter) were found in the ooplasm of the imposex females (Fig. 28D); whereas in the normal females, lipid droplets were not evident (Fig. 28E). A dominance of the electron-lucent vesicles (0.3 µm in diameter) in portions of the ooplasm was another prominent characteristic of the early vitellogenic oocytes. These vesicles subsequently dispersed throughout the ooplasm (Fig. 28E). Cortical granule formation was initiated in the early vitellogenic oocytes. In this stage, cortical granules were found in the endoplasm and cortical ooplasm. They were membrane-bound, spherical bodies (0.8 µm diameter) that were less electron-dense than the yolk bodies, and showed contrasting dark and light regions (Fig. 28D-E). In both imposex and normal females, the synthesis of the yolk bodies occurred mainly in the perinuclear ooplasm and the newly formed yolk bodies were generally positioned near a Golgi region. This process started when the maturing face of the Golgi bodies produced small Golgi vesicles

containing electron-dense material which then fused to form a homogenous, electron-dense yolk body (about 0.8 µm in diameter) (Fig. 28F). Furthermore, during early vitellogenesis the lamellar structures observed were annulate lamellae and found in clusters (Fig. 28G) or a single strand that had a swelling at one end (Fig. 28H).

Late vitellogenic oocytes: The late vitellogenic oocytes of imposex and normal females were similar in their structures. These oocytes were about 105 and 100 µm in diameter in imposex and normal females, respectively and were larger than the early vitellogenic oocytes. A round germinal vesicle occupied a large volume of the ooplasm containing a spherical, electron-dense nucleolus in the nucleoplasm (Fig. 29A). In this stage, the nucleus was active, although the number of nuclear pores decreased. In the perinuclear region, patches of nuage-like material (0.9 µm in diameter) with fine granules still persisted at this stage, and were often surrounded by small, round mitochondria (0.5 µm in diameter) (Fig. 29B). Oocyte electron-lucent vesicles, cortical granules and yolk bodies filled the ooplasm in a similar way to those seen at the early vitellogenic stage but they appeared in larger numbers (Fig. 29C-D). In addition, large lipid droplets (1.2 µm in diameter) with no limiting membrane were observed in a similar way to those of the early vitellogenic oocytes but only in the imposex females (Fig. 29D), and not in the normal females (Fig. 29C). Late vitellogenic oocytes of both groups of snails had abundant cortical granules (1.1 µm in diameter) throughout the ooplasm (Fig. 29C-D); this structure was found both in the endoplasm and cortical ooplasm.

As vitellogenesis proceeded, numerous elements of the Golgi bodies occurred extensively in the ooplasm and it appeared that they were involved in the process of yolk formation. This process was initiated by the production of numerous, small Golgi vesicles, containing electron-dense material. These vesicles with material of variable electron density were then released from the maturing face of the Golgi bodies and later fused to form growing yolk bodies which had two appearances: a light and homogenous one and a dark and heterogeneous one (Fig. 30A). In addition, Golgi bodies might also produce the electron-lucent vesicles (0.7 µm diameter) that were positioned near to the Golgi regions and were dispersed throughout the ooplasm. At the same time, some Golgi bodies formed elaborate whorls and stacks around their vesicles (Fig. 30B). These structures became denser (Fig. 30C) and fused to form the

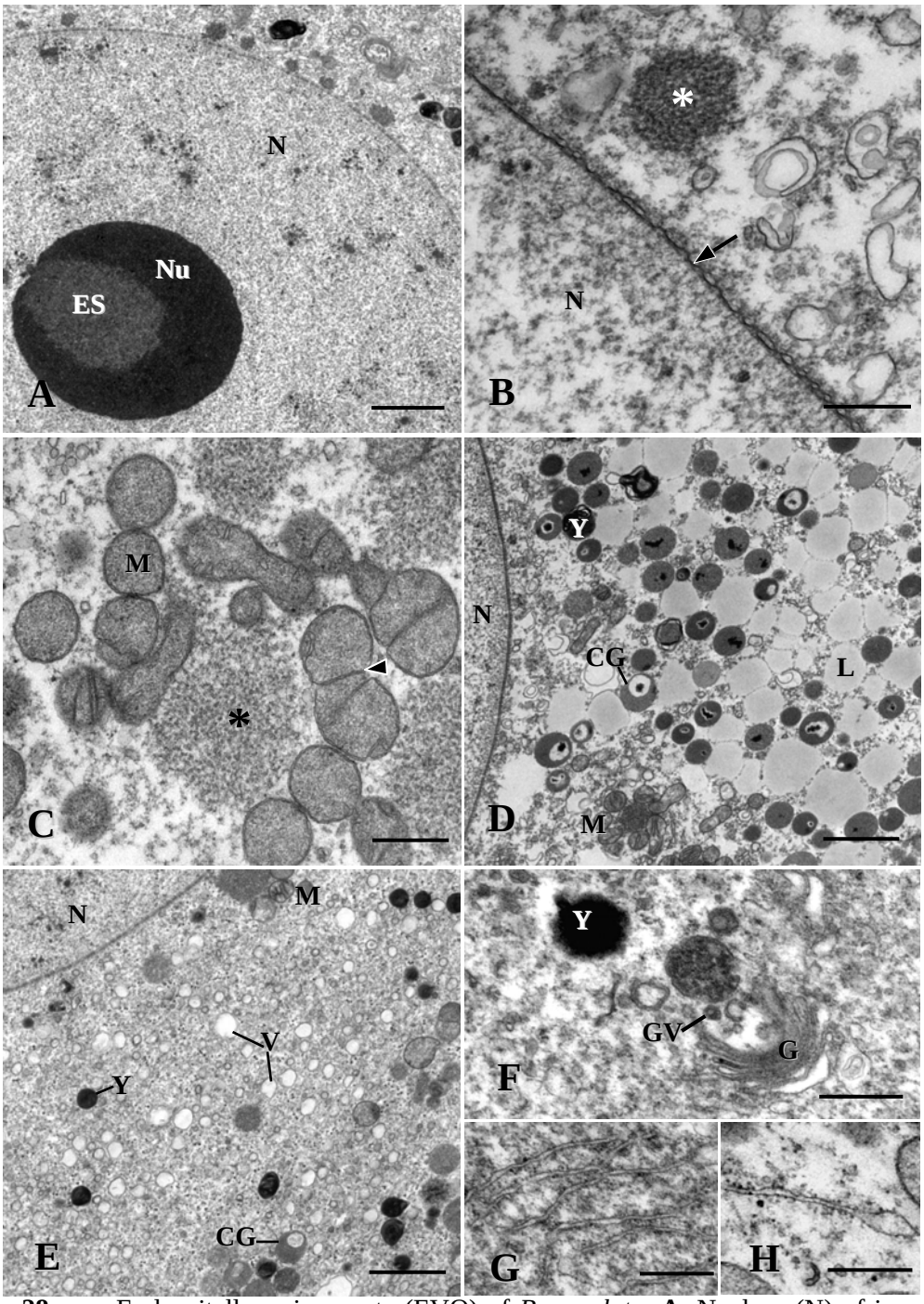

Figure 28. Early vitellogenic oocyte (EVO) of *B. areolata*. **A**: Nucleus (N) of imposex female EVO with a nucleolus (Nu) containing electron-lucent space (ES). **B**: Nuclear membrane with numerous nuclear pores (arrow) of imposex female EVO associated with nuage-like material (asterisk). **C**: EVO of imposex female showing nuage-like material (asterisk) surrounded by mitochondria that divide by bipartition (arrowhead). **D**: Ooplasm of imposex female EVO. **E**: Ooplasm of normal female EVO. **F**: Golgi body (G) of imposex female. **G-H**: Annulate lamellae in imposex female EVO CG-cortical granule; GV-Golgi vesicle; L-lipid droplet; M-mitochondria; V-electron-lucent vesicle; Y-yolk body. Scale bars = 0.5 µm (B, C, F, G, H) and 2 µm (A, D, E).

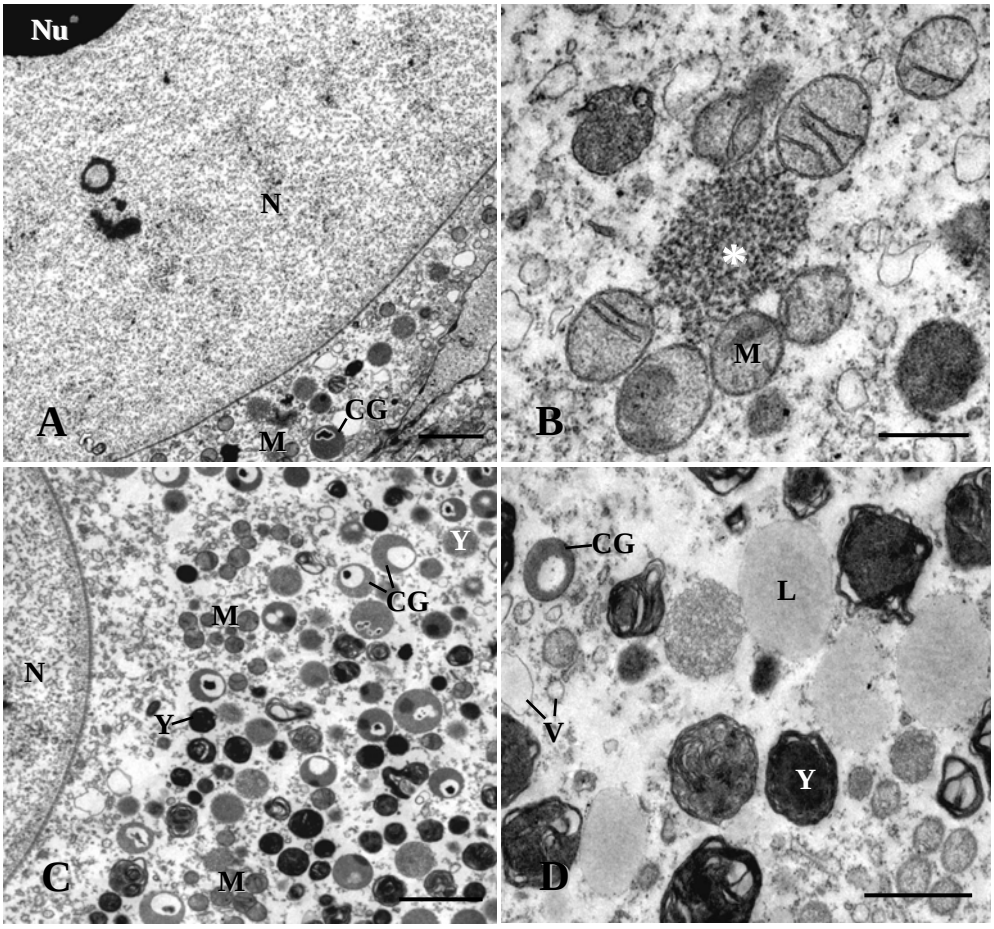

Figure 29. Late vitellogenic oocytes (LVO) of *B. areolata*. **A**: LVO of normal female. **B**: Nuage-like material (asterisk) surrounded by mitochondria (M) in LVO of normal female. **C**: Ooplasm of LVO of normal female. **D**: Ooplasm of LVO of imposex female showing many large lipid droplets (L). CG-cortical granule; N-nucleus; Nu-nucleolus; V-electron-lucent vesicle; Y-yolk body. Scale bars = 0.5 µm (B), 1 µm (D) and 2 µm (A, C).

growing yolk bodies of heterogeneous appearance, that originated from the fusion of two or three whorls inside (Fig. 30D). Another way in which the yolk bodies were formed was by surrounding the young yolk bodies with homogenous electron-dense, pre-yolk materials that were in a form of curly-shaped membranes (Fig. 30E). Eventually, the multi-vesicular bodies developed considerably, and often encompassed several small, young yolk bodies (Fig. 30E insert). These became the core of a single, larger maturing yolk body (Fig. 30F). The external envelope of the yolk bodies was formed by numerous membranes surrounding the core (Fig. 30G). Several of these membranes fused. Finally, the mature yolk body was formed, and showed a typical central, electron-dense core surrounded by a clear membranous envelope (Fig. 30H). As vitellogenesis progressed, the yolk material condensed and the ooplasm of the late vitellogenic oocytes was dominated by mature yolk bodies that were uniformly electron-dense and 2-5 µm in diameter.

As vitellogenesis progresses, endocytotic activity was seen along the oolemma in the form of pits (Fig. 30I). These pits appeared to invaginate to form a cup-like depression or an omega figure; they were then internalized into the cortical ooplasm to form a coated vesicle or endosome (Fig.30I-J). Newly formed endosomes were common near the oolemma. Subsequently, the spherical or irregularly shaped endosomes fused, coalesced their contents, and gradually transformed into homogenous, electron-dense yolk bodies (Fig. 30J).

Mature oocytes: Mature oocytes were the largest germinal cells. In both the imposex and normal females, oocytes were about 186 and 180 µm in diameter, respectively and possessed a very large germinal vesicle that displayed irregular outlines and dispersed chromatin. The round nucleolus (11.4 µm in diameter) was electron-dense with clearly defined light areas within it (Fig. 31A-B). The ooplasm contains numerous small, round mitochondria, cortical granules, yolk bodies, and electron-lucent vesicles (Fig. 31C-D). The mitochondria had a diameter of 0.7 µm and were commonly found in the clusters, while electron-lucent vesicles observed in the endoplasm were 0.5-0.7 µm in diameter (Fig. 31C-D). A marked increase in the number of the cortical granules (1.3 µm in diameter) also appeared (Fig. 31C, D, F). In addition, many elements of the Golgi bodies appeared to synthesize the yolk bodies that measured up to 4 µm in diameter (Fig. 31D). At this

stage, exocytotic vesicles resembling electron-lucent vesicles were normally found in the cortical ooplasm where they might be involved in the process of releasing material into the perivitelline space (Fig. 31E-F). A vitelline envelope was evident in the mature oocytes. This envelope consisted of evenly-spaced parallel microvilli penetrating an extracellular matrix or vitelline layer (Fig. 31F).

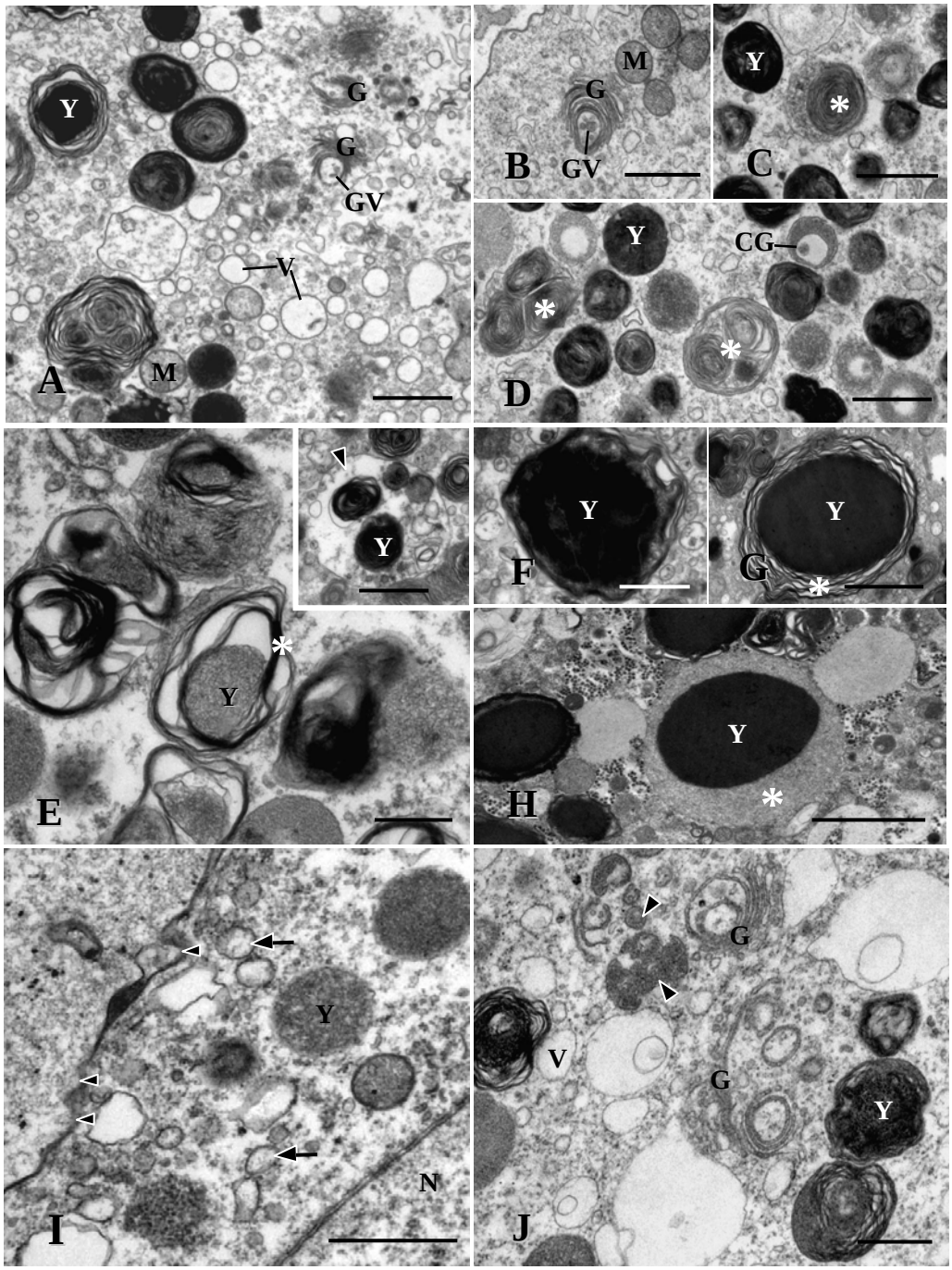

Figure 30. Late vitellogenic oocytes (LVO) of *B. areolata*. **A**: LVO of normal female showing Golgi body (G) and abundant electron-lucent vesicles (V). **B**: Golgi body of LVO of imposex female beginning to encompass its vesicles. **C**: Dense structure (asterisk) in LVO of imposex female. **D**: Many fused whorls (asterisks) in LVO of imposex female. **E**: Pre-yolk materials in a form of curly-shaped membranes (asterisk) surrounding the yolk body (Y). Insert: multi-vesicular body (arrowhead). **F**: The electron-dense core of yolk body. **G**: The fused membrane (asterisk) surrounding the core. **H.** The mature yolk body with a clear envelope (asterisk). **I**: Endocytotic pits (arrowheads) and endosomes (arrows). **J**: Irregularly shaped endosomes (arrowheads). CG-cortical granule; GV-Golgi vesicle; M-mitochondria; N-nucleus. Scale bars = 0.5 µm (J), 1 µm (A-F, I, Insert) and 2 µm (G-H).

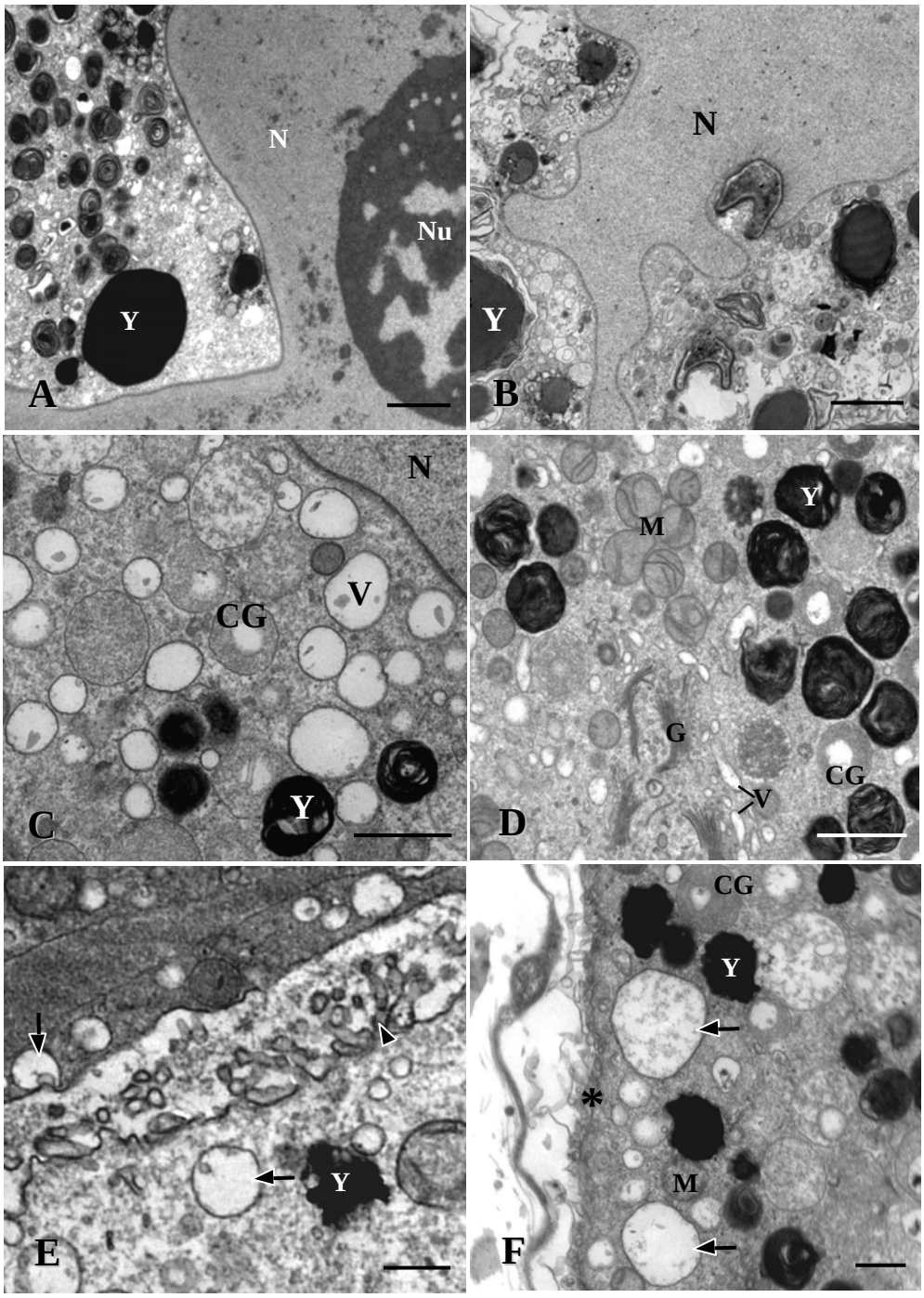

Figure 31. Mature oocyte (MO) of *B. areolata.* **A**: MO of the normal female**. B**: MO of imposex female. **C**: Ooplasm of the MO of normal female. **D**: Ooplasm of the MO of imposex female. **E**: The cortical ooplasm of the MO of the normal female. Note the exocytotic vesicles (arrows) and the outfolding of the ooplasmic membrane (arrowhead) before forming microvilli. **F**: The periphery of the MO of the normal female showing microvilli (asterisk) and exocytotic vesicles (arrows). CG-cortical granule; G-Golgi body; M-mitochondria; N-nucleus; Nu-nucleolus; V-electron-lucent vesicle; Y-yolk body. Scale bars = 0.4 µm (E), 0.8 µm (F), 2 µm (A, B) and 1 µm (C, D)**.**

4. Distribution of APGWamide in imposex female *B. areolata*

The central nervous system of *B. areolata* is composed of several paired ganglia, the cerebral, pleural, parietal, pedal ganglia, buccal and the unpaired visceral ganglion. The histology of these ganglia showed that they were surrounded by a layer of connective tissue as observed in the buccal (Fig. 32A), cerebral (Fig. 32B-C), pleural (Fig. 32D), pedal (Fig. 32E) and visceral (Fig. 32F) ganglia. All ganglia examined had the same features, exhibiting a “rind” of cells surrounding a central core of fibers. The cortical area of each ganglion contained two types of cell including neurons and neuroglia. The neurons were oval and contained round nuclei with heterochromatin and prominent nucleolus (Fig. 32A, C-F). The neuroglia cells were small and dispersed throughout the ganglia. Their darkly stained, round or spindle shaped nuclei possess a large amount of heterochromatin. The nucleolus and cytoplasm were hardly visible (Fig. 32A, C-F). In contrast to the cortical regions of the ganglia, the central core of each ganglion was composed of the axons and dendrites of neurons.

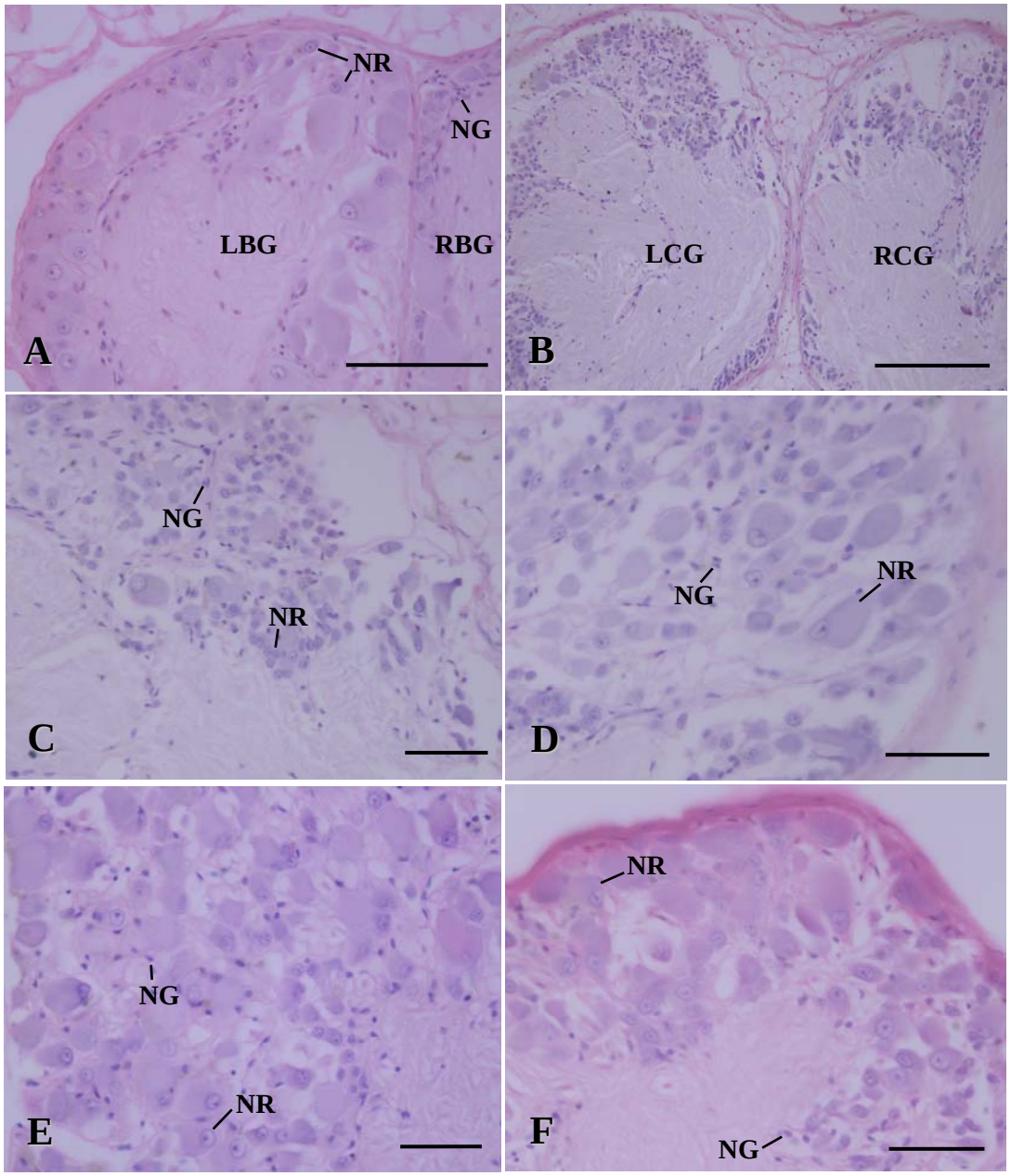

Figure 32. Histological structures of ganglia of *B. areolata* (H&E). **A:** Buccal ganglia. **B**: Cerebral ganglia. **C**-**F**: Various cell types in the cortical areas of the left cerebral ganglion (C), right pleural ganglion (D), right pedal ganglion (E) and visceral ganglia (F). LBG-left buccal ganglion; LCG-left cerebral ganglion; NG-neuroglia; NR-neuron; RBG-right buccal ganglion. RCG-right cerebral ganglion. Scale bars = 50 µm (C, D, E), 100 µm (F, A) and 200 µm (B).

4.1 Central nervous system or ganglia

On the basis of immunohistochemistry, the distribution of APGWamide-like immunoreactivity (APGWa-lir) in the central nervous system of *B. areolata* was determined and it was apparent that a strong APGWa-lir was observed in all ganglia of all groups of *B. areolata* examined (5 stages of imposex, normal female and normal male). In each ganglion the majority of neurons in *B. areolata* that appeared to contain APGWamide were localized in clusters and the average numbers of immunoreactive neurons per cluster were determined in each of the ganglia.

Cerebral ganglia: In serial sections through entire cerebral ganglia of all groups of *B. areolata*, anti-APGWamide consistently labeled 9 populations or clusters of immunoreactive neurons that were distributed throughout both the right and left cerebral ganglion (Fig. 33-36). Comparisons of the average number of immunostained neurons per cluster (NPC) (± S.E.) between groups of *B. areolata*, it was demonstrated that within both the left and right cerebral ganglion there were 5 clusters of neurons including cluster 1 (Fig. 33A-B), 2 (Fig. 33C-D), 3 (Fig. 33E-F), 5 (Fig. 34D-F) and 8 (Fig. 35E-F) where the NPC in each cluster were not different between groups of *B. areolata* ($p > 0.05$) (Table 9). The total mean values of the NPC for those clusters were 11.3 ± 1.1, 17.1 ± 2.5, 8.4 ± 1.6, 10.7 ± 1.3 and 24.3 ± 2.3 respectively for the left cerebral ganglion, and 15.1 ± 1.5, 12.7 ± 0.9, 9.9 ± 1.0, 11.8 ± 1.1 and 21.0 ± 2.2, respectively for the right cerebral ganglion. In the cluster 4 (Fig. 34A-C), 6 (Fig. 35A-B), and 7 (Fig. 35C-D) the observed NPC in the right cerebral ganglion in each cluster were similar among the groups of imposex females and did not differ from those of the normal snails ($p > 0.05$). The total mean values of the NPC for these three clusters were 10.5 ± 1.5, 12.9 ± 2.4 and 8.3 ± 2.4, respectively. In contrast to the right cerebral ganglion, in the left cerebral ganglion normal males showed significantly higher values of the NPC in each of the cluster 4, 6 and 7 (31.0 ± 5.0, 26.0 ± 1.0 and 28.0 ± 1.0, respectively) than those of the normal females and at all stages of imposex ($p < 0.05$). In these cases the NPC ranged from 4.5 ± 0.5 to 17.5 ± 8.5, 4.0 ± 2.0 to 14.3 ± 1.2 and 4.5 ± 0.5 to 16.5 ± 1.5, respectively. Furthermore cerebral ganglia of all groups of *B. areolata* had a single, larger cluster 9 (Fig. 36A-H) and there was a strong possibility that it seemed to be a major population of neurons that were immunoreactive to anti-APGWamide for the normal males and the imposex

5. As indicated in Table 9, the NPC in cluster 9 of the normal males and imposex 5 were identical within the left cerebral ganglion (88.3 ± 27.0 and 72.2 ± 9.0, respectively) and the right cerebral ganglion (95.2 ± 26.1 and 69.0 ± 19.0, respectively) ($p > 0.05$) and these values were significantly greater than those of the normal females as well as the imposex females from stages 1-4 whose NPC values ranged from 9.0 ± 3.0 to 29.6 ± 8.5 ($p < 0.05$).

Comparing the average numbers of total immunoreactive neurons (± S.E.) (computed from all clusters for each side of cerebral ganglia) between groups of *B. areolata* (n = 5 in each group), it was shown that the normal males and imposex 5 exhibited the same numbers of immunoreactive neurons within the left ganglion (180.4 ± 47.0 and 126.2 ± 21.9 respectively) ($p > 0.05$) and the right ganglion (162.4 ± 23.9 and 144.2 ± 35.8) ($p > 0.05$) and these values were significantly higher than those of all other remaining groups of *B. areolata* ($p < 0.05$) where the number of immunoreactive neurons ranged from 50.5 ± 12.4 to 93.8 ± 22.2 (Table 13). A similar trend was found for the average number of total immunostained neurons gathered from both sides of the cerebral ganglia and it is indicated in table 14 that the imposex 5 had a total number of immunostained neurons (288.6 ± 37.4) close to that of the normal males (324.6 ± 64.6) ($p > 0.05$) and these values were much higher than those of the normal females and all other stages of imposex where the number of immunostained neurons ranged from 89.3 ± 30.9 to 196.6 ± 37.1 ($p < 0.05$).

Pleural ganglia: From all groups of *B. areolata*, 7 clusters of neurons that stained well with the anti-APGWamide were distinguished in the pleural ganglia. To begin by evaluating the number of APGWamide-containing neurons in the left pleural ganglion, it was evident that the NPC in each of the following clusters: 1 (Fig. 37A, C), 2 (Fig. 37D), 6 (Figure 39D, F) and 7 (Fig. 40A, C) were similar between groups of *B. areolata* ($p > 0.05$) and the total mean values of the NPC for these clusters in all groups were 7.3 ± 1.1, 22.4 ± 3.0, 25.6 ± 3.6 and 25.3 ± 2.0, respectively (Table 10). However, there were significant differences in the NPC of the cluster 3 (Fig. 38A, C), 4 (Fig. 38D, F), and 5 (Fig. 39A, C) among groups ($p < 0.05$). In the cluster 3, 4 and 5, the NPC of the normal males (86.7 ± 29.0, 60.0 ± 1.0, 111.0 ± 22.6, respectively) and imposex 5 (94.3 ± 28.1, 59.5 ± 0.5, 118.3 ± 8.8, respectively) were the same for each cluster ($p > 0.05$) and extremely higher than

Table 9. Average number of APGWamide-like immunoreactive neurons per cluster (NPC) (± S.E.) in various cell clusters of cerebral ganglia in different groups of *B. areolata* (n = 5).

Groups	Clusters of neuron								
	1	2	3	4	5	6	7	8	9
Left ganglion									
Normal female	10.7 ± 4.1	11.7 ± 1.3	nd	4.5 ± 0.5^{a}	nd	4.0 ± 2.0^{a}	nd	15.0 ± 10.0	13.7 ± 8.2^{a}
Imposex 1	17.0 ± 1.5	35.0 ± 10.4	4.3 ± 0.9	7.5 ± 0.5^{ab}	7.8 ± 2.4	11.5 ± 0.5^{a}	4.5 ± 0.5^{a}	27.8 ± 2.6	29.6 ± 8.5^{a}
Imposex 2	10.5 ± 3.8	9.0 ± 1.5	5.7 ± 1.3	7.0 ± 1.0^{ab}	7.4 ± 2.3	8.3 ± 4.9^{a}	16.5 ± 1.5^{ab}	21.7 ± 4.3	10.3 ± 0.9^{a}
Imposex 3	11.3 ± 2.6	20.4 ± 7.1	5.0 ± 1.0	4.5 ± 0.5^{a}	7.5 ± 1.0	6.8 ± 1.5^{a}	nd	20.3 ± 5.4	27.3 ± 3.9^{a}
Imposex 4	8.0 ± 5.0	11.5 ± 2.5	3.0 ± 1.0	nd	17.0 ± 1.0	nd	9.5 ± 6.5^{a}	21.0 ± 2.0	11.5 ± 0.1^{a}
Imposex 5	9.3 ± 2.2	14.7 ± 1.9	16.0 ± 1.0	17.5 ± 8.5^{ab}	18.3 ± 3.7	14.3 ± 1.2^{a}	3.0 ± 1.0^{a}	33.0 ± 7.1	72.2 ± 9.0^{b}
Normal male	11.5 ± 1.3	16.0 ± 1.2	14.3 ± 3.8	31.0 ± 5.0^{b}	11.0 ± 3.2	26.0 ± 1.0^{b}	28.0 ± 1.0^{b}	24.4 ± 6.9	88.3 ± 27.0^{b}

Within each column, means sharing the same superscript letter are not significantly different from each other; means with different superscript letters are significantly different (one-way ANOVA, $p < 0.05$). nd = not detected.

Right ganglion									
Normal female	14.3 ± 3.0	10.8 ± 3.5	nd	nd	9.5 ± 0.5	nd	nd	27.5 ± 2.5	9.3 ± 3.4^{a}
Imposex 1	23.3 ± 3.5	17.3 ± 1.3	9.0 ± 1.2	15.0 ± 3.0	15.8 ± 3.9	14.0 ± 2.5	2.5 ± 0.5	22.5 ± 4.2	18.0 ± 1.8^{a}
Imposex 2	17.0 ± 2.1	13.8 ± 2.3	12.0 ± 2.5	7.7 ± 0.9	10.0 ± 1.2	7.0 ± 0.6	nd	14.0 ± 2.1	9.0 ± 3.0^{a}
Imposex 3	15.5 ± 5.1	11.6 ± 1.9	11.0 ± 1.0	10.0 ± 1.0	9.2 ± 1.8	8.8 ± 1.1	nd	20.3 ± 3.3	18.8 ± 5.2^{a}
Imposex 4	7.5 ± 2.5	10.0 ± 2.0	7.0 ± 1.0	nd	12.0 ± 8.0	nd	12.0 ± 1.0	7.5 ± 0.5	10.2 ± 3.2^{a}
Imposex 5	8.8 ± 2.5	12.8 ± 2.0	nd	12.0 ± 6.4	13.3 ± 1.8	13.3 ± 4.4	4.5 ± 1.5	22.4 ± 7.4	69.0 ± 19.0^{b}
Normal male	18.3 ± 2.3	12.5 ± 3.1	nd	8.5 ± 1.5	12.7 ± 2.3	20.5 ± 9.2	14.0 ± 8.0	29.3 ± 4.8	95.2 ± 26.1^{b}

Within each column, means sharing the same superscript letter are not significantly different from each other; means with different superscript letters are significantly different (one-way ANOVA, $p < 0.05$). nd = not detected.

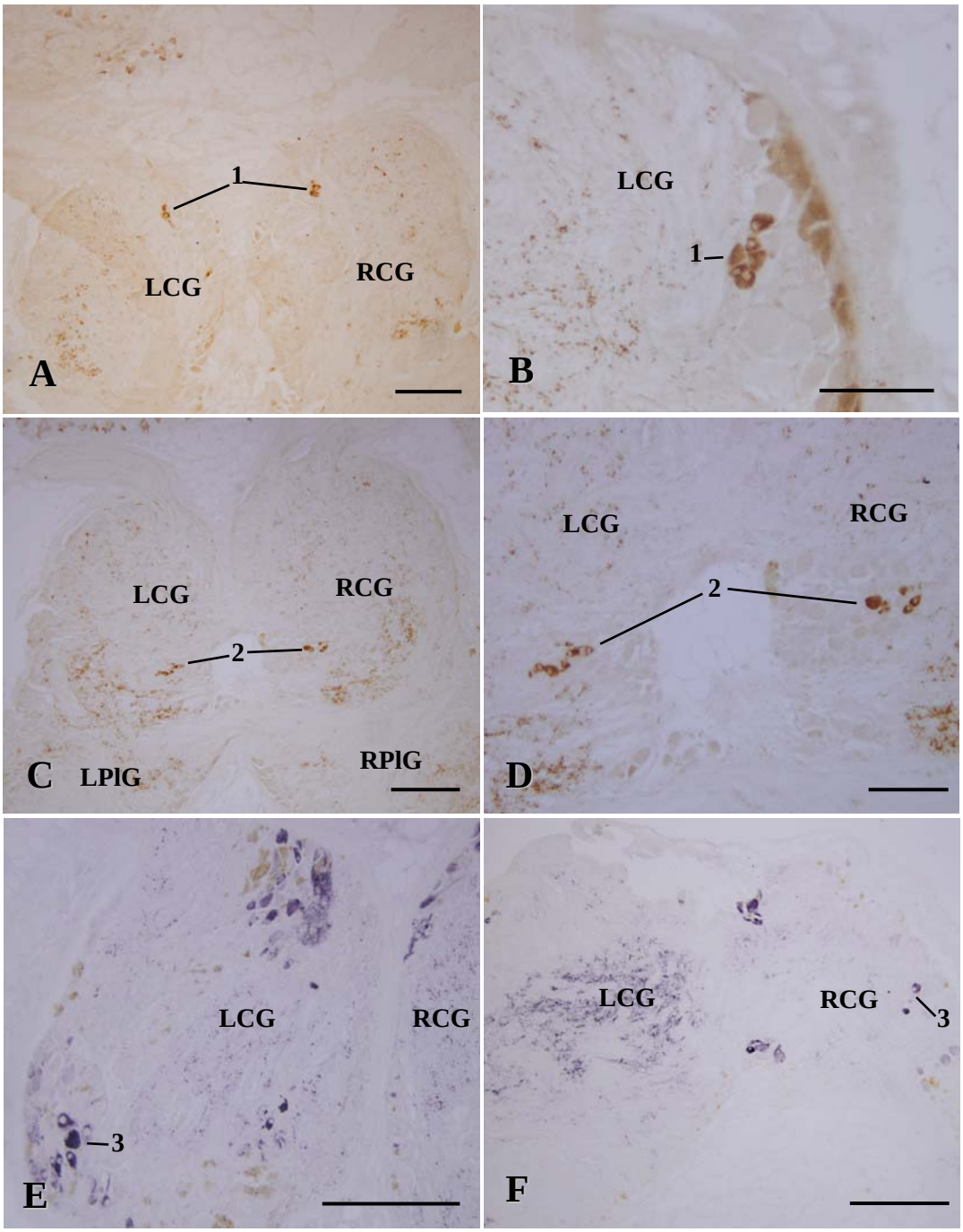

Figure 33. Cerebral ganglia of *B. areolata* with APGWamide-like immunoreactive neurons (cluster 1-3). **A-B**: Cluster 1 in imposex stage 5. **C-D**: Cluster 2 in imposex stage 5. **E-F**: Cluster 3 in normal male (E) and imposex stage 1 (F). LCG-left cerebral ganglion; LPlG-left pleural ganglion; RCG-right cerebral ganglion; RPlG-right pleural ganglion. Scale bars = 100 µm (B, D), 200 µm (A, C, E) and 250 µm (F).

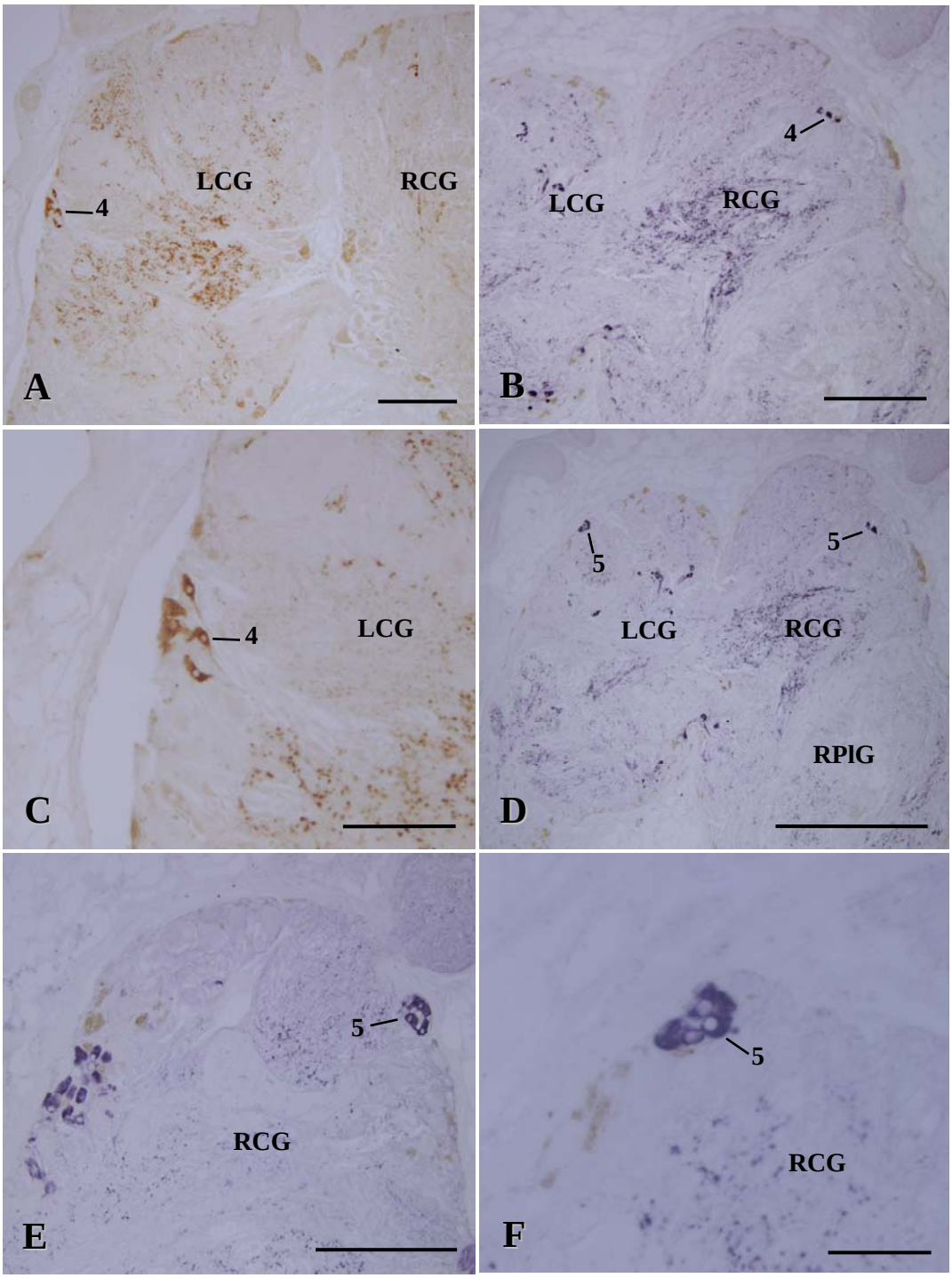

Figure 34. Cerebral ganglia of *B. areolata* with APGWamide-like immunoreactive neurons (cluster 4-5). **A-C**: Cluster 4 in imposex stage 5. **D-F**: Cluster 5 in normal male. LCG-left cerebral ganglion; RCG-right cerebral ganglion; RPlG-right pleural ganglion. Scale bars = 50 µm (F), 100 µm (C), 200 µm (A, E), 250 µm (B) and 500 µm (D).

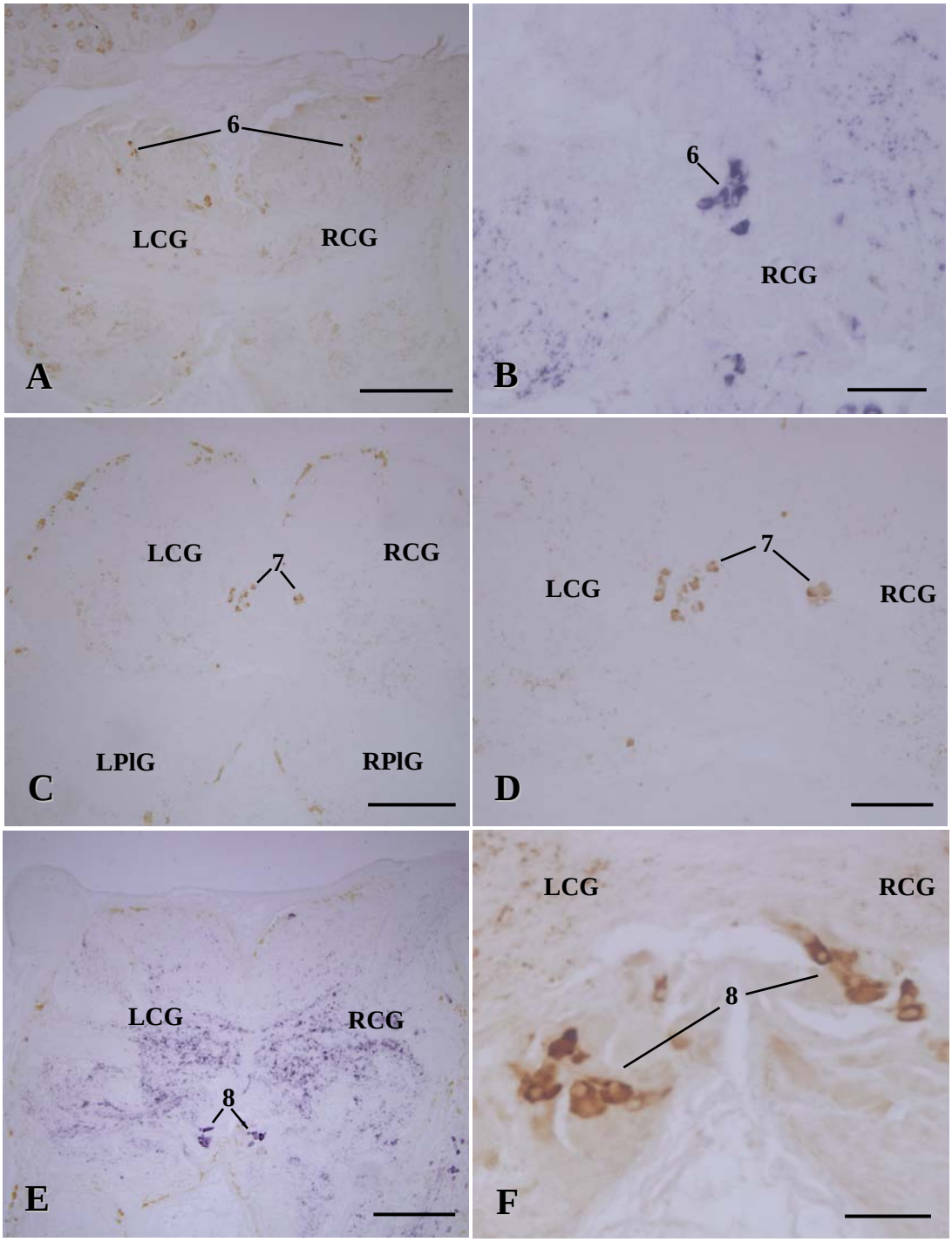

Figure 35. Cerebral ganglia of *B. areolata* with APGWamide-like immunoreactive neurons (cluster 6-8). **A-B**: Cluster 6 in imposex stage 5 (A) and normal male (B). **C-D**: Cluster 7 in normal male. **E-F**: Cluster 8 in imposex stage 5. LCG-left cerebral ganglion; LPlG-left pleural ganglion; RCG-right cerebral ganglion; RPlG-right pleural ganglion. Scale bars = 50 µm (B, F), 100 µm (D), and 250 µm (A, C, E).

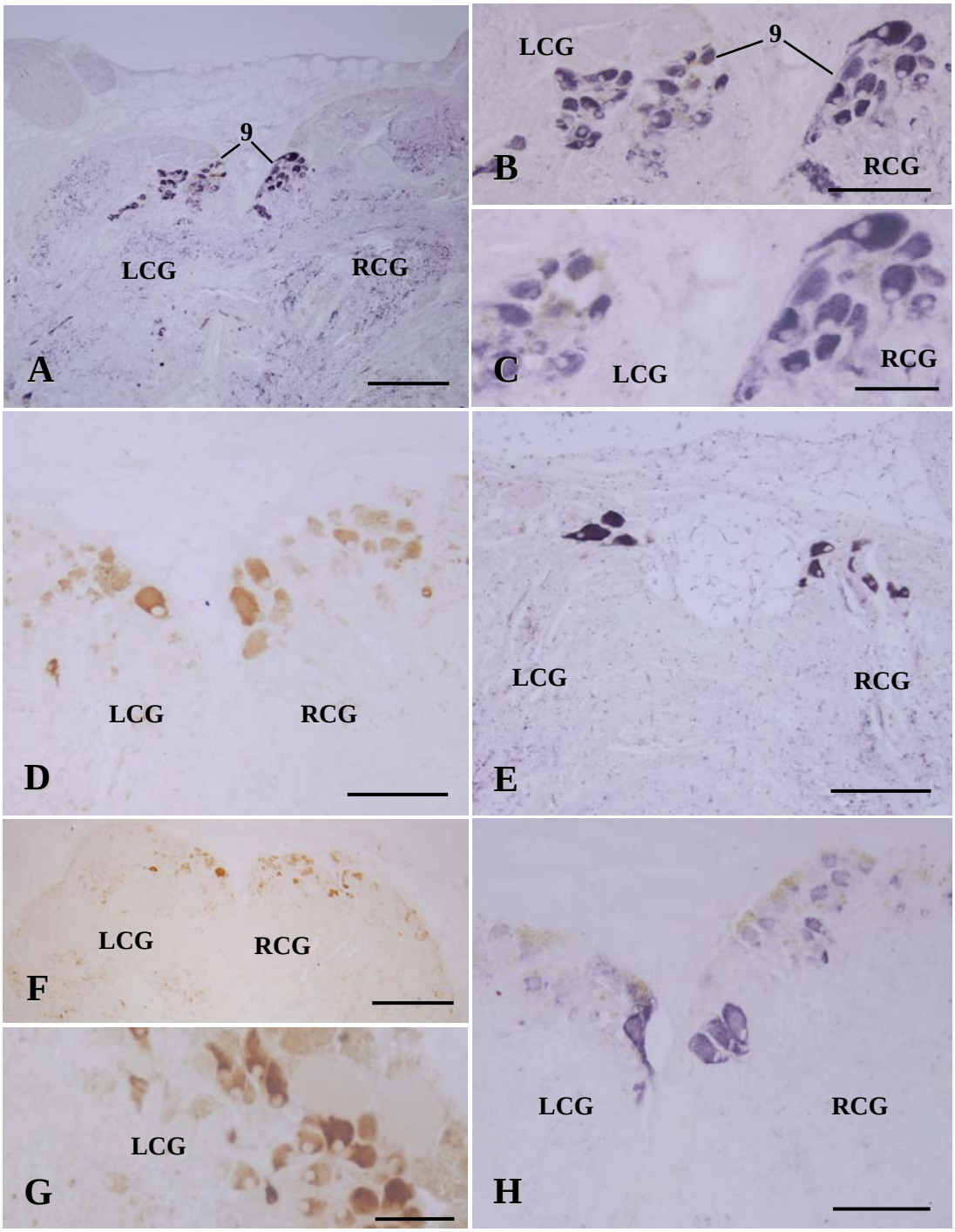

Figure 36. Cerebral ganglia of *B. areolata* with APGWamide-like immunoreactive neurons (cluster 9). **A-C**: Cluster 9 in normal male. **D**: Cluster 9 in imposex stage 1. **E**: Cluster 9 in imposex stage 3. **F-G**: Cluster 9 in imposex stage 5. **H**: Cluster 9 in normal female. LCG-left cerebral ganglion; RCG-right cerebral ganglion. Scale bars = 50 µm (C, G), 100 µm (B, D, E, H), 200 µm (A) and 250 µm (F).

those of the normal females and the imposex females with stages 1 - 4 ($p < 0.05$) where the NPC ranged from 17.3 ± 3.2 to 31.2 ± 10.6, 7.5 ± 0.5 to 32.3 ± 2.3, and 9.0 ± 2.0 to 67.0 ± 59.0 (for cluster 3, 4 and 5, respectively). In the left pleural ganglion, the evidence for clusters 3, 4 and 5 were that they were likely to be the main clusters of neurons that were immunoreactive to APGWamide for the normal male and imposex 5. After determining the NPC in various clusters of the right pleural ganglion, it appeared that the imposex 1-5, normal females and normal males had similar values of the NPC in each of the following clusters: 1 (Fig. 37B), 2 (Fig. 37E-F) and 3 (Fig. 38B) and the total mean values of the NPC of these three clusters in all groups of *B. areolata* were 4.4 ± 2.0, 53.2 ± 7.1 and 43.8 ± 4.9, respectively (Table 10). In the remaining clusters: 4 (Fig. 38E), 5 (Fig. 39B), 6 (Fig. 39E), and 7 (Fig. 40B, D), it was shown that the NPC of all groups of imposex as well as the normal females were identical for each of clusters 4 and 7 ($p > 0.05$), but slightly different for each of the clusters 5 and 6 ($p < 0.05$), and ranged from 20.5 ± 1.5 to 25.5 ± 0.5, 4.0 ± 1.0 to 28.0 ± 5.6, 3.0 ± 1.0 to 21.3 ± 2.0, and 14.0 ± 2.0 to 22.5 ± 2.5 (for cluster 4, 5, 6 and 7, respectively). However, all values of the NPC of those groups (imposex females and normal females) in each cluster were significantly lower than those of the normal male ($p < 0.05$) where the observed NPC were 61.5 ± 1.5, 32.0 ± 9.2 and 38.5 ± 1.5 for the cluster 4, 5 and 7, respectively.

Comparing the average numbers of total immunoreactive neurons (± S.E.) between groups of *B. areolata* on each side of the pleural ganglia, the left pleural ganglion of imposex females at stages 1-4 and normal females had similar numbers of immunoreactive neurons ranging from 56.0 ± 19.7 to 126.7 ± 47.8 ($p > 0.05$) whereas for the imposex stage 5 there was no difference in the number of immunoreactive neurons (238.2 ± 55.7) from that of the untreated males (305.3 ± 38.8) ($p > 0.05$) and these values were significantly higher than those of the imposex females at stages 1-4 and the normal females ($p < 0.05$) (Table 13). In the right pleural ganglion, the number of total immunoreactive neurons of all groups of imposex and the normal females ranging from 65.5 ± 18.2 to 155.0 ± 30.2 were significantly lower than that of the normal males (194.0 ± 24.5) ($p < 0.05$). For the average number of total immunostained neurons gathered from both sides of the pleural ganglia, the results showed that the number of total immunostained neurons of the imposex 5

(460.3 ± 68.6) and the normal males (432.2 ± 72.1) was the same ($p > 0.05$) and significantly greater than those of all other groups of *B. areolata* ($p < 0.05$) with values that ranged from 108.4 ± 22.8 to 248.4 ± 67.8 (Table 14).

Parietal ganglia: Although the entire nerve ring consisting of 5 ganglia including a pair of buccal, cerebral, pleural, parietal and pedal ganglia was dissected and serially sectioned during the steps of tissue preparation, the right parietal ganglion was not present in the sections, therefore could not be analyzed. Therefore, the distribution of APGWamide was described only in the left parietal ganglion. From the total 9 clusters of immunopositive neurons, there were 4 clusters where the NPC of each cluster were similar when comparing between groups of *B. areolata* ($p > 0.05$). These included cluster 2 (Fig. 41C-D), 5 (Fig. 42C-D), 7 (Fig. 43A-B) and 8 (Fig. 43C-D) and the total mean values of the NPC of these clusters were 21.1 ± 3.3, 16.8 ± 2.0, 39.0 ± 6.3 and 15.3 ± 1.5, respectively (Table 11). In each of the cluster 1 (Fig. 41A-B) and 6 (Fig. 42E-F), the NPC of all groups of imposex females as well as the normal females were similar ($p > 0.05$), ranging from 1.3 ± 0.3 to 9.7 ± 3.2 and 2.5 ± 1.5 to 20.5 ± 8.9 for cluster 1 and 6 respectively, but significantly lower than those of the normal males (20.5 ± 0.5 and 42.0 ± 2.0, respectively) ($p < 0.05$). A similar trend was found in the cluster 3 (Fig. 41E-F) but in this cluster the NPC of the imposex 5 (29.3 ± 4.4) was close to those of the normal males (30.3 ± 10.0) ($p > 0.05$) and significantly higher than those of the remaining groups of the imposex females as well as the normal females ($p < 0.05$) where the NPC ranged from 1.7 ± 0.7 to 10.0 ± 3.0. In the last two clusters: 4 (Fig. 42A-B) and 9 (Fig. 43E-F), no stained neurons were observed in the normal males and in each cluster there were slight differences in the NPC among the groups of normal females and all stages of the imposex females ($p < 0.05$). The total mean values of the NPC for these two clusters were 12.6 ± 2.5 and 9.3 ± 0.9, respectively.

Comparing the average number of total immunoreactive neurons in the left parietal ganglia, it was demonstrated that the number of immunoreactive neurons in all groups of imposex and normal females ranged from 28.0 ± 6.1 (in imposex 4) to 123.3 ± 38.1 (in imposex 5) and were significantly lower than that of the normal males (159.8 ± 15.0) ($p < 0.05$) (Table 13).

Table 10. Average number of APGWamide-like immunoreactive neurons per cluster (NPC) (± S.E.) in various cell clusters of pleural ganglia in different groups of *B. areolata* (n = 5).

Groups	Clusters of neuron						
	1	2	3	4	5	6	7
Left ganglion							
Normal female	3.7 ± 3.7	12.7 ± 4.1	19.0 ± 8.2^{a}	21.5 ± 9.5^{ab}	13.8 ± 2.9^{a}	13.5 ± 8.5	34.0 ± 1.0
Imposex 1	3.3 ± 3.3	37.5 ± 18.7	17.3 ± 3.2^{a}	32.3 ± 2.3^{ab}	67.0 ± 59.0^{ab}	37.3 ± 9.9	23.3 ± 5.8
Imposex 2	10.6 ± 10.6	22.8 ± 2.6	21.6 ± 6.7^{a}	22.7 ± 2.8^{ab}	17.4 ± 3.7^{a}	28.0 ± 22.0	24.8 ± 6.0
Imposex 3	6.7 ± 6.7	15.8 ± 3.0	31.2 ± 10.6^{a}	26.0 ± 4.0^{ab}	13.0 ± 2.8^{a}	20.0 ± 7.6	17.7 ± 0.9
Imposex 4	2.0 ± 2.0	14.3 ± 4.9	20.8 ± 6.5^{a}	7.5 ± 0.5^{a}	9.0 ± 2.0^{a}	12.0 ± 1.0	29.0 ± 1.0
Imposex 5	7.5 ± 7.5	20.3 ± 6.2	94.3 ± 28.1^{b}	59.5 ± 0.5^{c}	118.3 ± 8.8^{b}	35.5 ± 0.5	28.3 ± 7.3
Normal male	11.2 ± 11.2	30.6 ± 3.3	86.7 ± 29.0^{b}	60.0 ± 1.0^{c}	111.0 ± 22.6^{b}	27.8 ± 6.6	23.5 ± 0.5

Within each column, means sharing the same superscript letter are not significantly different from each other; means with different superscript letters are significantly different (one-way ANOVA, $p < 0.05$). nd = not detected.

Right ganglion							
Normal female	1.5 ± 0.5	34.3 ± 18.1	31.2 ± 16.9	23.5 ± 1.5^{a}	10.5 ± 3.5^{abc}	3.0 ± 1.0^{a}	14.5 ± 0.5^{a}
Imposex 1	1.0 ± 0.0	49.0 ± 35.6	31.8 ± 14.0	25.5 ± 0.5^{a}	7.0 ± 2.0^{ab}	12.3 ± 3.9^{ab}	14.0 ± 2.0^{a}
Imposex 2	1.7 ± 0.3	66.7 ± 20.3	44.5 ± 13.6	24.0 ± 1.5^{a}	28.0 ± 5.6^{bc}	21.3 ± 2.0^{b}	18.0 ± 1.2^{a}
Imposex 3	1.0 ± 0.0	57.3 ± 12.1	43.2 ± 11.3	23.5 ± 1.5^{a}	16.0 ± 5.3^{abc}	9.3 ± 0.9^{ab}	18.3 ± 1.9^{a}
Imposex 4	nd	23.5 ± 15.5	40.0 ± 13.8	nd	4.0 ± 1.0^{a}	nd	nd
Imposex 5	nd	77.0 ± 20.7	56.5 ± 11.2	20.5 ± 1.5^{a}	nd	nd	22.5 ± 2.5^{a}
Normal male	14.7 ± 5.8	60.4 ± 12.0	59.2 ± 10.5	61.5 ± 1.5^{b}	32.0 ± 9.2^{c}	nd	38.5 ± 1.5^{b}

Within each column, means sharing the same superscript letter are not significantly different from each other; means with different superscript letters are significantly different (one-way ANOVA, $p < 0.05$). nd = not detected.

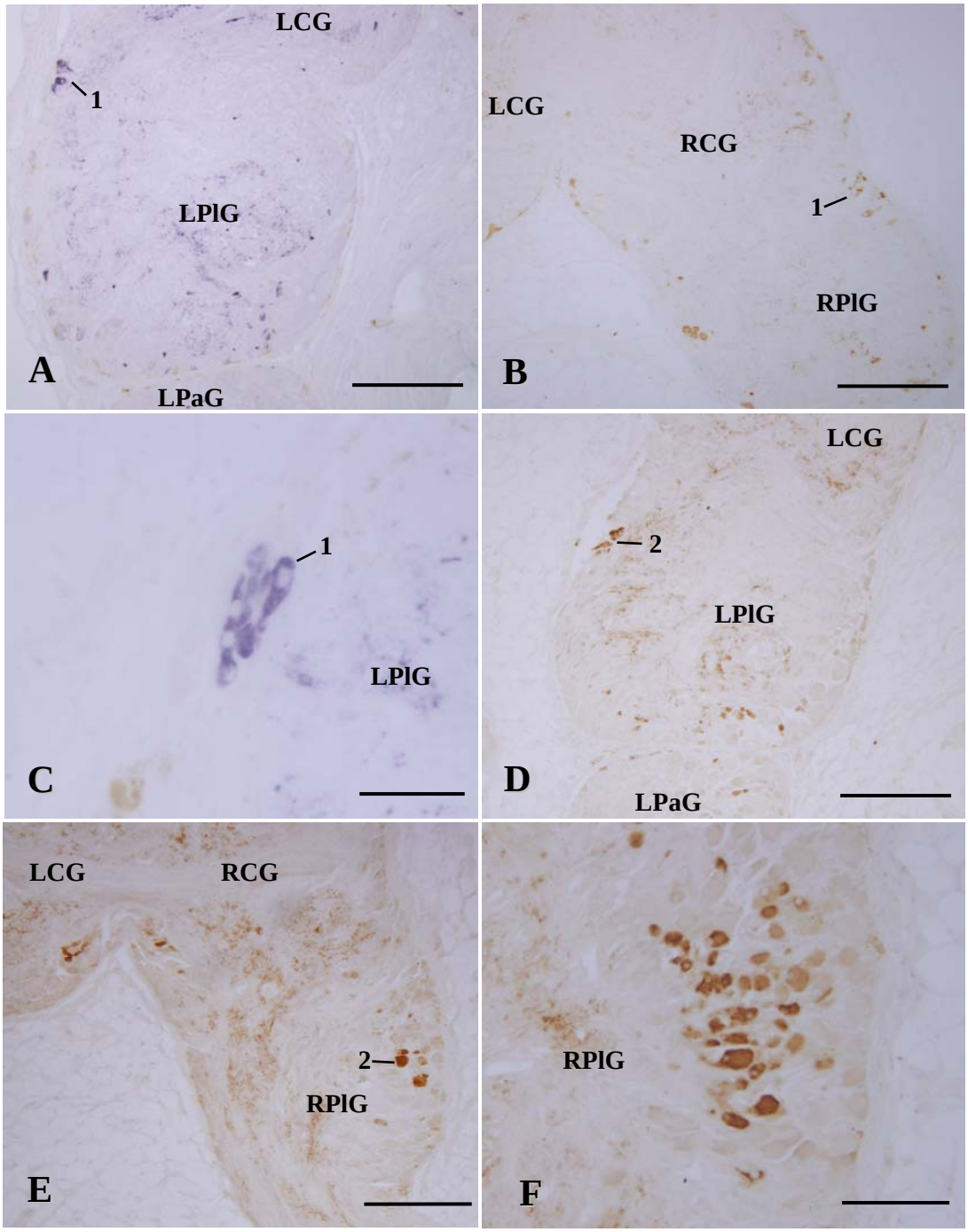

Figure 37. Pleural ganglia of *B. areolata* with neurons immunoreactive to anti-APGWamide (cluster 1-2). **A-C**: Cluster 1 in normal female (A) and normal male (B-C). **D-F**: Cluster 2 in imposex stage 5. LCG-left cerebral ganglion; LPaG-left parietal ganglion; LPlG-left pleural ganglion; RCG-right cerebral ganglia; RPlG-right pleural ganglion. Scale bars = 50 µm (C), 100 µm (F) and 250 µm (A, B, D, E).

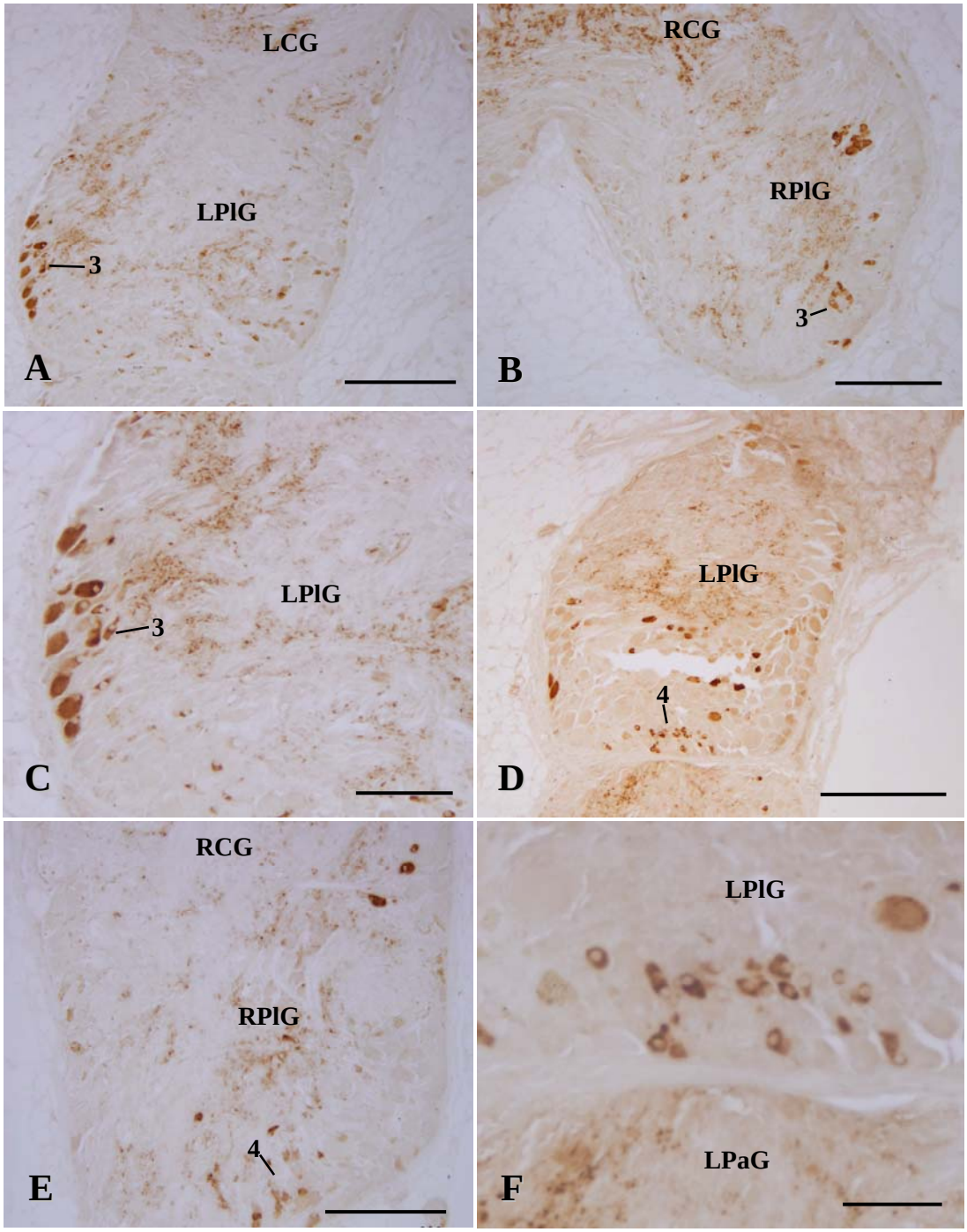

Figure 38. Pleural ganglia of *B. areolata* with neurons immunoreactive to anti-APGWamide (cluster 3-4). **A-C**: Cluster 3 in normal male. **D-F**: Cluster 4 in imposex stage 5. LCG-left cerebral ganglion; LPaG-left parietal ganglion; LPlG-left pleural ganglion; RCG-right cerebral ganglia.; RPlG-right pleural ganglion. Scale bars = 50 µm (F), 100 µm (C), 200 µm (E) and 250 µm (A, B, D).

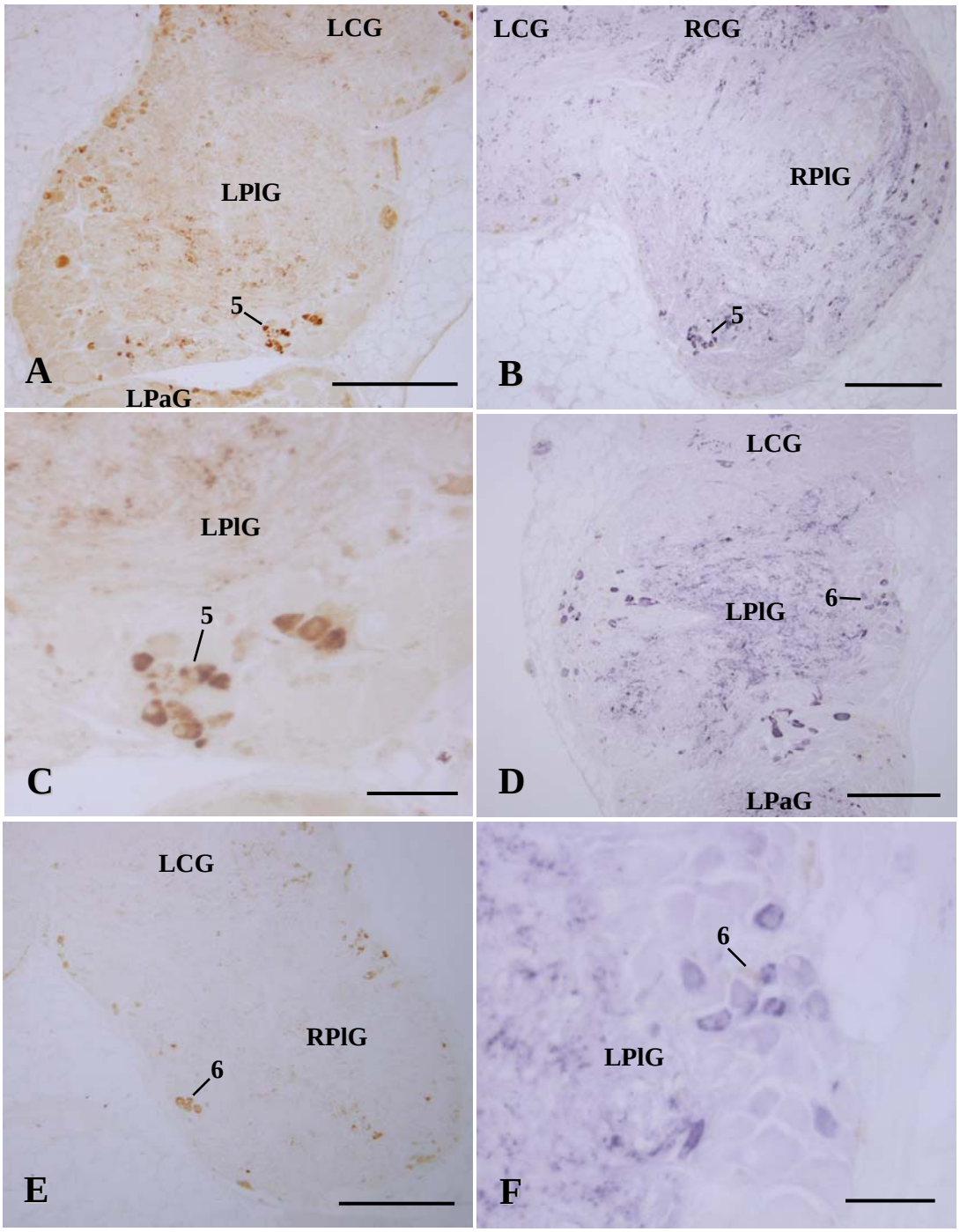

Figure 39. Pleural ganglia of *B. areolata* with neurons immunoreactive to anti-APGWamide (cluster 5-6). **A-C**: Cluster 5 in normal male. **D-F**: Cluster 6 in imposex stage 1. LCG-left cerebral ganglion; LPaG-left parietal ganglion; LPlG-left pleural ganglion; RCG-right cerebral ganglia; RPlG-right pleural ganglion. Scale bars = 50 µm (C, F), 200 µm (D) and 250 µm (A, B, E).

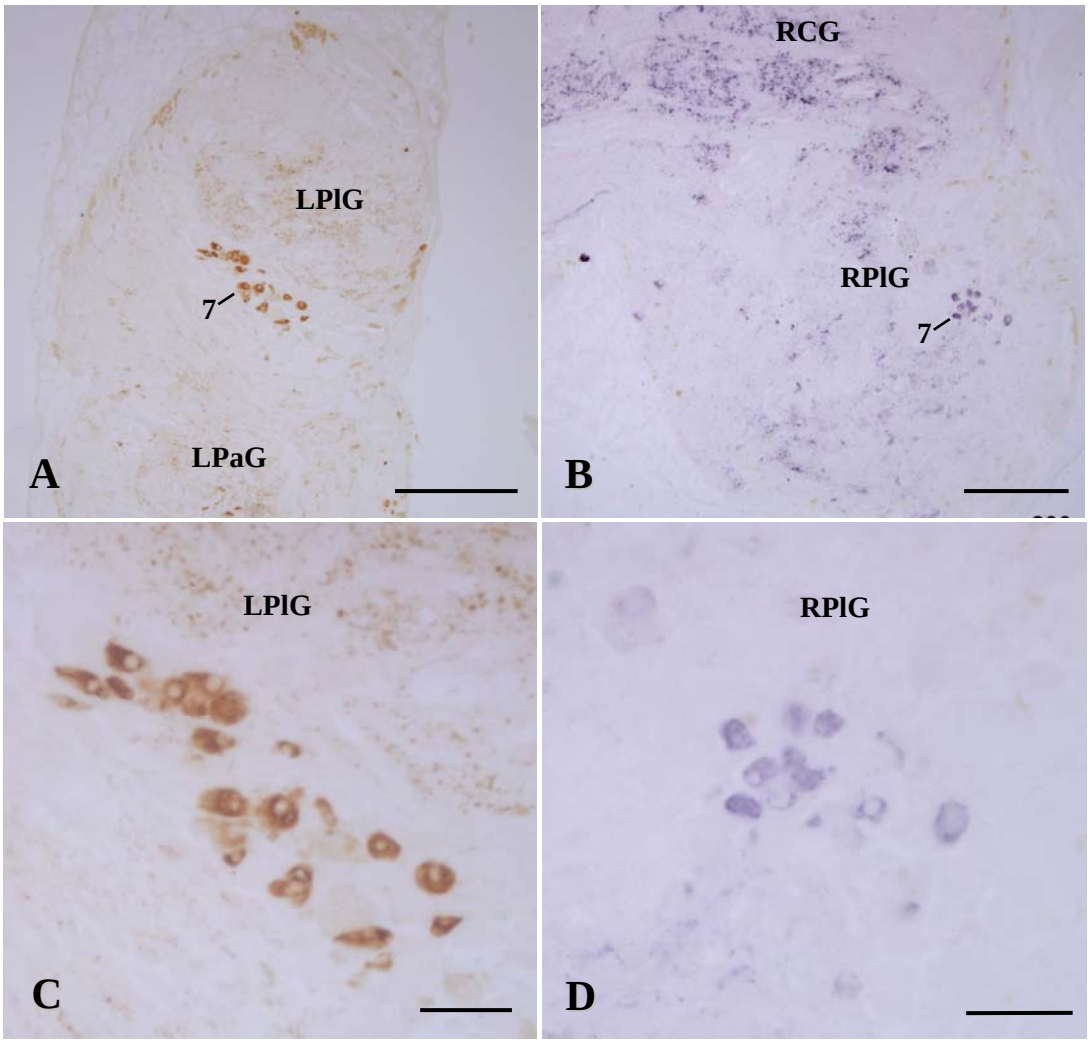

Figure 40. Pleural ganglia of *B. areolata* with neurons immunoreactive to anti-APGWamide (cluster 7). **A, C**: Cluster 7 in imposex stage 5. **B, D**: Cluster 7 in normal male. LPaG-left parietal ganglion; LPlG-left pleural ganglion; RCG-right cerebral ganglia; RPlG-right pleural ganglion. Scale bars = 50 µm (C, D), 200 µm (B) and 250 µm (A).

Pedal ganglia: After examining the presence of APGWamide in all groups of *B. areolata*, it was obvious that the pedal ganglia contained 4 clusters of neurons immunoreactive to anti-APGWamide. Comparing the NPC between the different groups of *B. areolata*, it was shown that within both the left and right pedal ganglion the NPC for each of the clusters: 1 (Fig. 44A-C), 2 (Fig. 44D-F), 3 (Fig. 45A-C) and 4 (Fig. 45D-F) were not different between all stages of imposex females, normal female and normal male ($p > 0.05$) (Table 12) and the total mean values for these clusters were 7.6 ± 0.7, 17.0 ± 1.9, 10.0 ± 1.3, and 8.7 ± 0.8 respectively for the left pedal ganglion and 9.3 ± 0.9, 10.6 ± 1.4, 12.4 ± 0.9, and 6.2 ± 0.9 respectively for the right pedal ganglion. Comparing the average numbers of total immunoreactive neurons for each side of the pedal ganglia between *B. areolata* groups, it was evident that in the left pedal ganglion the number of immunoreactive neurons in the imposex 4 (23.0 ± 5.1) and normal females (20.6 ± 4.1) were not different ($p > 0.05$) and significantly lower than those of all other groups where the values ranged from 39.0 ± 6.8 to 49.3 ± 4.7, while in the right pedal ganglion the number of immunoreactive neurons did not differ among the groups ($p > 0.05$) (Table 13). For the average number of total immunoreactive neurons calculated from both sides of the pedal ganglia, the results clearly showed that there was no difference in the values, that ranged from 38.7 ± 6.5 to 93.6 ± 31.1, between the groups of *B. areolata* ($p > 0.05$) (Table 14).

Buccal ganglia: One cluster of immunoreactive neurons was observed in the buccal ganglia (Fig. 46A-F). Both in the left and right buccal ganglion, the NPC of this cluster were not different between the groups of imposex females, untreated males and imposex females ($p > 0.05$) (Table 13) and the total mean values were 7.8 ± 0.6 and 6.6 ± 0.5 for left and right ganglion respectively. Comparisons of the average numbers of total immunoreactive neurons gathered from both sides of the buccal ganglia showed that the numbers of immunoreactive neurons were similar in all groups of *B. areolata* ($p > 0.05$) (Table 14).

Table 11. Average number of APGWamide-like immunoreactive neurons per cluster (NPC) (± S.E.) in various cell clusters of parietal ganglia in different groups of *B. areolata* (n = 5).

Groups	Clusters of neuron								
	1	2	3	4	5	6	7	8	9
Left ganglion									
Normal female	5.0 ± 1.5^{a}	23.0 ± 9.0	5.0 ± 1.0^{a}	12.0 ± 6.9^{ab}	23.5 ± 1.5	6.0 ± 4.0^{a}	25.3 ± 18.5	nd	6.5 ± 0.5^{a}
Imposex 1	1.3 ± 0.3^{a}	19.0 ± 3.0	5.5 ± 1.7^{a}	7.3 ± 1.3^{ab}	13.8 ± 5.0	13.0 ± 1.5^{a}	56.3 ± 0.9	nd	9.7 ± 0.9^{ab}
Imposex 2	7.3 ± 0.3^{a}	23.3 ± 6.8	10.0 ± 3.0^{a}	10.3 ± 3.5^{ab}	18.3 ± 4.5	10.2 ± 3.1^{a}	41.0 ± 14.8	nd	6.3 ± 0.3^{a}
Imposex 3	7.3 ± 2.3^{a}	20.8 ± 6.0	6.8 ± 2.8^{a}	28.0 ± 6.5^{b}	21.8 ± 4.6	20.5 ± 8.9^{ab}	45.0 ± 13.7	nd	9.8 ± 1.8^{ab}
Imposex 4	5.3 ± 3.0^{a}	5.5 ± 3.5	1.7 ± 0.7^{a}	3.0 ± 1.0^{a}	5.0 ± 1.5	2.5 ± 1.5^{a}	nd	13.0 ± 1.0	nd
Imposex 5	9.7 ± 3.2^{a}	12.5 ± 7.5	29.3 ± 4.4^{b}	8.8 ± 1.7^{ab}	23.5 ± 0.5	nd	nd	17.5 ± 1.5	15.0 ± 1.0^{b}
Normal male	20.5 ± 0.5^{b}	42.5 ± 19.5	30.3 ± 10.0^{b}	nd	16.0 ± 8.0	42.0 ± 2.0^{b}	18.5 ± 7.5	nd	nd

Within each column, means sharing the same superscript letter are not significantly different from each other; means with different superscript letters are significantly different (one-way ANOVA, $p < 0.05$). nd = not detected.

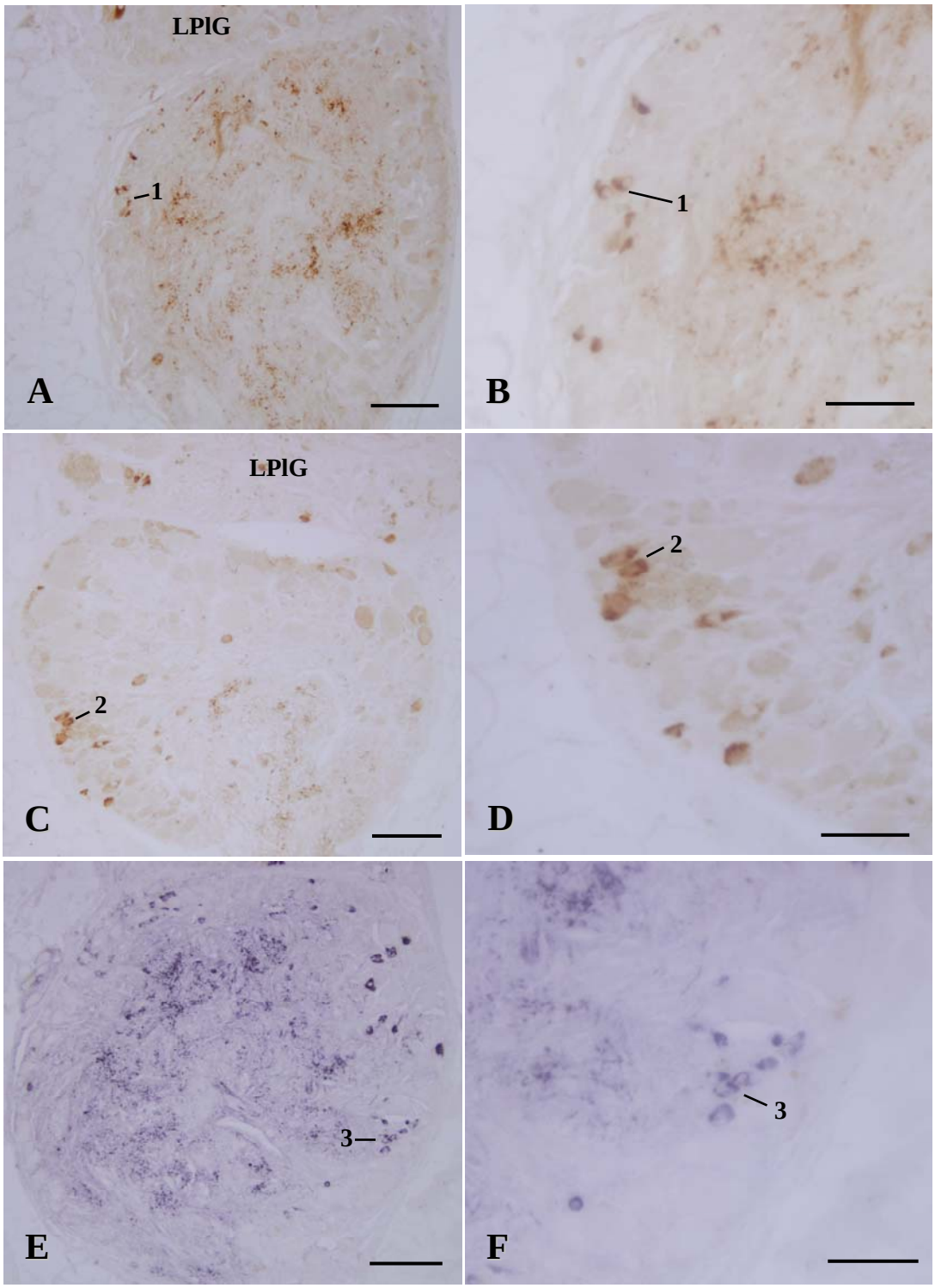

Figure 41. Left parietal ganglion of *B. areolata* with APGWamide-immunopositive neurons (cluster 1-3). **A-B**: Cluster 1 in imposex stage 5. **C-D**: Cluster 2 in normal male. **E-F**: Cluster 3 in imposex stage 2. LPlG-left pleural ganglion. Scale bars = 50 µm (B, D, F) and 100 µm (A, C, E).

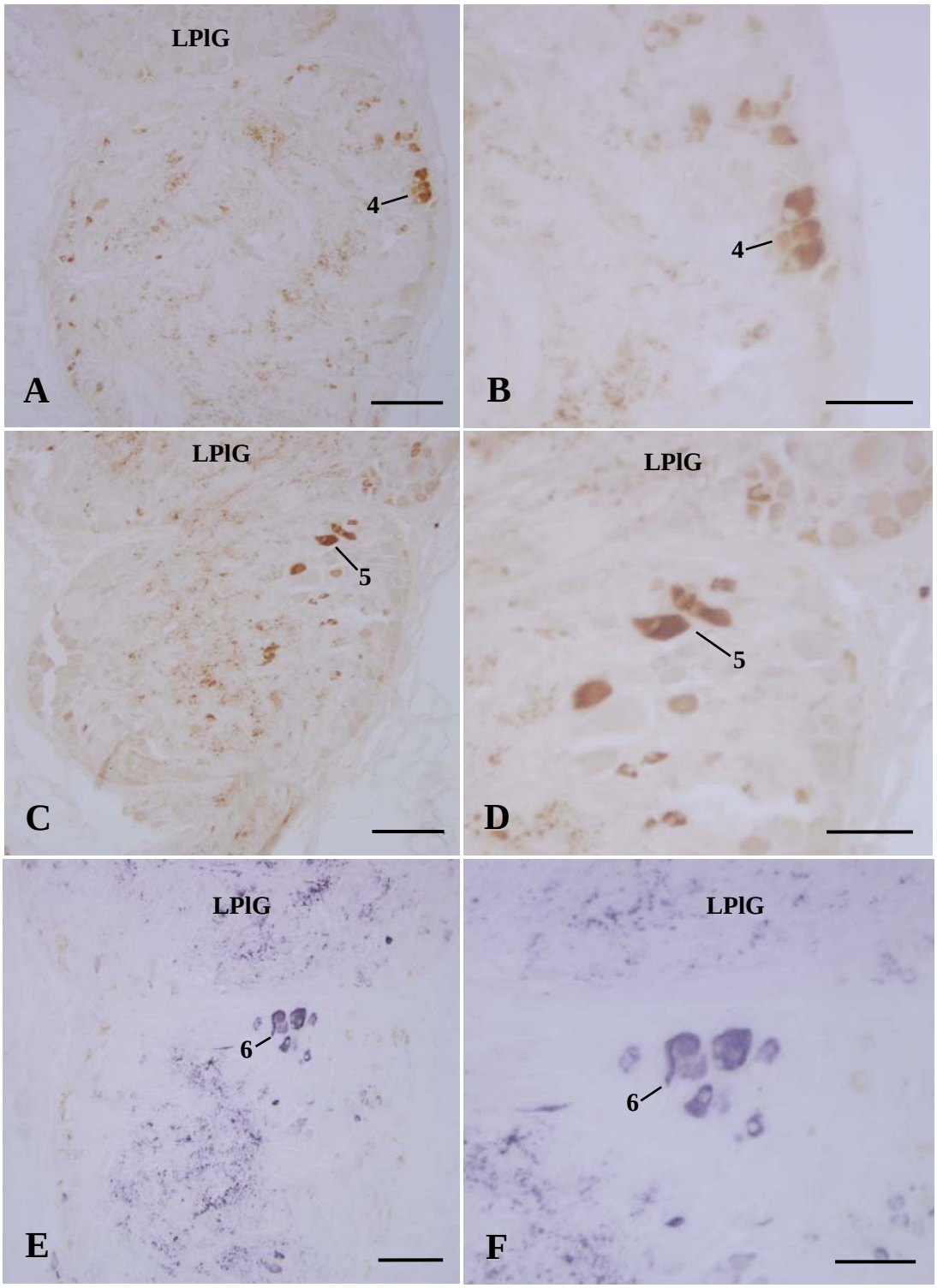

Figure 42. Left parietal ganglion of *B. areolata* with APGWamide-immunopositive neurons (cluster 4-6). **A-B**: Cluster 4 in imposex stage 5. **C-D**: Cluster 5 in normal male. **E-F**: Cluster 6 in imposex stage 2. LPlG-left pleural ganglion. Scale bars = 50 µm (B, D, F) and 100 µm (A, C, E).

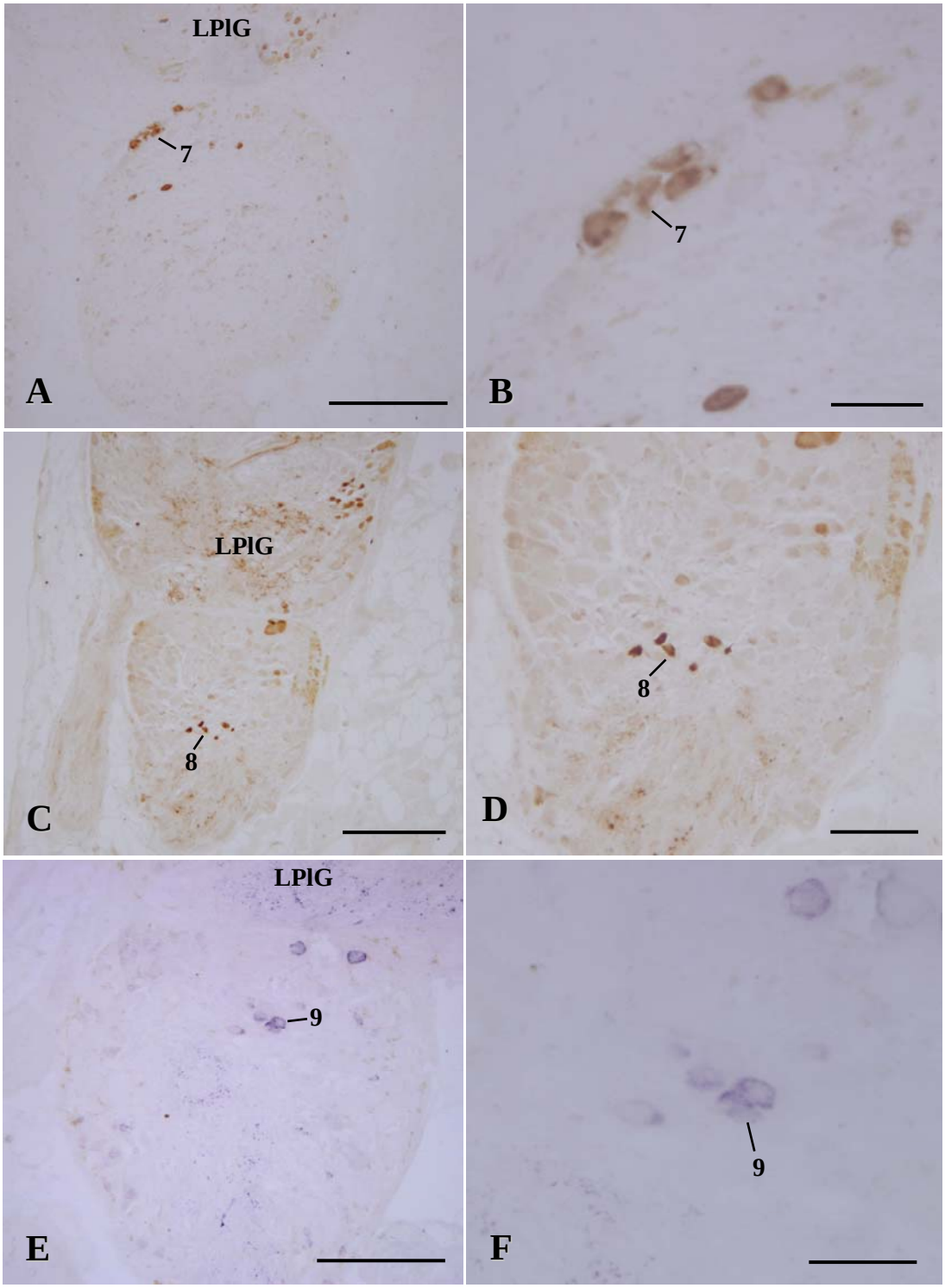

Figure 43. Left parietal ganglion of *B. areolata* with APGWamide-immunopositive neurons (cluster 7-9). **A-B**: Cluster 7 in normal male. **C-D**: Cluster 8 in imposex stage 5. **E-F**: Cluster 9 in normal female. LPlG-left pleural ganglion. Scale bars = 50 µm (B, F), 100 µm (D), 200 µm (E) and 250 µm (A, C).

Table 12. Average number of APGWamide-like immunoreactive neurons per cluster (NPC) (± S.E.) in various cell clusters of pedal ganglia in different groups of *B. areolata* (n = 5).

Groups	Clusters of neuron			
	1	2	3	4
Left ganglion				
Normal female	7.4 ± 1.9	7.7 ± 5.7	6.3 ± 0.7	12.0 ± 1.0
Imposex 1	6.7 ± 0.9	14.3 ± 0.9	12.0 ± 2.1	10.0 ± 0.6
Imposex 2	7.0 ± 1.5	21.0 ± 7.5	12.7 ± 4.2	8.7 ± 0.9
Imposex 3	6.5 ± 2.5	20.0 ± 7.5	15.7 ± 6.2	6.0 ± 4.0
Imposex 4	5.7 ± 2.3	15.7 ± 6.8	nd	2.5 ± 0.5
Imposex 5	10.2 ± 1.5	22.0 ± 2.4	6.6 ± 1.6	8.5 ± 1.2
Normal male	8.0 ± 1.5	15.5 ± 5.1	9.0 ± 1.0	11.7 ± 1.2

Within each column, means without any superscript letters are not significantly different from each other (one-way ANOVA, $p > 0.05$). nd = not detected.

Right ganglion				
Normal female	9.3 ± 2.4	9.7 ± 5.8	7.0 ± 1.0	3.5 ± 2.5
Imposex 1	6.3 ± 0.3	6.7 ± 0.7	13.0 ± 1.5	9.7 ± 1.9
Imposex 2	12.3 ± 2.0	10.0 ± 4.5	16.7 ± 0.3	1.0 ± 0.0
Imposex 3	12.0 ± 0.0	9.7 ± 4.4	11.0 ± 5.0	4.0 ± 2.0
Imposex 4	8.5 ± 3.5	8.0 ± 2.0	nd	3.0 ± 2.0
Imposex 5	9.2 ± 2.5	14.6 ± 4.1	11.0 ± 1.4	7.8 ± 1.4
Normal male	8.0 ± 2.0	12.5 ± 2.9	14.3 ± 0.7	9.3 ± 1.7

Within each column, means without any superscript letters are not significantly different from each other (one-way ANOVA, $p > 0.05$). nd = not detected.

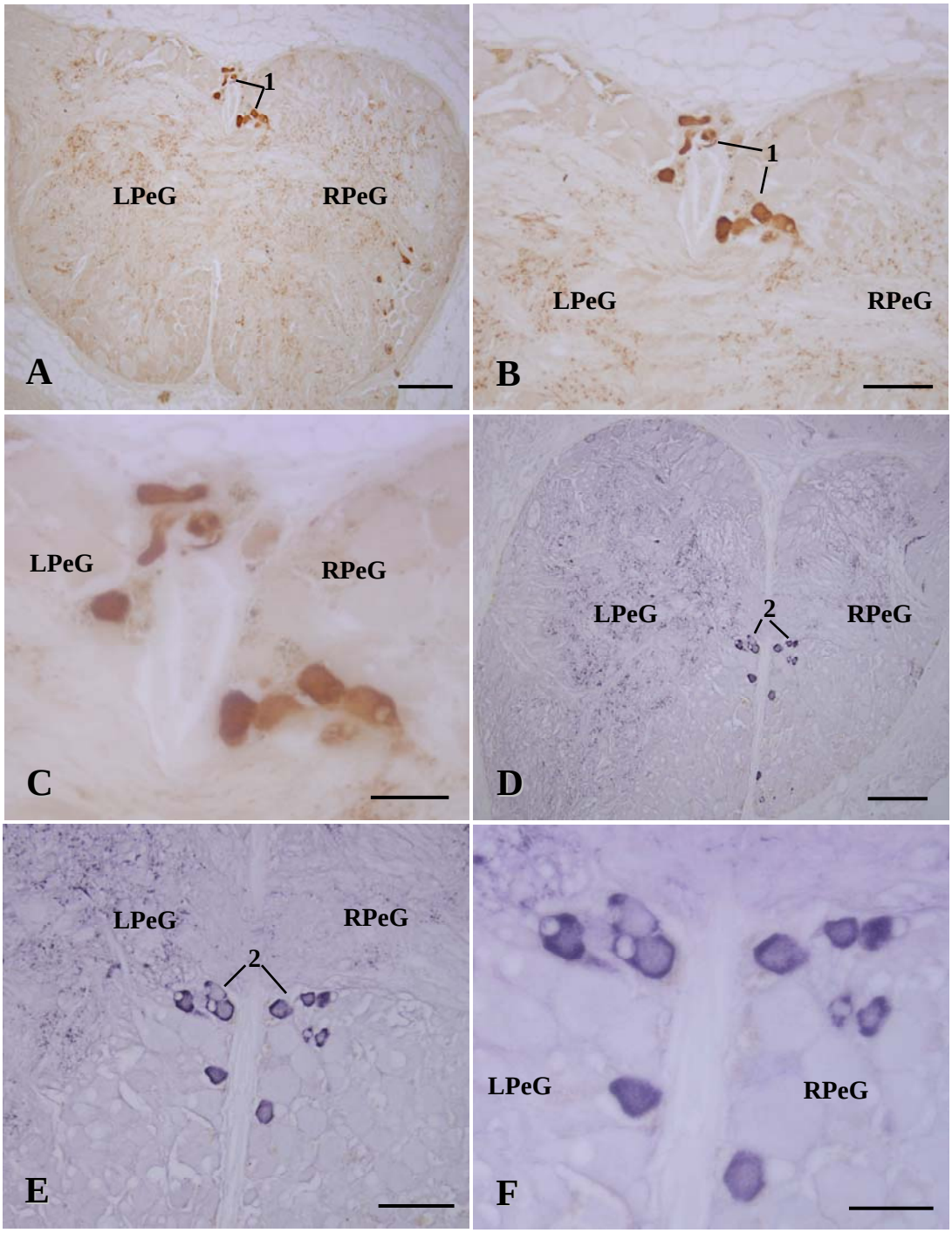

Figure 44. Pedal ganglia of *B. areolata* with neurons stained well with anti-APGWamide (cluster 1-2). **A-C**: Cluster 1 in imposex stage 5. **D-F**: Cluster 2 in normal female. LPeG-left pedal ganglion; RPeG-right pedal ganglion. Scale bars = 50 µm (C, F), 100 µm (B, E) and 200 µm (A, D).

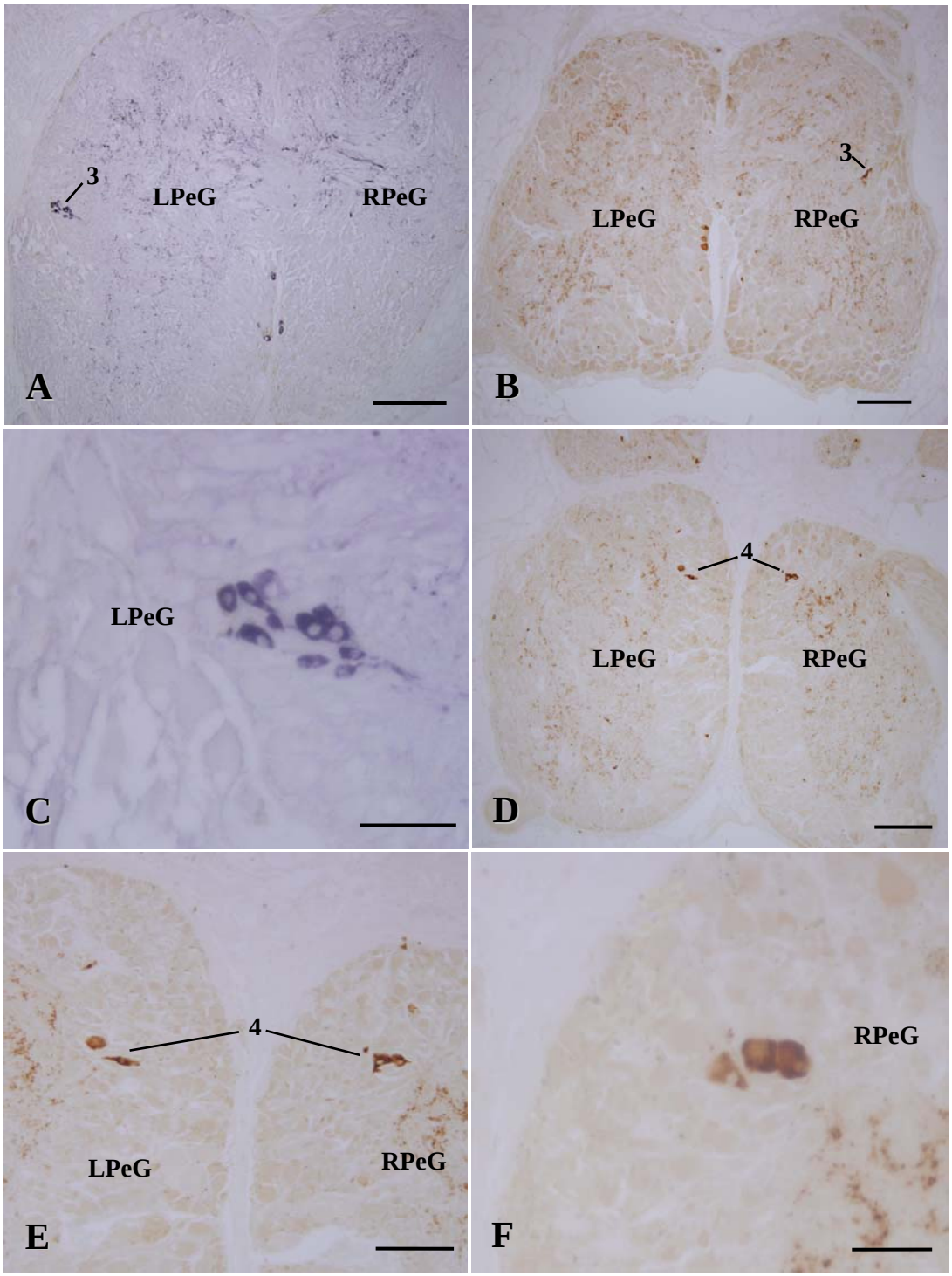

Figure 45. Pedal ganglia of *B. areolata* with neurons stained well with anti APGWamide (cluster 3-4). **A-C**: Cluster 3 normal female. **D-F**: Cluster 4 in normal male. LPeG-left pedal ganglion; RPeG-right pedal ganglion. Scale bars = 50 µm (C, F), 100 µm (E), 200 µm (B, D) and 250µm(A).

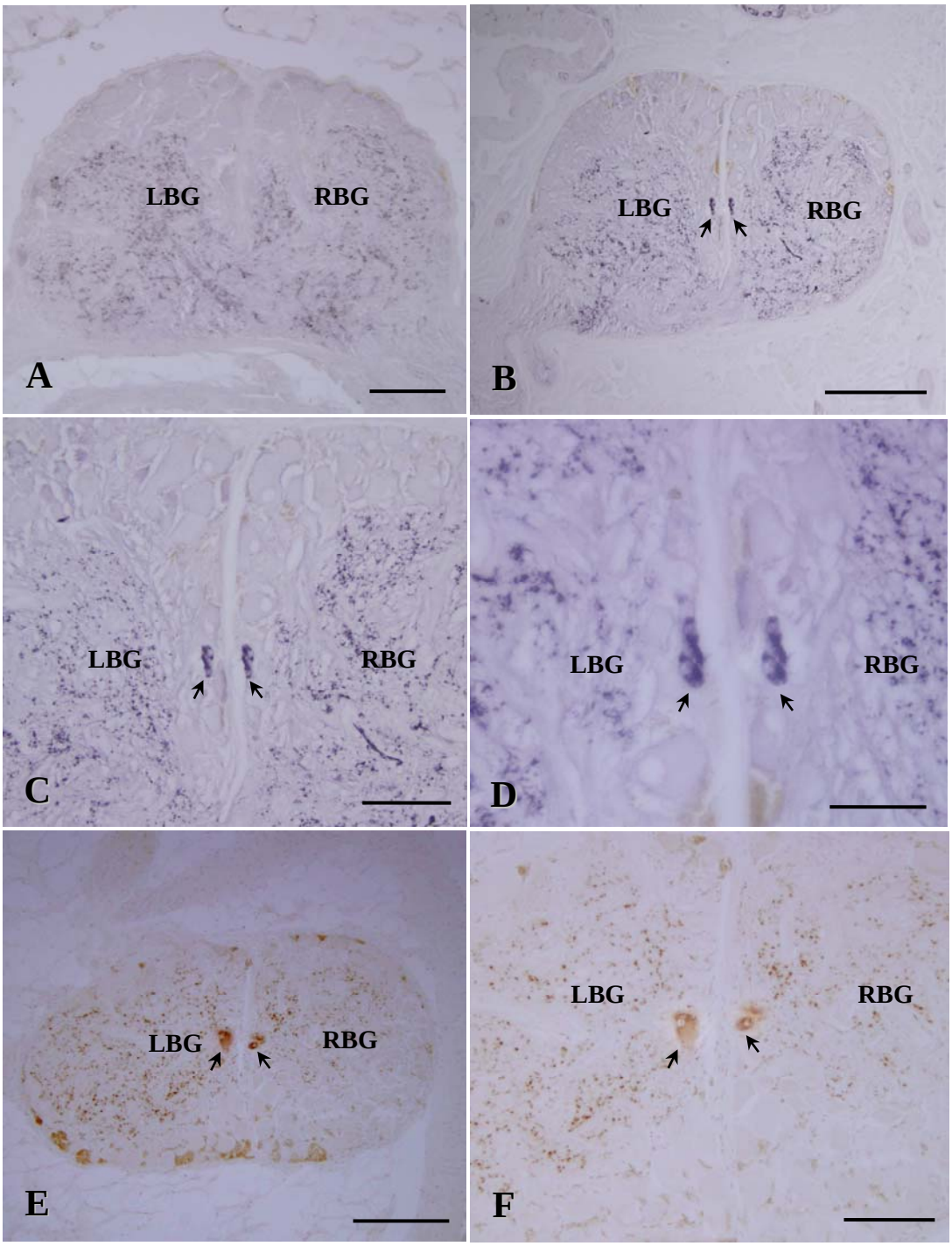

Figure 46. Buccal ganglia of *B. areolata* showing APGWamide-like immunoreactivity in one cluster of neurons (arrows). **A**: In imposex stage 4 with no stained neurons. **B-D**: In normal female. **E-F**: In imposex stage 5. LBG-left buccal ganglion; RBG-right buccal ganglion. Scale bars = 50 µm (D), 100 µm (A, C, F), 200 µm (E) and 250 µm (B).

Table 13. Average numbers of total immunoreactive neurons (± S.E.) gathered from each side of ganglia in different groups of *B. areolata* (n = 5).

Groups	Ganglia				
	Cerebral	Pleural	Parietal	Pedal	Buccal
Left ganglion					
Normal female	51.7 ± 20.7[a]	67.4 ± 30.7[a]	66.8 ± 28.7[ab]	20.6 ± 4.1[a]	7.5 ± 1.5
Imposex 1	65.0 ± 16.2[a]	126.7 ± 47.8[a]	82.2 ± 24.0[ab]	43.0 ± 2.5[b]	7.5 ± 1.5
Imposex 2	60.0 ± 17.8[a]	117.0 ± 21.3[a]	94.4 ± 30.4[ab]	49.3 ± 4.7[b]	6.5 ± 0.5
Imposex 3	82.6 ± 21.2[a]	104.8 ± 22.6[a]	7 2.3 ± 27.5[ab]	44.0 ± 5.6[b]	7.5 ± 1.5
Imposex 4	73.0 ± 18.3[a]	56.0 ± 19.7[a]	28.0 ± 6.1[a]	23.0 ± 5.1[a]	nd
Imposex 5	126.2 ± 21.9[b]	238.2 ± 55.7[b]	123.3 ± 38.1[ab]	45.6 ± 2.7[b]	11.0 ± 0.0
Normal male	180.4 ± 47.0[b]	305.3 ± 38.8[b]	159.8 ± 15.0[b]	39.0 ± 6.8[b]	6.5 ± 0.5

Within each column, means sharing the same superscript letter are not significantly different from each other; means with different superscript letters are significantly different (one-way ANOVA, $p < 0.05$). nd = not detected.

Right ganglion					
Normal female	50.5 ± 12.4[a]	73.0 ± 27.5[a]	nd	73.0 ± 27.5	8.0 ± 3.0
Imposex 1	93.8 ± 22.2[ab]	105.3 ± 51.5[ab]	nd	35.7 ± 1.2	6.0 ± 1.0
Imposex 2	60.0 ± 17.8[a]	164.3 ± 44.3[ab]	nd	39.7 ± 4.9	6.5 ± 1.5
Imposex 3	85.6 ± 11.7[ab]	128.2 ± 22.3[ab]	nd	27.7 ± 14.1	5.5 ± 0.5
Imposex 4	56.0 ± 11.0[a]	65.5 ± 18.2[a]	nd	15.7 ± 5.5	nd
Imposex 5	144.2 ± 35.8[b]	155.0 ± 30.2[ab]	nd	41.0 ± 2.9	7.0 ± 1.0
Normal male	162.4 ± 23.9[b]	194.0 ± 24.5[b]	nd	38.8 ± 7.4	6.5 ± 0.5

Within each column, means sharing the same superscript letter are not significantly different from each other; means with different superscript letters are significantly different (one-way ANOVA, $p < 0.05$). nd = not detected.

Table 14. Comparisons of the total immunoreactive neurons (mean ± S.E.) (computed from both sides of ganglia) between groups of *B. areolata* (n = 5).

Groups	Ganglia			
	Cerebral	Pleural	Pedal	Buccal
Normal female	89.3 ± 30.9[a]	140.4 ± 55.5[a]	93.6 ± 31.1	15.5 ± 4.5
Imposex 1	196.6 ± 37.1[a]	200.3 ± 85.2[a]	78.7 ± 2.0	13.5 ± 0.5
Imposex 2	120.0 ± 35.6[a]	248.4 ± 67.8[a]	89.0 ± 9.5	13.0 ± 2.0
Imposex 3	168.2 ± 31.2[a]	233.0 ± 43.7[a]	71.7 ± 19.6	13.0 ± 1.0
Imposex 4	110.3 ± 38.0[a]	108.4 ± 22.8[a]	38.7 ± 6.5	nd
Imposex 5	288.6 ± 37.4[b]	460.3 ± 68.6[b]	86.6 ± 4.5	18.0 ± 1.0
Normal male	324.6 ± 64.6[b]	432.2 ± 72.1[b]	77.8 ± 12.9	13.0 ± 1.0

Within each column, means sharing the same superscript letter are not significantly different from each other; means with different superscript letters are significantly different (one-way ANOVA, $p < 0.05$). nd = not detected.

4.2. Peripheral reproductive organs

To validate the role of the APGWamide immunoreactive neurons in the control of reproductive activity, in addition to the ganglia, the presence of immunoreactivity in the reproductive organs of *B. areolata* (normal male, normal female, and imposex female in stage 5) was investigated. These organs consisted of gonads (testes in normal males as well as ovaries in normal females and imposex stage 5) and penis (in normal males and imposex stage 5). Based on the immunohistochemistry, no peripheral APGWamide immunoreactive somata were observed in any of these reproductive tissues examined, but intense APGWa-lir in nerve processes was detected. To start with the APGWamide distribution in the gonads, the sections taken from a testis in the mature stage of the normal male showed that the entire testis was surrounded by a layer of loose connective tissue at its outermost and contained numerous seminiferous tubules where sperm was produced (Fig. 47A, C). In this testis APGWamide immunopositive signals were clearly observed in both the seminiferous tubules and outer connective tissue that contained muscle, nerve fibers, and epithelial cells (Fig. 47B, D). Similarly, intense APGWa-lir was found in the spawned testes particularly in the connective tissue separating the seminiferous tubules (Fig. 47E). For the negative control, there was no APGWa-lir in the testicular section that stained with pre-immune serum (Fig. 47F).

The ovaries of the normal females were surrounded by a layer of loose connective tissue and had many ovarian follicles where various stages of female germ cell were developed (Fig. 48A, C). The APGWa-lir was confined to the interfollicular connective tissue of both the spawning (Fig. 48B) and developing (Fig. 48D-E) stages of ovaries, whereas no immunoreactivity was detected in the ovarian sections treated as the negative control (Fig. 48F). The spawned ovary of the imposex stage 5 displayed histological structures similar to those of the normal female ovary (Fig. 49A, C, E). In this group of snail, the APGWamide immunopositive staining was also generally like that seen in the normal female ovary and localized in the interfollicular connective tissue (Fig. 49B, D, F).

In transverse sections through the entire penis, it was obvious that the penis ducts of imposex females (stages 2-5) (Fig. 50C-F) consisted of a similar tissue

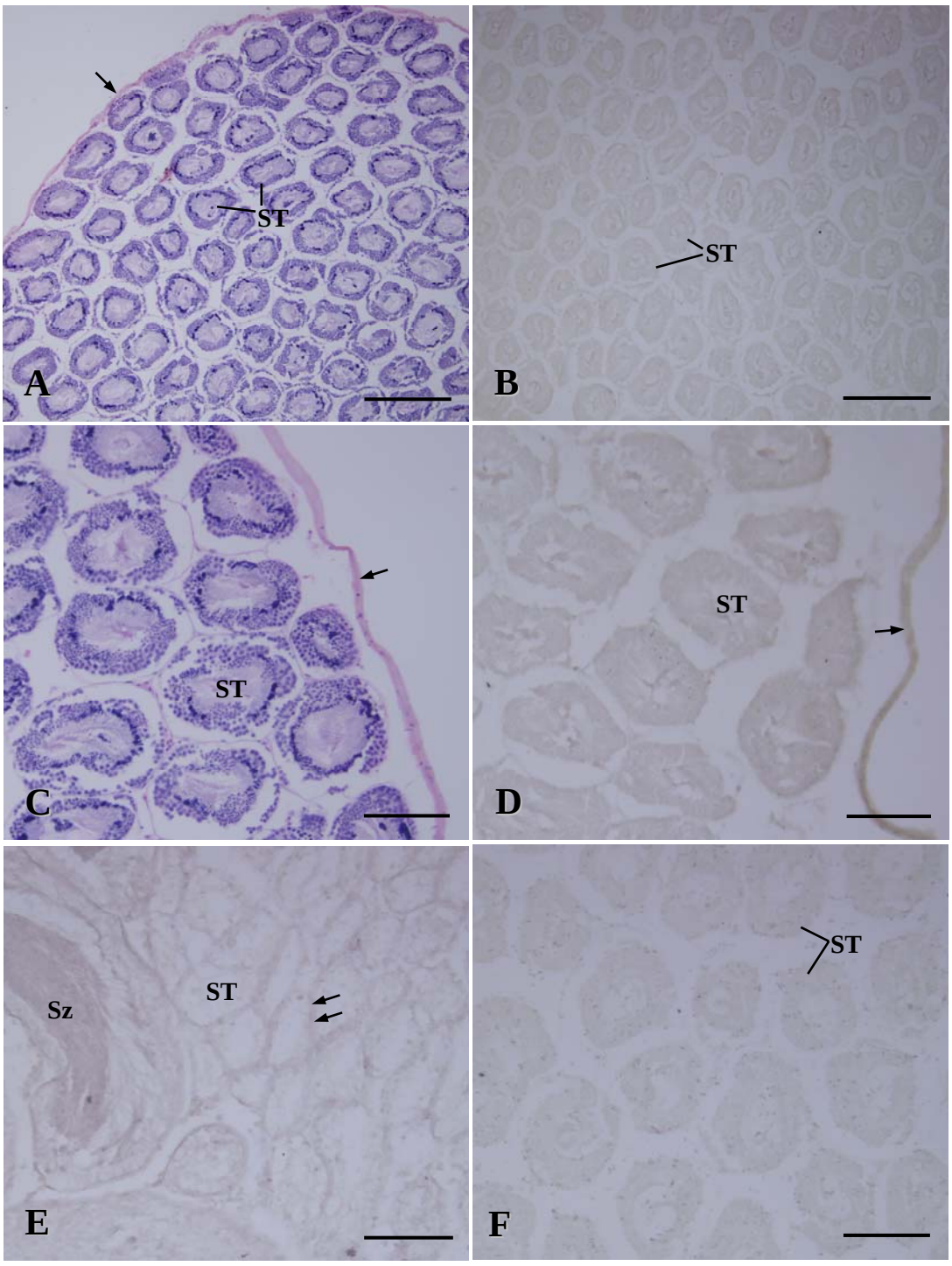

Figure 47. APGWamide-like immunoreactivity (APGWa-lir) in the testes of normal male *B. areolata*. **A-B**: Low power micrographs of testicular sections stained with H&E (A) and anti-APGWamide (B) showing a layer of loose connective tissue (arrows) and seminiferous tubules (ST). **C-F**: Medium power micrographs of testicular sections stained with H&E (C), anti-APGWamide (D-E), and pre-immune serum (negative control) (F). Note. APGWa-lir (double arrows) observed in the connective tissue of seminiferous tubules. Sz-spermatozoa. Scale bars = 100 µm (C-F) and 250 µm (A, B).

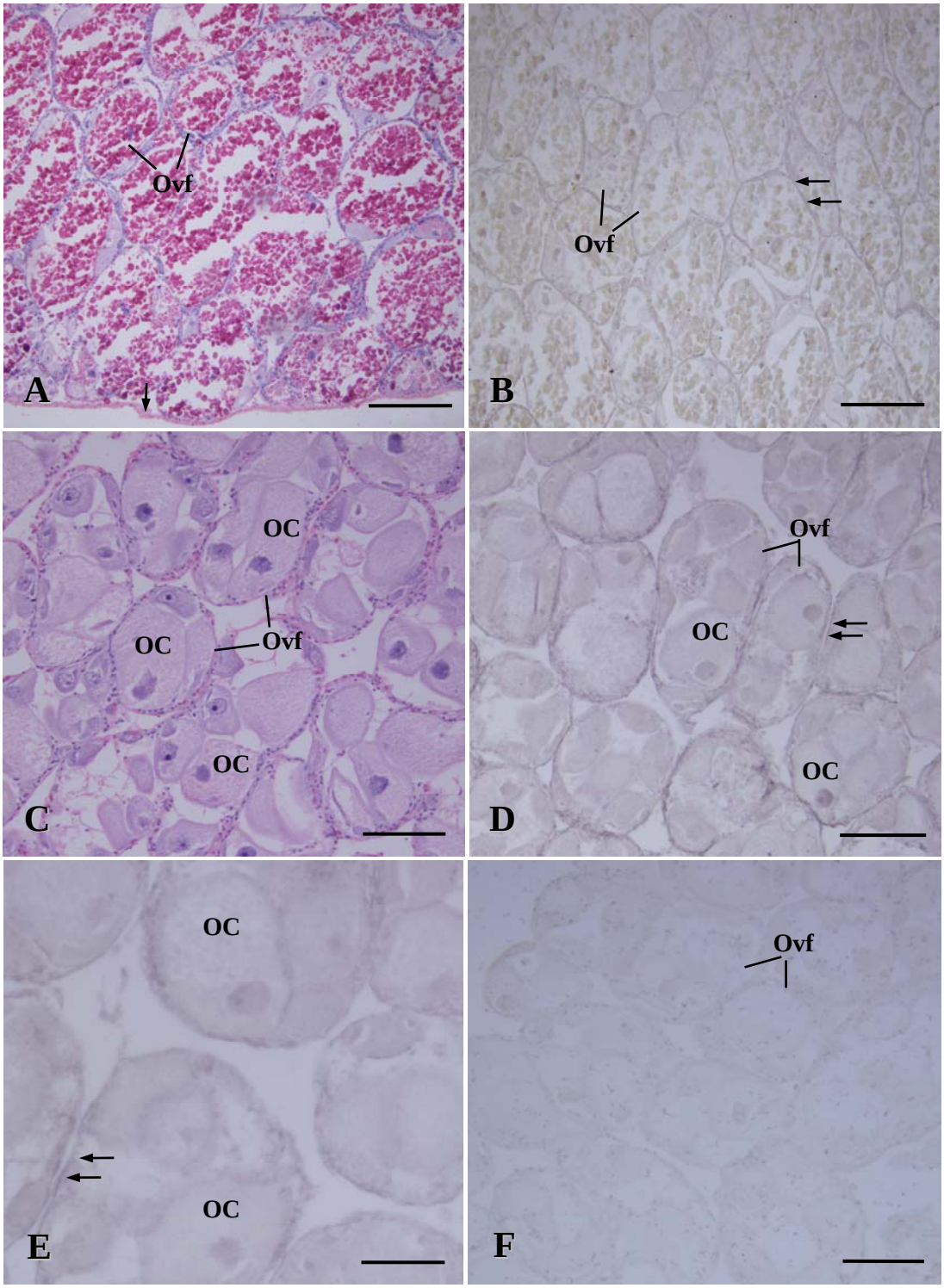

Figure 48. APGWamide-like immunoreactivity in the ovaries of normal female *B. areolata*. **A, C:** Ovarian sections stained with H&E. Note. A layer of loose connective tissue (arrow). **B, D, E:** Ovarian sections stained with anti-APGWamide. Note. APGWa-lir (double arrows) in the connective tissue between ovarian follicles. **F:** An ovarian section stained with pre-immune serum (negative control). OC-oocyte; Ovf-ovarian follicles. Scale bars = 50 µm (E), 100 µm (C, D, F) and 250 µm (A, B).

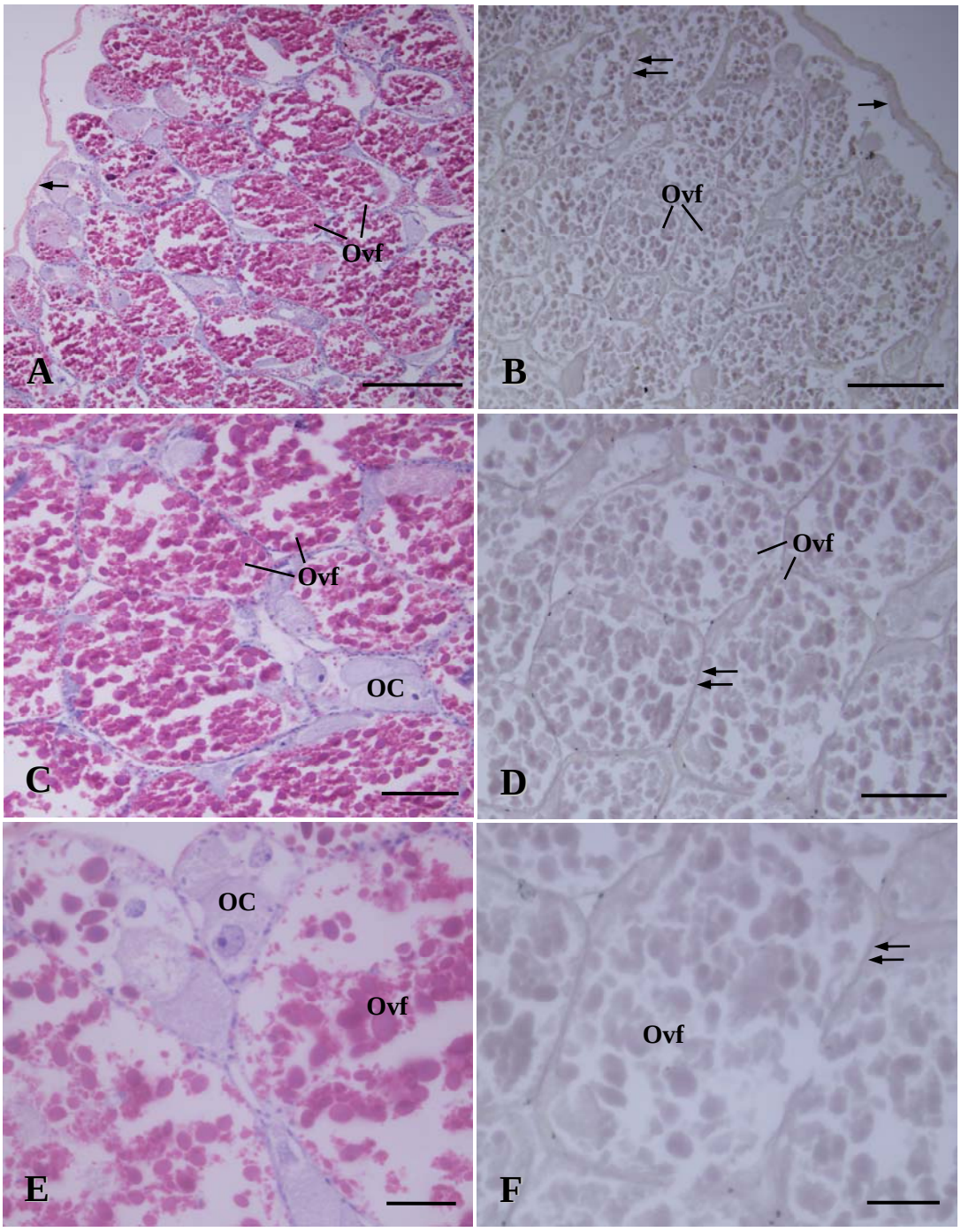

Figure 49. APGWamide-like immunoreactivity in the ovaries of female *B. areolata* in stage 5 of imposex. **A, C, E:** Ovarian sections stained with H&E. Note. A layer of loose connective tissue (arrow). **B, D, F:** Ovarian sections stained with anti-APGWamide. Note. APGWa-lir (double arrows) in the connective tissue between ovarian follicles. OC-oocytes; Ovf-ovarian follicles. Scale bars = 50 µm (E, F), 100 µm (C, D) and 250 µm (A, B).

component to those of the normal males (Fig. 50A-B) and was basically composed of three regions: an outer epithelium layer covering the entire penis and consisting of a loose connective tissue and a simple cuboidal epithelium, the layers of muscle fibers surrounding the penis ducts, and an inner epithelium layer (simple ciliated pseudostratified columnar epithelium) that lined the lumen of the penis duct. After investigating the presence of APGWa-lir in the penis of both the normal male (Fig. 51A-C) and imposex stage 5 (Fig. 52A-C), immunoreactive fibers and axons were detected in both the outer epithelium surrounding the entire penis, and a layer of loose connective tissue and muscle fibers underlying the outer epithelium. Furthermore, immunoreactive fibers and axons were also located in the layers of both the outer, longitudinal and inner, circular muscle fibers. In contrast the penile sections of the negative control displayed no APGWa-lir (Fig. 51D and Fig. 52D).

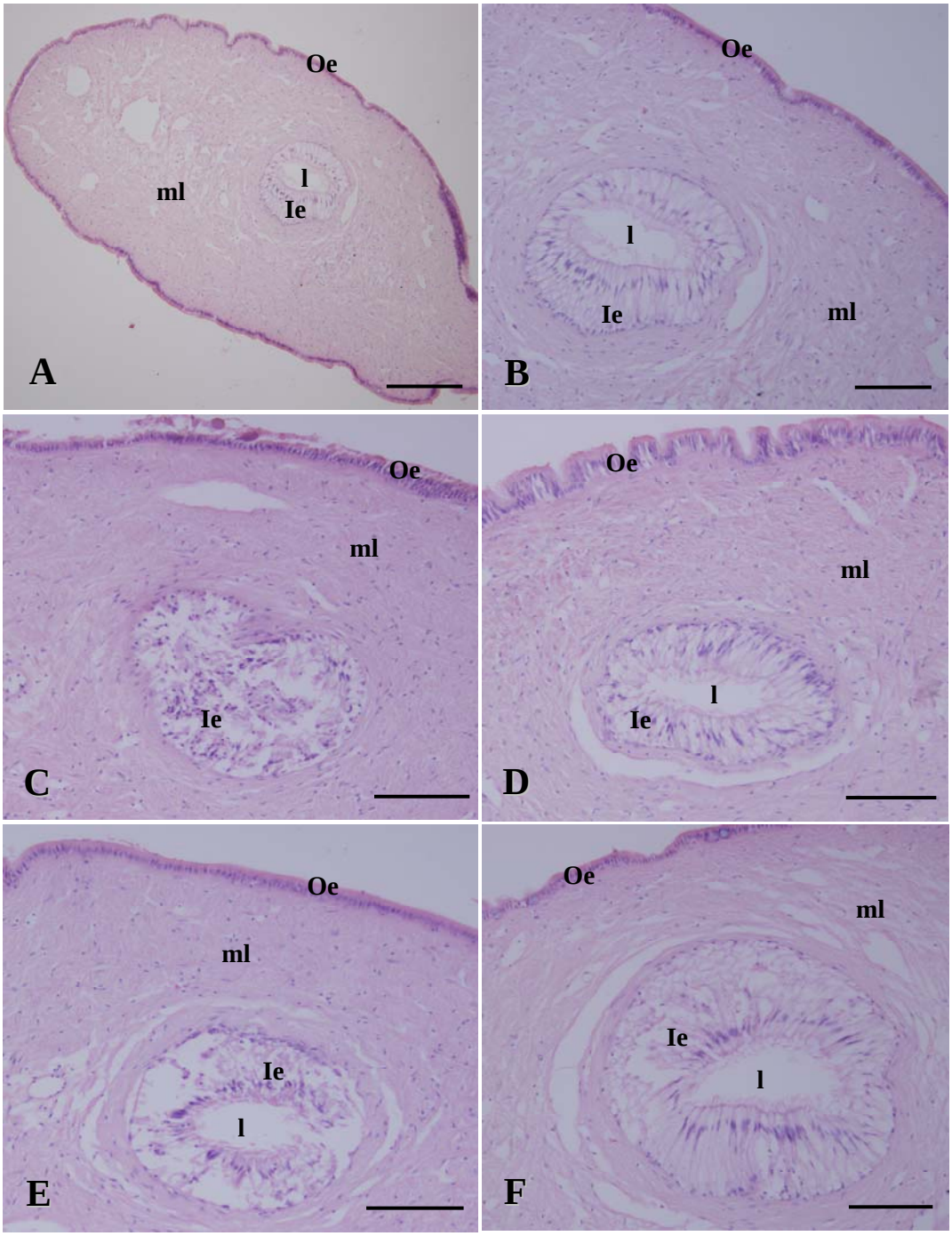

Figure 50. X-sections through the penis of *B. areolata* (H&E). **A-B**: Normal males. **C**: Imposex stage 2. **D**: Imposex stage 3. **E**: Imposex stage 4. **F**: Imposex stage 5. Ie-inner epithelium layer; l-lumen; m-muscle layers; Oe-outer epithelium layer. Scale bars = 100 µm (B-F) and 250 µm (A).

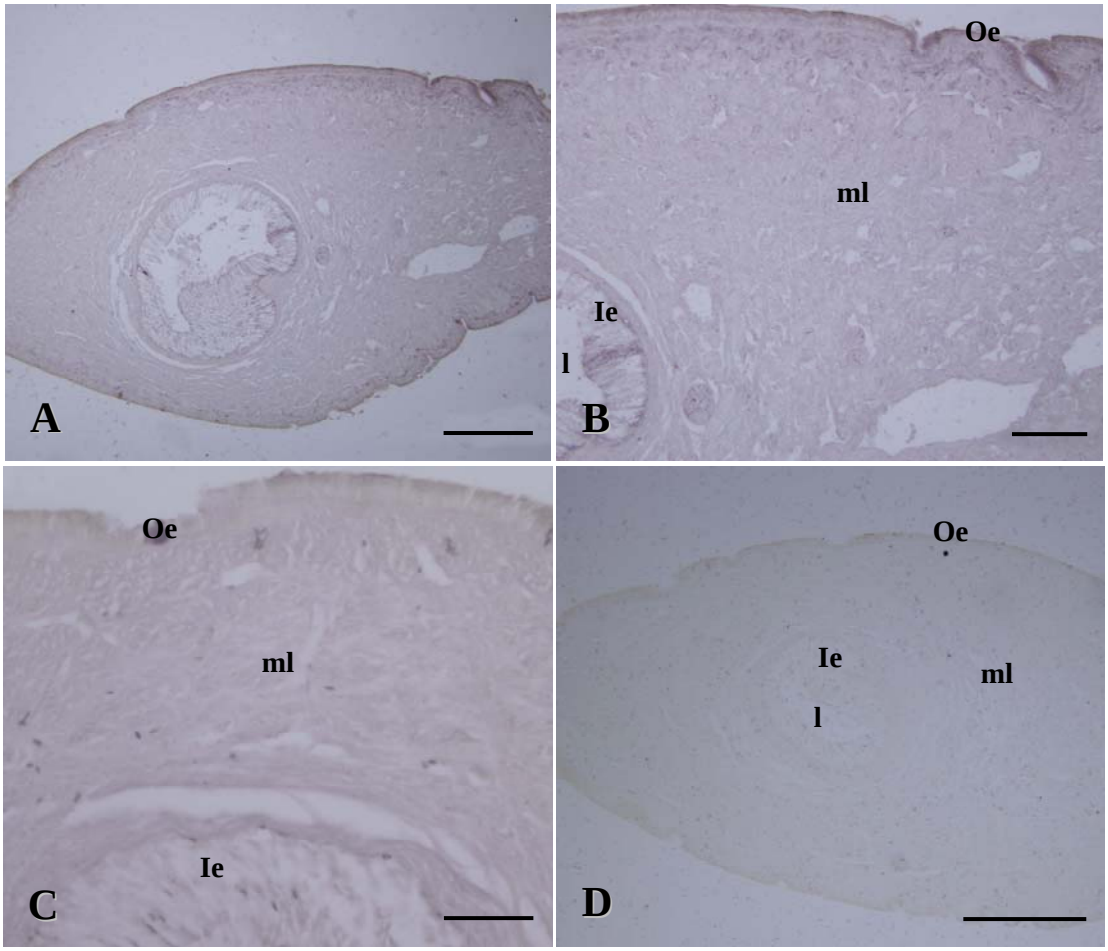

Figure 51. APGWamide-like immunoreactivity in the penis of the normal male *B. areolata*. **A-C:** Penile sections stained with anti-APGWamide showing immunopositive signals. **D**: A penile section stained with pre-immune serum (negative control). Ie-inner epithelium layer; l-lumen; ml-muscle layer; Oe-outer epithelium layer. Scale bars = 50 µm (C), 100 µm (B) and 250 µm (A, D).

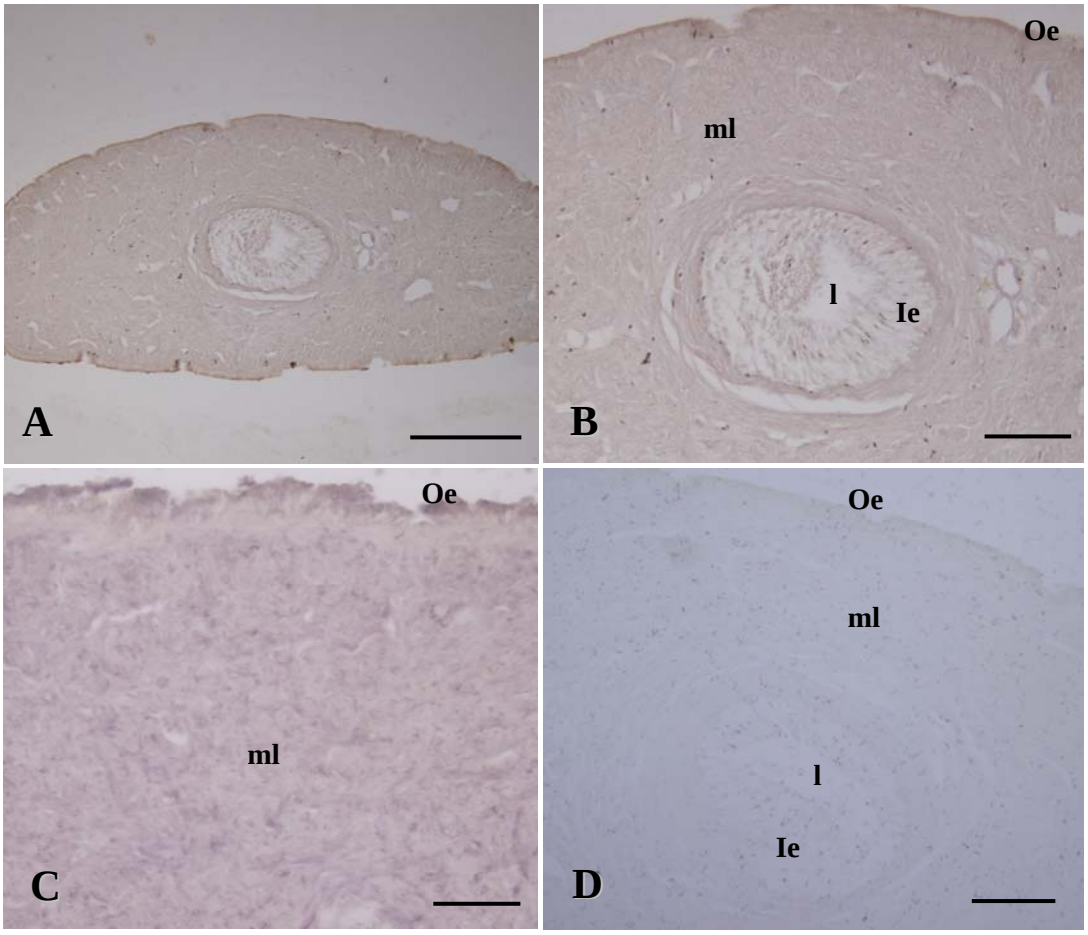

Figure 52. APGWamide-like immunoreactivity in the penis of the female *B. areolata* in stage 5 of imposex. **A-C**: Penile sections stained with anti-APGWamide exhibiting immunopositive signals. **D**: A penile section stained with pre-immune serum (negative control). Ie-inner epithelium layer; l-lumen; ml-muscle layer; Oe-outer epithelium layer. Scale bars = 50 µm (C), 100 µm (B, D) and 250 (A).

CHAPTER 4
DISCUSSION

This work has investigated the possible effects of TBT on the mortality of adult *B. areolata* and showed that in general the behavior of *B. areolata* adults was negatively affected by exposure to concentrations of 10 and 100 µg TBT/L, and the 96-h LC_{100} value was 100 µg/L. Although there are no reports on concentrations of TBT in Thai inshore seawaters, previous investigations on the concentrations of TBT in seawater in many countries have indicated that actual TBT concentrations in seawaters of Thailand may be less than 10 µg/L (Jamari, 2001) (below the LOEC and LC_{100}). Therefore, TBT pollution may have little effect on the mortality of the adult *B. areolata* in contaminated areas, particularly in the Gulf of Thailand. The chronic TBT-exposure experiment was performed using sublethal concentrations to test whether TBT is the sole cause of imposex and whether imposex effects could result in a low reproductive performance in *B. areolata*. The results clearly showed that all TBT concentrations (1, 10, 50, 100 and 500 ng TBT as Sn/L) had the potential to induce imposex in *B. areolata* in a time and concentration manner. The minimum concentration of 1 ng TBT as Sn/L that induced imposex in female *B. areolata* was also found in *I. obsoleta* (Gooding *et al*., 2003) at the same dose. Previous reports of the lowest concentration that caused imposex was 0.1 ng/L as Sn in the *I. obsoleta* (Gooding *et al*., 2003), whereas 1,000 ng TBT as Sn/L was the highest concentration tested in *B. undatum* (Mensink *et al*., 2002). The maximum concentration used in this study was 500 ng TBT as Sn/L; however, *B. areolata* was also exposed to the 1,000 ng TBT as Sn/L and it did induce imposex, but all of them died after 2 months of exposure (data not shown).

The VDSI is known to be the best index to determine the imposex intensity both in field and laboratory observations and its value exhibits a significant dependence on the TBT concentration (Gibbs *et al*., 1987). In this study, all VDSI values for *B. areolata* were never higher than 3. This indicated a low to moderate imposex intensity; this is in contrast to many gastropods taken from the field and laboratory surveys where the VDSI values are higher than 4, indicating a high degree

or intensity of imposex (Pellizzato *et al*., 2004; Staglicic *et al*., 2008). By using VDSI, it is possible to compare the TBT-sensitivity of different gastropod species and *B. areolata* seems to be less sensitive than others. On the other hand, the results clearly showed that TBT had an effect on the *B. areolata* by inducing imposex females to produce a penis that was almost the same length as that of a normal male penis. This contrast with other studies in which the FPL of imposex females was always smaller that those of the normal males as found in *B. undatum* (Mensink *et al*., 2002), and *Cymbiola nobilis* and *Melo melo* (Swennen and Horpet, 2008). In addition, a penis size of the imposex female *B. areolata* is > 60% that of the male (at the highest concentration of TBT at 500 ng as Sn/L where all RPSI values were above 60), and sometimes greater than that of the male (at the same dose where the values were > 100); this is in contrast to those of other species in which the female imposex penis size is always never larger than that of males (Blackmore, 2000). Furthermore, the *B. areolata* males treated with TBT showed malformation (excrescence) on their vas deferens that have not been previously reported in TBT-exposure experiments. This finding corroborates the field survey in *B. brandaris* from TBT-contaminated areas where one male exhibited excrescence on the penis and another one on the vas deferens (Ramon and Amor, 2001). Another interesting malformation observed in female *B. areolata* at stage 4 imposex was the development of a double penis which had been previously reported only in *B. undatum* (Mensink *et al*., 2002).

This thesis is the first attempt to detail the development of imposex in *B. areolata* from stage 1 to 6, although the final stage 6 was not found in this experiment. In general, TBT has no effect on reproduction in the imposex females of stages 1 to 4 (Mensink *et al*., 2002; Axiak *et al*., 2003) but it commonly causes the imposex females in the stages 5 and 6 to be effectively sterilized by two modes. The stage 5 females of *B. areolata* are sterilized by the first mode which is the blockage of the female genital opening by the tissue of the newly developed sperm duct (vas deferens and/or prostate gland) that prevents the release of egg capsules. This observation was similar to the findings in many gastropod species such as *O. aciculata* (Oehlmann *et al*., 1996), *T. clavigera* (Blackmore, 2000) and *H. trunculus* (Axiak *et al*., 2003). The second mode is a split of the bursa copulatrix and the capsule gland, preventing copulation and capsule formation, as found only in *O.*

aciculata (Oehlmann *et al*., 1996). Oehlmann *et al*. (1996) concluded this was a general symptom for population decline. They pointed out that if VDSI values are > 4.0, it indicates that part of the population is sterilized, leading to a high female mortality and low reproductive performance, as observed in *O. aciculata* (Oehlmann *et al*., 1996). This is not consistent with the results of the present study in which the imposex intensity in *B. areolata* is low to moderate (VDSI values ≤ 3) and there is also a low number of specimens from stage 5 (10 individuals) in *B. areolata*. It is suggested that TBT did not have any affects on the reproductive capacity of *B. areolata*.

Spermatogenesis in TBT-treated males

By using both light and electron microscopic investigations, the possible effect of TBT on the spermatogenesis was investigated in the male *B. areolata* exposed to 500 ng TBT as Sn/L for a period of six months and the results provided compelling evidence that the spermatogenesis in TBT-treated males was intact with no histological and ultrastructural changes. These results are comparable to the findings in *H. gigantea* exposed to 100 ng TBT/L for 2 months in which no significant histological changes were observed in the testis of males (Horiguchi *et al*., 2002). Although there are no other reports of such effect of TBT from those results it is reasonable to speculate that TBT, at environmentally relevant concentrations, may have no effect on the spermatogenesis in the TBT-treated males. However, in some cases, not TBT, but triphenyltin (TPT) can affect spermatogenesis in the male. For example, in *Marisa cornuarietis* exposed to nominal aqueous concentrations of 500 ng TPT as Sn/L for 2 and 3 months, and *Hinia reticulate* exposed to concentrations of 50, 125 and 500 µg TPT as Sn/kg (dry wt.) in artificial sediments for 1 month, a marked impairment of spermatogenesis (both species) was observed, including a disruption of germ cell formation, a high degree of testis atrophy, and maturation depletion containing degenerated spermatogonia and spermatids (Schulte-Oehlmann *et al*., 2000).

In addition to its advantage in detecting the adverse effect of various pollutants or toxins, the ultrastructures of spermatogenesis have been shown to be of great value for tracing phylogenetic and taxonomic relationships between gastropod

species (Riedal *et al*., 2001; Ropstorf *et al*., 2002; Giminenz *et al*., 2008; Zabala *et al*., 2009). In the present study, thus, the ultrastructural features of spermatogenesis in *B. areolata* were delineated and compared to others. *B. areolata* shows characteristic features of modified euspermatozoa as described by Maxwell (1983) and Voltzow (1994). In general, the euspermatogenesis and mature sperm of *B. areolata* conform to the type characteristic of most caenogastropods (Healy, 1996; Giminenz *et al*., 2008; Zabala *et al*., 2009). As in numerous other species studied (Suwanjarat and Klepal, 2001; Singhakaew *et al*., 2003; Hodgson *et al*., 2009), the spermatogonia of *B. areolata* posses a large spherical nucleus with one nucleolus and the cytoplasmic organelles are poorly developed. In early spermatids, the presence of a well-developed Golgi body indicates that it could be involved in acrosome and midpiece development during spermiogenesis. Many of the spermiogenesis features found in *B. areolata* are in line with those of the caenogastropods. These include substructural changes in the nucleus. In *B. areolata*, the pattern of nuclear condensation passing through the granular, fibrillar and lamellar phase is consistent with that reported in other prosobranchs (Suwanjarat and Klepal, 2001; Singhakaew *et al*., 2003; Hodgson *et al*., 2009). The euspermatozoa features of *B. areolata* closely correspond to many other neogastropods and also the so-called 'higher' mesogastropods (Buckland-Nicks and Chia, 1973; Healy, 1982). The diagnostic, shared characteristics of this euspermatozoa morphology include the following: (1) morphology of the acrosomal complex (shape of acrosomal vesicle, apical bleb, accessory membrane, basal plate and axial rod), (2) a solid electron-dense nucleus, (3) a midpiece composed of the axoneme surrounded by multiple (6-10) helical coiled mitochondria, (4) a glycogen piece with nine tracts of granules associated with the axonemal doublets, and (5) presence of a dense ring structure at the midpiece-glycogen piece junction. A truly conical acrosomal vesicle of *B. areolata* that is associated with the apical bleb at its extremity and the short accessory membrane at its base is similar to most caenogastropods (Ropstorf *et al*., 2002; Giminenz *et al*., 2008; Zabala *et al*., 2009). The *B. areolata* nucleus is short, rod-shaped and solid, with a short, shallow basal invagination for the insertion of the centriole/axoneme complex; this nuclear morphology has been found in many caenogastropods such as the Littorinoidea (Healy, 1996), Rissooidea (Ropstorf *et al*., 2002) and Muricoidea (Giminenz *et al*.,

2008). In relation to the midpiece of *B. areolata*, the outer layer of each mitochondrial element is considerable more electron-dense than the remainder of the matrix component (this dense layer having an angular, U-shaped profile in longitudinal section) and no recognizable cristae are observed. These findings are identical to those observed in some caenogastropod species of the superfamily Muricoidea such as *Zidona dufresnei* and *Provocator mirabilis* (Giminenz *et al*., 2008), *Adelomelon ancilla* (Zabala *et al*., 2009). The glycogen piece of *B. areolata* does not differ in any respect from the configuration shown to exist in many other caenogastropods (Ropstorf *et al*., 2002; Giminenz *et al*., 2008; Zabala *et al*., 2009), showing the typical microtubular pattern (9+2) associated with glycogen granules for each pair. The glycogen piece of *B. areolata* is separated from the midpiece by the junction that presents a complex ring elements attached to the plasma membrane. This complex structure of the double ring is similar to that recorded in many caenogastropods (Riedal *et al*., 2001; Ropstorf *et al*., 2002; Giminenz *et al*., 2008) and differs from the single ring annulus observed in the basal caenogastropods such as the Cerithioidea (Healy, 1982).

Oogenesis in imposex females

This study tried to characterize the overall effects of TBT on the process of gametogenesis in the ovaries of imposex female *B. areolata* using light and electron microscopy. At the lower imposex stages, at least up to 4, all *B. areolata* ovaries examined exhibited normal histological structures, similar to those of many prosobranch species affected by imposex e.g. *O. aciculata* (Oehlmann *et al*., 1996), *B. brandaris* (Ramon and Amor, 2001) *B. undatum* (Mensink *et al*., 2002) and *Thais rufotincta* (Cheng and Liu, 2004). In contrast imposex females (at stage 5 and 6) induced by TBT-after a severe spill incident could generally result in an occurrence of spermatogenesis in the ovaries as reported in *O. aciculate* (Oehlmann *et al*., 1996), *H. trunculus* (Axiak *et al*., 2003) and *B. japonica* (Horiguchi *et al*., 2006) from field observations as well as *N. lapillus* (Gibbs *et al*., 1988) and *H. gigantea* (Horiguchi *et al*., 2002) from laboratory studies of exposure to TBT. In the present study, histological and ultrastructural evidence, however, undoubtedly showed that no male tissue was developed in any specimens analyzed from imposex female *B. areolata* in

the stage 5 (totally ten individuals). This could be explained probably by the fact that ovarian spermatogenesis may normally occur with a low frequency or proportion. For example, in *O. aciculata* (Oehlmann *et al*., 1996), 11 of the 721 imposex female specimens analysed (1.5%) were characterized by having male gonads with seminiferous tubules and normal spermiogenesis in the ovaries. In *B. japonica,* a closely related species to *B. areolata*, ovarian spermatogenesis was observed in 6 of 92 imposex females for a frequency of about 6.5% (Horiguchi *et al*., 2006). At present the ultrastructures of ovarian spermatogenesis have been documented only in *H. trunculus* with the most advanced imposex stage (5); sperm-like structures were found with complete acrosomes and characteristic axonemes (9+2 microtubular structures) (Axiak *et al*., 2003). For the effects of TBT on oogenesis, at the light microscopic level two types of histopathological disorders were observed in the ovarian tissue of imposex female *B. areolata*: a diffused hemocytic infiltration and oocyte degeneration. The former was previously found in *T. clavigera* (Cheng and Liu, 2004) but the effect of this disorder on reproductive activity is unknown. The latter was indicated by the presence of egg atrophy and decreased yolk production, and found in many gastropod species such as has been reported by Gibbs *et al.* (1988) and Oehlmann *et al*. (1996). On the basis of TEM study, oogenesis in the imposex female *B. areolata* (stage 5) was similar to that of the normal female, indicating that an alteration of this process at the ultrastructural level did not occur as previously observed in *B. brandaris* (Amor *et al*. 2004). However, a significant difference in oogenesis of the imposex female *B. areolata* from the normal female was the presence of numerous lipid droplets in the cytoplasm at almost all stages of the oocytes development (especially in the vitellogenic oocytes) as well as of the follicle cells, and this is similar to those found in the imposex females of *H. trunculus* (Axiak *et al*. 2003). The occurrence of the lipid may be a first sign of oocyte degeneration that could finally lead to the suppression of oogenesis and the follicle cells might degenerate together with the oocytes. In this case, TBT is thought to be a causative agent for this histopathological disorder through a shift in energy balance from reproduction to detoxicification (Axiak *et al*. 2003).

The association between follicle cells and oocytes in gastropods is typical (review in Voltzow, 1994) but the structure and function of the follicles seem

to vary between species. The follicle cells of *B. areolata* are associated with all stages of oocytes, particularly the oogonia and pre-vitellogenic oocytes, and contain proliferated, proteosynthetic organelles including extensive, parallel arrays of RER and the well-developed Golgi bodies. In general, these active follicle cells are similar to those described in other caenogastropods: *I. obsoleta* (Taylor and Anderson, 1969) and *Colus stimpsoni* (West, 1981) as well as in the pulmonates, *Siphonaria serrata and Siphonaria capensis* (Pal and Hodgson, 2002) and appear to play an important role in oocyte nutrition. It is suggested in particular that *B. areolata* follicle cells might synthesize at least some yolk precursors which are then transported to the oocytes. Results of the present study provides evidence that vitellogenesis in oocytes of *B. areolata* involves both autosynthetic and heterosysthetic processes, whereas many species in the caenogastropods: a nassariid *I. obsoleta* (Taylor and Anderson, 1969), a muricid *B. brandaris* (Amor *et al*., 2004) and a buccinid *Neptunea arthritica cumingii* (Chung *et al*., 2006), a vitigastropod: *Haliotis varia* (Najmudeen, 2008) as well as a pulmonate: *S. capensis* (Pal and Hodgson, 2002) formed their yolk bodies only by autosynthesis involving the producing of yolk materials by the combined activities among proteosynthetic organelles. In *B. areolata*, this process is initiated in the early vitellogenic oocytes and involved with RER and Golgi bodies that increase in number and appear to synthesize one type of yolk body. As vitellogenesis proceeds in the late vitellogenic oocytes of *B. areolata*, it is evidence that the production of yolk body via autosynthesis is sometimes complemented by multivesicular bodies that develop considerably throughout the ooplasm. These structures have also been involved in yolk formation in the vitellogenic oocytes of *N. arthritica cumingii* (Chung *et al*., 2006) and *I. obsoleta* (Gerin, 1976). However, it is not possible to determine how the multivesicular bodies originate. As mentioned above, autosynthesis in *B. areolata*, like many other species, give rise to only one type of yolk body; however there is a possibility for gastropods to produce more than one types of yolk body, e.g. in the nerittid *Bathynerita naticoidea* in which a second type of yolk body may be derived from mitochondria (Eckelbarger and Young, 1997) but its exact origin and function still remain unclear. The formation of a yolk body via heterosynthesis involving endocytosis (West, 1981; Eckelbarger and Young, 1997) are less widespread than those for autosynthesis which has been suggested to be a

fundamental yolk-forming means in molluscs (Medina *et al*., 1986). In prosobranch gastropods, endocytotic activity in the oocytes, similar to that of *B. areolata*, seems to be confined to some species like the caenogastropods: the buccinid *C. stimpsoni* (West, 1981) and the neritimorph: the neritid *B. naticoidea* (Eckelbarger and Young, 1997), the patellogastropods: *Patella* spp. and *Helcion pectunculus* (Hodgson and Eckelbarger, 2000) as well as the pulmonate: *S. serrata* (Pal and Hodgson, 2002). This process appears in the cortical ooplasm of the late vitellogenic oocytes of *B. areolata* and is detected by the presence of endocytotic pits which later become vesicles that gradually fuse to form a yolk body. The appearance of these pits probably indicates the uptake of extra-ovarian substances but their origin has still to be identified. The mature yolk bodies of *B. areolata* are similar to those found in *B. brandaris* (Amor *et al*., 2004) and *N. arthritica cumingii* (Chung *et al*, 2006), as they exhibit an electron-dense core surrounded by a clear envelope that is typically composed of protein and carbohydrate, respectively (Gerin, 1976). Apart from these two components, there is also a limiting membrane at the outermost position of the yolk body in *N. arthritica cumingi* (Chung *et al*., 2006). In addition, the presence of the cortical granules that proliferate throughout the ooplasm of the late vitellogenic oocytes of *B. areolata* is similar to those found in the primitive gastropods such as the patellogastropods (*Patella* spp and *H. pectunculus*) (Hodgson and Eckelbarger, 2000), and the vitigastropod (*H. varia*) (Najmudeen, 2008). In contrast, this structure was not found in most of the studied caenogastropods such as *B. naticoidea* (Eckelbarger and Young, 1997), *B. brandaris* (Amor *et al*., 2004), and *N. arthritica cumingii* (Chung *et al*, 2006). Until now the origin of the cortical granules is still unclear for gastropods but some studies have suggested that they arise through the fusion of the Golgi vesicles (Hodgson and Eckelbarger, 2000). The mature oocytes of *B. areolata* develop microvilli similar to those found in *Patella* spp and *H. pectunculus* (Hodgson and Eckelbarger, 2000), and *H. varia* (Najmudeen, 2008). Apart from forming junctions with adjacent oocytes, microvilli help in absorption, transportation, and secretion of egg envelopes (Norrevang, 1968). It is interesting to note, however, that not all gastropod oocyes have microvilli, e.g. *B. naticoidea* (Eckelbarger and Young, 1997) and *N. arthritica cumingii* (Chung *et al*., 2006). Exocytosis is a process of releasing materials into the perivitelline space and has been observed in bivalves (Pipe, 1987;

Eckelbarger and Young, 1999). For the buccinid *B. areolata* this is the first report of such a process; however its role should be further investigated.

Distribution of APGWamide in imposex females.

To determine whether APGWamide plays a role in imposex induction in *B. areolata*, it was hypothesized that the distribution of APGWamide in the central nervous system (ganglia) and in reproductive organs (penis and ovary) of imposex females should be detected, and that imposex females should have an increase in APGWamide immunoreactive neurons. To our present knowledge, there have been no reports to determine the distribution of APGWamide in the ganglia of any species of gastropod imposex females. The present study with *B. areolata* is the first attempt to verify this issue and the results clearly showed, that from the total of five neural ganglia (cerebral, pleural, parietal, pedal and buccal) examined in all groups of *B. areolata* (5 stages of imposex females, normal male and normal female), the vast majority of immunoreactive neurons containing APGWamide was localized in these three ganglia: cerebral, pleural and parietal, while less abundant immunoreactive neurons was present in the pedal and buccal ganglia. The localization of APGWamide containing neurons in cerebral ganglia of male *B. areolata* corroborates to the findings in other gastropod species (Croll and Van Minnen, 1992; Li and Chase, 1995; De Lange and Van Minnen, 1998; Koene *et al*., 2000) and supports the idea that the cerebral ganglia is a major part of the central nervous system in secreting APGWamide in gastropods. Clusters of APGWamide containing neurons in the cerebral ganglia are well known to be associated with the control of male sexual behaviors as was found in many gastropod species such as the prosobranch *Rapana thomasiana* (Minakata *et al*., 1991), the opisthobranch *Aplysia* (Fan *et al*, 1997) and the pulmonate *Bulinus truncatus* (De Lange and Van Minnen, 1998). In addition, the presence of numerous APGWamide immunoreactive neurons in the pleural and parietal ganglia of male *B. areolata* provides the first evidence that they also appear to be the main ganglia producing APGWamide in this prosobranch species, and may play a similar role as those in the cerebral ganglia. This result is in contrast to other previously studied species where the pleural and parietal ganglia contain small number of the APGWamide immunoreactive cells, and appear to play less important

roles related to gastropod reproduction (Croll and Van Minnen, 1992; (Fan *et al*., 1997; De Lange and Van Minnen, 1998). For instance, each of the paired pleural ganglia in opisthobranch *Aplysia californica* occasionally contained 2-4 cells (Fan *et al*., 1997). In the right parietal ganglia of pulmonate *L. stagnalis*, the number of APGWamide containing neurons ranged from 8-10 (Croll and Van Minnen, 1992). Furthermore, although the pedal and buccal ganglia of *B. areolata* were not the main ganglia and had the APGWamide expressing neurons with lower amounts, similar to those found in other species (Croll and Van Minnen, 1992; Fan *et al*., 1997; De Lange and Van Minnen, 1998) but in some species, however, the pedal ganglia seem to be involved in the male reproduction as observed in *Lymnaea* where a cluster of excitatory motor neurons in the right pedal ganglia innervates the penis retractor muscle (PRM) (Rock *et al*., 1977). From that information, future investigations should be explored to determine the exact role of APGWamide containing neurons related to the male reproduction in each ganglia of other prosobrachs.

A growing body of evidence indicates that neuropeptides have been implicated in imposex induction by exogenous administration or bioassays (Feral and Le Gall, 1983; Oberdoster *et al*., 2005). The finding of an increase of an unidentified neurohormone, termed Penis Morphogenic Factor (PMF) in the cerebropleural and pedal ganglia of *O. erinacea* after exposure to TBT for 24 h provides the first evidence for a peptide hormone being involved in imposex induction, and implies in particular that TBT could cause an abnormal release of PMF to induce penis growth in imposex females (Feral and Le Gall, 1983). The role of the PMF in the control of the development of male Accessory Sex Organs (ASO) including the sperm duct, seminal vesicle, external sperm groove and the penis is supported by the fact that PMF produced by pedal ganglia induces the differentiation of penis in male *I. obsoleta* (Joosse, 1988). At present PMF has been identified in several species affected by imposex or intersex (Feral and Le Gall, 1983; Joosse, 1988; Deutsch and Fioroni, 1996), but it has not been chemically characterized. Recently, APGWamide has been proposed to be the putative PMF, because after seven and fourteen days of injection, only APGWamide (with a threshold dose near 10^{-16} moles), out of four neuropeptides, induces imposex in the mud snail *I. obsoleta* (Oberdorster and McClellan-Green, 2000). From this experiment, it is proposed that TBT has potent

biological activity to induce imposex via an abnormal release of APGWamide. This proposal is confirmed by the results of the present study in which although the numbers of total APGWamide immunoreactive neurons of imposex at stages 1 to 4 in each of the main ganglia (cerebral, pleural, and parietal) were similar and did not differ statistically from those of normal females, it was biologically apparent that their numbers tended to be slightly increased comparing to those of normal females. Taking these results together with the findings that the numbers of total APGWamide immunoreactive neurons in each of the main ganglia for the late stage of imposex (5) were increased up to those of the normal males, and were extremely higher than those of the early stages of imposex (1-4) and normal females, it was clear, in the present study, that an increase in the numbers of APGWamide immunoreactive neurons in the main ganglia caused by TBT seemed to play an important role in imposex induction in *B. areolata*. These results are comparable to the findings of Oberdoster *et al*. (2005) in *I. obsoleta* where the endogenous levels of APGWamide were measured by Western blotting of whole animal homogenates, not in the ganglia, and their results showed that imposex females had levels of APGWamide similar to control males and significantly higher than control females, indicating that endogenous changes in APGWamide also play a role in imposex induction in this species.

The above findings that APGWamide has an ability to induce imposex in *I. obsoleta* (Oberdorster and McClellan-Green, 2000) and that there is an increase in the levels of APGWamide in imposex females of *I. obsoleta* (Oberdorster *et al.,* 2005) and in the numbers of APGWamide immunoreactive neurons in *B. areolata* (present study) provides compelling evidence that APGWamide may be responsible for the control the generation and growth of the penis and vas deferens in the imposex females. This possible role of APGWamide in the control of the development of male sexual characteristics in females corresponds well to its widespread functions, that have been largely reported to acts as sex hormones in a variety of mollusc species such as gastropods (Fan *et al*., 1997; De Lange and Van Minnen, 1998; Koene *et al*., 2000), bivalves (Smith *et al*., 1997), and cephalopods (Di Cristo *et al*., 2005), and particularly to control male reproductive activity in gastropods (De Lange *et al*., 1998; De Lange and Van Minnen, 1998; Koene *et al*., 2000). The major role of APGWamide in the control of male reproductive behaviour of gastropods includes

controlling such diverse processes such as ejaculation of semen during copulation (Van Golgen *et al*., 1995), inhibition of the contractions of the penis retractor during penis eversion (Li and Chase, 1995) and induction of the preputium (De Boer *et al*., 1997). In the present study, this role of APGWamide was investigated by determining the presence of APGWamide immunoreactivity in the penis and gonads of *B. areolata*. The results showed that in both imposex females (stage 5) and normal males, APGWamide immunoreactive fibers and axons were mainly identified in the muscle layers surrounding their penis ducts. This innervation of a penial complex by the APGWamide immunoreactive neurons from the central nervous system (ganglia) has been previously reported elsewhere in gastropods (Croll and Van Minnen, 1992; Van Golgen *et al*., 1995; De Lange *et al*., 1997; Fan *et al*., 1997; De Lange and Van Minnen, 1998), and indicates that APGWamide may play a role in regulating reproductive function in normal male *B. areolata,* as it does in other gastropods, and supports the idea that this neuropeptide may be directly involved in the formation of the imposex female penis. In addition, APGWamide immunoreactivity was particularly found in the connective tissue of both outer epithelium and the seminiferous tubules in testis of normal male *B. areolata*. This pattern of APGWa-lir distribution corroborates to that observed in *Haliotis asinina* (Chansela *et al*., 2008) and its connective tissue, similar to that found in *B. areolata*, was composed of varicosed nerve fibers and muscle cells (Apisawetakan *et al*., 2001). It is believed that APGWamide stored in the nerve fibers may be released to stimulate the contraction of muscle cells in the outer epithelium and the seminiferous tubules, so that this contraction initiates the release of sperm from the testis (Chansela *et al*., 2008). Furthermore, APGWamide immunoreactivity was confined to the interfollicular connective tissue within the ovaries of both imposex and normal females of *B. areolata*. This result is consistent to that of the sea scallop, *Placopecten magellanicus* where APGWa-lir was localized to the gonadal integument and interacinal connective tissue (Smith *et al*., 1997). It is suggested, that in the present study, perhaps APGWamide is involved in the modulation of muscular contractions within the ovary of *B. areolata* during spawning, as this neuropeptide is known to have myoactive and modulating effects on muscles of some gastropods (Van Golgen *et al*., 1995; De Lange *et al*., 1997).

In general, three different suggested pathways (steroid, retinoid and neuroendocrine) have been proposed to explain imposex induction mechanisms. Previous studies related to first two pathways have been aimed to verify how TBT initially causes the development of male sexual organs in females (Bettin *et al*., 1996; Castro *et al*., 2007). Firstly, in the steroid hypothesis, it is proposed that TBT may inhibit at the steps of the aromatase system (Bettin *et al*., 1996) and/or excretion of testosterone to fatty acid (Ronis and Mason, 1996), leading to an increase in testosterone levels in females. Secondly, in *N. lapillus*, TBT effectively binds to the orthologue of the nuclear receptor Retinoid X Receptor (RXR) and moreover, injection experiment with 9cisRA, have suggested that the natural ligand of RXR, promoted the development of imposex to the same degree as TBT (in 100% of the injected females) (Castro *et al*., 2007), indicating that imposex induction may be mediated through the modulation of the RXR signaling pathways. In the present study for neuroendocrine hypothesis, it is not possible to determine whether an increase in APGWamide immunoreactive neurons is a primary factor, acting at the initial step of imposex induction, or just maintains the development of male sexual organs in the imposex female *B. areolata*. Although multiple hypotheses still exist for the exact mechanism of imposex induction, in the present study it is clear, that endogenous changes in neuropeptide APGWamide play an important role in this process in *B. areolata*.

CHAPTER 5
CONCLUSION

The findings of this study are as follows:

1. An acute toxicity test indicated that TBT at the concentrations of 0.001, 0.01, 0.1, 1 and 10 µg as Sn/L did not increase mortality of adult *B. areolata*. In addition, the LOEC (lowest observed effect concentration) and 96-h LC_{100} values were 10 and 100 µg TBT as Sn/L, respectively.

2. The chronic toxicity study indicated that TBT at a range of environmentally relevant concentrations (1-500 ng TBT as Sn/L) induced imposex in female *B. areolata* at a low to moderate intensity whereas at the highest dose it increased the length and size of the imposex female penis close to those of normal males. In addition, TBT also caused sterilization in the most advanced stage of the imposex female.

3. Based on the LM and TEM studies, TBT did not affect either spermatogenesis in the TBT-treated males or oogenesis in imposex females of *B. areolata*. Although imposex females did not exhibit male testicular tissue, the findings indicated that TBT has an impact on the reproductive function of *B. areolata*. In addition, the ultrastructure of euspermatogenesis in *B. areolata* is similar to those found in other species in the Buccinidae.

4. Vitellogenesis in *B. areolata* is generally consistent with that of prosobranchs and also related to that of pulmonates in having both auto and heterosynthetic processes. However, the appearance of cortical granules in the ooplasm and microvilli on the vitelline envelope appears to be a unique feature of *B. areolata,* which differs from other gastropods in the Buccinidae.

5. An immunohistochemical investigation revealed that the majority of APGWamide expressing neurons reside in the cerebral, pleural, and parietal ganglia of *B. areolata*. This finding is in line with the observation that TBT caused an increase in APGWamide positive neurons in these ganglia of imposex females, and might be responsible for the induction of imposex in this species.

6. The presence of APGWamide immunoreactivity in the reproductive organs of *B. areolata* might suggest the role of this neuropeptide in the control of reproductive activity in gastropods.

Author's comments:

The investigation of gametogenesis (oogenesis and ovarian spermatogenesis) in imposex females of *B. areolata* at the ultrastructural level was the main focus of the present study. However, the data obtained are insufficient to draw conclusions of the overall effects of TBT. Thus, additional investigations in *B. areolata* and/or other closely related species affected by imposex will be needed. In addition, in view of the wide-spread presence of APGWamide in the central ganglia and reproductive tract, it will be necessary to determine the role that APGWamide plays in the control of reproduction in *B. areolata*.

REFERENCES

Amor, M.J., Ramón, M. and Durfort, M. 2004. Ultrastructural studies of oogenesis in *Bolinus brandaris* (Gastropoda: Muricidae). Scientia Marina. 68(3): 343-353.

Apisawetakan, S., Chanpoo, M., Wanichanon, C., Linthong, V., Kruatrachue, M., Upatham, E.S., Pumthong, T. and Sobhon, P. 2001. Characterization of trabecular cells in the gonad of *Haliotis asinina* Linnaeus. Journal of Shellfish Research. 20: 717–724.

Axiak, V., Micallef, D., Muscat, J., Vella, A. and Mintoff, B. 2003. Imposex as a biomonitoring tool for marine pollution by tributyltin: some further observations. Environment International. 28(8): 743-749.

Bancrof, J.D. and Gamble, M. 2002. Theory and Practice of Histological Techniques. Churchill Livingstone: London.

Barroso, C.M. and Moreira, M.H. 2002. Spatial and temporal changes of TBT pollution along the Portuguese coast: Inefficacy of the EEC directive 89/677. Marine Pollution Bulletin. 44(6): 480-486.

Barroso, C.M., Moreira, M.H. and Bebianno, M.J. 2002. Imposex, female sterility and organotin contamination of the prosobranch *Nassarius reticulatus* from the Portuguese coast. Marine Ecology Progress Series. 230: 127-135.

Bauer, B., Fioroni, P., Ide, I., Liebe, S., Oehlmann, J., Stroben, E. and Watermann B. 1995. TBT effects on the female genital system of *Littorina littorea* - a possible indicator of tributyltin pollution. Hydrobiologia. 309:15–27.

Bettin, C., Oehlmann, J. and Stroben, E. 1996. TBT-induced imposex in marine neogastropods is mediated by an increasing androgen level. Helgolander Meeresuntersuchungen. 50(3): 299-317.

Blaber, S.J.M. 1970. The occurrence of a penis like out growth behind the right tentacle in spent females of *Nucella lapillus* (L.). Proceeding of the Malacological Society of London. 39: 231-233.

Blackmore, G. 2000. Imposex in *Thais clavigera* (Neogastropoda) as an indicator of TBT (tributyltin) bioavailability in coastal waters of Hong Kong**.** Journal of Molluscan Studies. 66(1): 1-8.

Bryan, G.W., Gibbs, P.E., Hummerstone, L.G. and Burt, G.R. 1986 The decline of the gastropod *Nucella lapillus* around south-west England: evidence for the effect of tributylin from antifouling paints. Journal - Marine Biological Association. 66(3): 611-640.

Buckland-Nicks, J.A. and Chia, F. 1973. The fine structure of the spermatozooan of *Littorina* (Gastropoda: Prosobranchia), with special reference to sperm motility. Zeitschrift für Zellforschung. 144: 111–129.

Castro, L.F.C., Lima, D., Machado, A., Melo, C., Hiromori, Y., Nishikawa, J., Nakanishi, T., Reis-Henriques, M.A. and Santos, M.M. 2007. Imposex induction is mediated through the Retinoid X Receptor signalling pathway in the neogastropod *Nucella lapillus.* Aquatic Toxicology. 85(1): 57-66.

Chansela, P., Saitongdee, P., Stewart, P., Soonklang, N., Stewart, M., Suphamungmee, W., Poomtong, T. and Sobhon, P. 2008. Existence of APGWamide in the testis and its induction of spermiation in *Haliotis asinina* Linnaeus. Aquaculture. 279(1-4): 142-149.

Chase, R. 1986. Brain cells that command sexual behavior in the snail *Helix aspersa*. Journal of Neurobiology. 17: 669-679.

Cheng, C.Y. and Liu, L.L. 2004. Gametogenesis in the imposex-affected oyster drills, *Thais clavigera* and *Thais rufotincta*. Journal of Fisheries Society of Taiwan. 31: 55-65.

Chung, E., Kim, S.Y. and Park, G. 2006. Germ cell differentiation and sexual maturation of the female *Neptunea (barbitonia) arthritica cumingii* (Crosse, 1862) (Gastropoda: Buccinidae). Malacologia. 48: 65-76.

Coelho, M.R., Fuentes, S. and Bebianno, M.J. 2001. TBT effects on the larvae of *Ruditapes decussate*. Journal of Marine Biological Association of United Kingdom. 81: 259-265.

Croll, R.P. and Van Minnen, J. 1992. Distribution of the peptide ala-pro-gly-trp-NH2 (APGWamide) in the nervous system and periphery of the snail *Lymnaea stagnalis* as revealed by immunocytochemistry and in situ hybridization. Journal of Comparative Neurology. 324(4): 67-574.

De Boer, P.A.C.M., Jansen, R.F. and Ter Maat, A. 1997. Copulation in the hermaphroditic snail *Lymnaea stagnalis*: A review. Invertebrate Reproduction and Development. 30(1-3): 167-176.

deFur, P.L., Crane, M., Ingersoll, C. and Tattersfield, L. (Eds.). 1999. "Endocrine disruption in invertebrates: Endocrinology, testing, and assessment. Proceedings of the Workshops on Endocrine Disruption in Invertebrates, 12-15 December 1998, Noordwijkerhout, The Netherlands." SETAC Press: Pensa cola.

De Lange, R.P.J., De Boer, P.A.C.M., Ter Maat, A., Tensen, C.P. and Van Minnen, J. 1998. Transmitter identification in neurons involved in male copulation behavior in *Lymnaea stagnalis*. Journal of Comparative Neurology. 395(4): 440-449.

De Lange, R.P.J. and Van Minnen, J. 1998. Localization of the neuropeptide APGWamide in gastropod molluscs by in situ hybridization and immunocytochemistry. General and Comparative Endocrinology. 109(2): 166-174.

Deutsch, U. and Fioroni, P. 1996. Effects of tributyltin (TBT) and testosterone on the female genital system in the mesogastropod *Littorina littorea* (Prosobranchia). Helgolander Meeresuntersuchungen. 50: 105–15.

Di Cristo, C., Minnen, J.V. and Di Cosmo, A. 2005. The presence of APGWamide in *Octopus vulgaris*: A possible role in the reproductive behavior. Peptides. 26 (1): 53-62.

Eckelbarger, K.J. and Young, C.M. 1997. Ultrastructure of the ovary and oogenesis in the methane-seep mollusc *Bathynerita naticoidea* (Gastropoda: Neritidae) from the Louisiana slope. Invertebrate Biology. 116: 299-312.

Eckelbarger, K.J. and Young, C.M. 1999. Ultrastructure of gametogenesis in a chemosynthetic mytilid bivalve *(Bathynerita childresi)* from a bathyal, methane seep environment (Northern Gulf of Mexico). Marine Biology. 135: 635-646.

Evans, S.M., Hutton, A., Kendell, M. A. and Samosir, A.M. 1991. Recovery in poulations of Dogwhelks, *Nucella lapillus* (L.) suffering from imposex. Marine Pollution Bulletin. 22: 331-333.

Evans, S.M., Leksono, T. and McKinnell, P.D. 1995. Tributyltin pollution: A diminishing problem following legislation limiting the use of TBT-based anti-fouling paints. Marine Pollution Bulletin. 30(1): 14-21.

Fan, X., Croll, R.P., Wu, B., Fang, L., Shen, Q., Painter, S.D. and Nagle, G.T. 1997. Molecular cloning of a cDNA encoding the neuropeptides APGWamide and cerebral peptide 1: Localization of APGWamide-like immunoreactivity in the central nervous system and male reproductive organs of *Aplysia*. Journal of Comparative Neurology. 387(1): 53-62.

Fent, K. 2006. Worldwide occurrence of organotins from antifouling paints and effects in the aquatic environment. Handbook of Environmental Chemistry. 5, Part 0: 71-100.

Fe´ral, C and Le Gall, S. 1983. The influence of a pollutant factor (tributyltin) on the neuroendocrine mechanism responsible for the occurrence of a penis in the females of *Ocenebra erinacea*. In: Molluscan neuro-endocrinology. Lever, J. and Boer, H.H., Eds. Amsterdam: North Holland Publ. Co., pp 173–175.

Finney, D.J. 1971. Probit analysis. Cambridge University Press: Cambridge.

Gerin, Y. 1976. Origin and evolution of some organelles during oogenesis in the mud snail *Ilyanassa obsoleta*. I. The yolk platelets. Acta Embryologie Experimentalis. 1: 15-26.

Gibbs, P.E., Bryan, G.W., Pascoe, P.L. and Burt, G.R. 1987. The use of the dog-whelk, *Nucella lapillus*, as an indicator of tributyltin (TBT) contamination. Journal - Marine Biological Association. 67(3): 507-523.

Gibbs, P.E., Pascoe, P.L. and Burt, G.R.. 1988. Sex change in the female dog-whelk, *Nucella lapillus*, induced by tributyltin from antifouling paints. Journal - Marine Biological Association. 68(4): 715-731.

Giménez, J., Healy, J.M., Hermida, G.N., Nostro, F.L. and Penchaszadeh, P.E. 2008. Ultrastructure and potential taxonomic importance of euspermatozoa and paraspermatozoa in the volutid gastropods *Zidona dufresnei* and *Provocator mirabilis* (Caenogastropoda, Mollusca). Zoomorphology. 127(3): 161-173.

Goldberg, E.D. 1986. TBT: an environmental dilemma. Environment. 28: 17-44.

Gooding, M.P., Wilson, V.S., Folmar, L.C., Marcovich, D.T. and LeBlanc, G.A. 2003. The biocide tributylin reduces the accumulation of testosterone as fatty

acid esters in the mud snail (*Ilyanassa obsoleta*). Environmental Health Perspectives. 111(4): 426-430.

Harino, H., Ohji, M., Wattayakorn, G., Arai, T., Rungsupa, S. and Miyazaki, N. 2006. Occurrence of antifouling biocides in sediment and green mussels from Thailand. Archives of Environmental Contamination and Toxicology. 51: 400-407.

Healy, J.M. 1982. Ultrastructure of paraspermatozoa, euspermatozoa and eusperm-like spermatozoa of *Obtortio cf. fulva* (Prosobranchia: Cerithiacea). Helgoländer Meeresuntersuchungen. 35(4): 489-500.

Healy, J.M. 1996. An ultrastructural study of euspermatozoa in *Bembicium auratum* including a comparison with other Caenogastropoda, especially Littorinoidea. Journal of Molluscan Studies. 62: 57–63.

Hodgson, A.N. and Eckelbarger, K.J. 2000. Ultrastructure of the ovary and oogenesis in six species of patellid limpets (Gastropoda: Petellogastropoda). Invertebrate Biology. 119(3): 265-277.

Hodgson, A.N., Eckelbarger, K.J. and Young, C.M. 2009. Sperm ultrastructure and spermatogenesis in the hydrothermal vent gastropod *Rhynchopelta concentrica* (Peltospiridae). Journal of Molluscan Studies. 75(2): 159-165.

Horiguchi, T., Kojima, M., Hamada, F., Kajikawa, A., Shiraishi, H., Morita, M. and Shimizu, M. 2006. Impact of Tributyltin and Triphenyltin on Ivory Shell (*Babylonia japonica*) Populations. Environmental Health Perspectives. 2006: 114(S-1): 13-19.

Horiguchi, T., Kojima, M., Kaya, M., Matsuo, T., Shiraishi, H., Morita, M. and Adachi, Y. 2002. Tributyltin and triphenyltin induce spermatogenesis in ovary of female abalone, *Haliotis gigantean*. Marine Environmental Research. 54(3-5): 679-684.

Horiguchi, T., Kojima, M., Takiguchi, N., Kaya, M., Shiraishi, H. and Morita, M. 2005. Continuing observation of disturbed reproductive cycle and ovarian spermatogenesis in the giant abalone, *Haliotis madaka* from an organotin-contaminated site of Japan. Marine Pollution Bulletin. 51(8-12): 817-822.

Horiguchi, T., Shiraishi H. and Morita, M. 2003. Specific tissue distributions of organotin compounds in prosobranch gastropods [Abstract]. SETAC 24th Annual Meeting Abstract Book. Pensacola, FL:SETAC, 290.

Jamari, Z. 2001. Asean Marine Water Quality Criteria for Tributyltin (TBT). ASEAN-Canada CPMS-II. Cooperative Programme on Marine Science, Malasia. March, 2001.

Jha, A.N., Hagger, J.A. and Hill, S.J. 2000. Tributyltin induces cytogenetic damage in the early life stages of the marine mussel, *Mytilus edulis*. Environment and Molecular Mutagenesis. 35: 343-350.

Joosse J. 1988. The hormones of molluscs. In: Endocrinology of selected invertebrate types. Laufer, H. and Downer, G.H., Eds. New York: Alan R. Liss, Inc., pp 89–140.

Kan-Atireklap, S., Tanabe, S. and Sanguansin, J. 1997. Contamination by butyltin compounds in sediments from Thailand. Marine Pollution Bulletin. 34 (11): 894-899.

Kobayashi, M. and Moneoka, Y. 1990. Structure and function of molluscan neuropeptides. Zoological Science. 7: 801–14.

Koene, J.M., Jansen, R.F., Ter Maat, A. and Chase, R. 2000. A conserved location for the central nervous system control of mating behaviour in gastropod molluscs: Evidence from a terrestrial snail. Journal of Experimental Biology. 203(6): 1071-1080.

Kuroki, Y., Kanda, T., Kubota, I., Fujisawa, Y., Ikeda, T., Miura, A., Minamitake, Y. and Muneoka, Y. 1990. A molluscan neuropeptide related to the crustacean hormone, RPCH. Biochemical and Biophysical Research Communications. 167(1): 273-279.

Legierse, K.C.H.M., Sijm, D.T.H.M., Van Leeuwen, C.J., Seinen, W. and Hermens, J.L.M. 1988. Bioconcentration kinetics of chlorobenzenes and the organophosphorus pesticide chlorthion in the pond snail *Lymnaea stagnalis* - A comparison with the guppy *Poecilia reticulate.* Aquatic Toxicology. 41(4): 301-323.

Li, G. Y., and Chase, R. 1995. Correlation of axon projections and peptide immunoreactivity in mesocerebral neurons of the snail *Helix aspersa.* Journal of Comparative Neurology. 353: 9-17.

Leung, K.M.Y., Kwong, R.P.Y., Ng, W.C., Horiguchi, T., Qiu, J.W., Yang, R., Song, M. and Lam, P.K.S.. 2006. Ecological risk assessments of endocrine disrupting organotin compounds using marine neogastropods in Hong Kong. Chemosphere. 65 (6): 922-938.

Maxwell, W. 1983. Mollusca. In: Reproductive Biology of Invertebrates Vol II: Spermatogenesis and sperm function. Adiyodi, K. and Adiyodi, G., Eds. New York: John Wiley and Sons., pp 275-319.

Medina, A., Garcia, J.C., Moreno, F.J and Lopez-Campos, J.P. 1986. Comparative studies on the histology of the ovo- testis in *Hypselodoris tricolor* and *Godiva banyulensis* (Gastropoda, Opisthobranchia), with special reference to yolk formation. Journal of Morphology. 186: 105-118.

Mensink, B.P., Kralt, H., Vethaak, A.D., Ten Hallers-Tjabbes, C.C., Koeman, J.H., Van Hattum, B. and Boon, J.P. 2002. Imposex induction in laboratory reared juvenile *Buccinum undatum* by tributyltin (TBT). Environmental Toxicology and Pharmacology. 11(1): 49-65.

Minakata, H., Kuroki, Y., Ikeda, T., Fujisawa, Y., Nomoto, K., Kubota, I. and Muneoka, Y. 1991. Effects of the neuropeptide APGW-amide and related compounds on molluscan muscle—GWamide shows potent modulatory effects. Comparative Biochemestry and Physiology Part C. 100: 565–571.

Moore, D.R.J., Noble, D.G., Walker, S.L., Trotter, D.M., Wong, M.P. and Pierce, R.C. 1992. Canadain Quality Guidelines for Organotins. Ecosystem Science and Evaluation Directorate, Environment Canada, Ottawa, Ontario. 144 pp.

Najmudeen, T.M. 2008. Ultrastructeral studies of oogenesis in the variable abalone *Haliotis varia* (vetigastropoda: Haliotidae). Aquatic Biology. 2: 143-151.

Norrevang, A. 1968. Electron microscopic morphology of oogenesis. International Review of Cytology. 23: 113-186.

Oberdörster, E. and McClellan-Green, P. 2000. The neuropeptide APGWamide induces imposex in the mud snail, *Ilyanassa obsoleta*. Peptides. 21(9): 1323-1330.

Oberdörster, E., Romano, J. and McClellan-Green, P. 2005. The neuropeptide APGWamide as a penis morphogenic factor (PMF) in gastropod mollusks. Integrative and Comparative Biology. 45(1): 28-32.

Oehlmann, J., Fioroni, P., Stroben, E. and Markert, B. 1996. Tributyltin (TBT) effects on *Ocinebrina aciculata* (Gastropoda: Muricidae): Imposex development, sterilization, sex change and population decline. Science of the Total Environment. 188(2-3): 205-223.

Oehlmann, J., Schulte-Oehlmann, U., Tillmann, M. and Markert, B. 2000. Effects of endocrine disruptors on prosobranch snails (Mollusca: gastropoda) in the laboratory. Part I: Bisphenol A and octylphenol as xeno-estrogens. Ecotoxicology. 9 (6): 383-397.

Pal, P. and Hodgson, A.N. 2002. An ultrastructeral study of oogenesis in a planktonic and a direct-development species of *Siphonaria* (Gastropoda: Pulmonata). Journal of Molluscan Studies. 68: 337-334.

Pellizzato, F., Centanni, E., Marin, M.G., Moschino, V. and Pavoni, B. 2004. Concentrations of organotin compounds and imposex in the gastropod *Hexaplex trunculus* from the Lagoon of Venice. Science of the Total Environment. 332 (1-3): 89-100.

Pepe, R.K. 1987. Oogenesis in the marine mussel *Mytilus edulis*: an ultrastructural study. Marine Biology. 95: 405-414.

Quintela, M., Barreiro, R. and Ruiz, J.M. 2000. The use of *Nucella lapillus* (L.) transplanted in cages to monitor tributyltin (TBT) pollution. Science of the Total Environment. 247 (2-3): 227-237.

Ramón, M. and Amor, M.J. 2001. Increasing imposex in populations of *Bolinus brandaris* (Gastropoda: Muricidae) in the north-western Mediterranean. Marine Environmental Research. 52(5): 463-475.

Riedel, F., Healy, J.M., Röpstorf, P. and Sitnikova, T.Y. 2001. Ecology, shell morphology, anatomy and sperm ultrastructure of the caenogastropod *Pyrgula annulata*, with a discussion of the relationship between the 'pyrgulidae' and caspian and baikalian rissooideans. Limnologica. 31(4): 289-302.

Rock, M.K., Blankenship, J.E. and Lebeda, F.J. 1977. Penis-retractor muscle of *Aplysia*: Excitatory motor neurons. Journal of Neurobiology. 8: 569-579.

Röpstorf, P., Healy, J.M., Riedel, F. and Sitnikova, T.Y. 2002. Comparative sperm ultrastructure of Baikalian endemic prosobranch gastropods. Journal of Molluscan Studies. 68(2): 111-126.

Ruppert, E.E., Fox, R.S. and Barnes, R.D. 2004. Invertebrate zoology : a functional evolutionary approach**.** 7th ed. Brooks/Cole: Australia . 963 pp.

Schulte-Oehlmann, U., Tillmann, M., Markert, B., Oehlmann, J., Watermann, B. and Scherf, S. 2000. Effects of endocrine disruptors on prosobranch snails (mollusca: gastropoda) in the laboratory. Part II: Triphenyltin as a xeno-androgen. Ecotoxicology. 9(6): 399-412.

Singhakaew, S., Seehabutr, V., Kruatrachue, M., Sretarugsa, P. and Romratanapun, S. 2003. Ultrastructure of male germ cells in the testes of abalone, *Haliotis ovina* Gmelin. Mulluscan Research. 23(2): 109-121.

Smith, B.S. 1971. Sexuality in the American mud snail, *Nassarius obsoletus* Say. Proceeding of the Malacological Society of London. 39: 337-378.

Smith, P.J. 1996. Selective decline in imposex levels in the dogwhelk *Lepsiella scobina* following a ban on the use of TBT antifoulants in New Zealand. Marine Pollution Bulletin. 32(4): 362-365.

Smith, S.A., Nason, J. and Croll, R.P. 1997. Detection of APGWAamide-like immunoreactivity in the sea scallop, *Placopecten magellanicus*. Neuropeptides. 31(2): 155-165.

Stagličić, N., Prime, M., Žoko, M., Erak, Z., Brajčić, D., Blaževic, D., Madiraza, K., Jelić, K. and Peharda, M. 2008. Imposex incidence in *Hexaplex trunculus* from Kaštela Bay, Adriatic Sea. Acta Adriatica. 49(2): 159-164.

Stroben, E., Oehlmann, J. and Fioroni, P. 1992. The morphological expression of imposex in *Hinia reticulata* (Gastropoda: Buccinidae): a potential indicator of tributultin pollution. Marine Biology. 113(4): 625-636.

Sujatha, C.H., Nair, S.M. and Chacko, J. 1996. Tributyltin oxide induced physiological and biochemical changes in a tropical estuarine clam. Bulletin of Environmental Contamination and Toxicology. 56: 303-310.

Suwanjarat, J. and Klepal, W. 2001. Ultrastructural investigations of Euspermatogenesis and euspermatozoa in *Cerithidea obtus*a (Lamarck 1822) (Caenogastropoda: Potamididae). Marine Ecology. 22(1-2): 23-34.

Swennen, C. and Horpet, P. 2008. Pseudo-imposex; male features in female volutes not TBT-induced (Gastropoda: Volutidae). Contributions to Zoology. 77(1): 17-24.

Swennen, C., Ruttanadakul, N., Ardseungnern, S., Singh, H.R., Mensink, B.P. and Ten Hallers-Tjabbes, C.C. 1997. Imposex in sublittoral and littoral gastropods from the Gulf of Thailand and Strait of Malacca in relation to shipping. Environmental Technology. 18(12): 1245-1254.

Taylor, G.T. and Anderson, E. 1969. Cytochemical and fine structural analysis of oogenesis in the gastropod *Ilyanassa obsoleta*. Journal of Morphology. 129: 211-248.

Thaweethamsewee, P., Boonyoung, P. and Vongvatcharanon, U. 2010. Morphology and histology of the central nervous system and neurosecretory cells in male and female *Babylonia areolata,* Link 1807. 33rd AAT Annual Conference Proceedings of the Anatomy Association of Thailand.

Van Golen, F.A., Li, K.W., DeLange, R.P.J., Van Kesteren, R.E., Van Der Schors, R.C. and Geraerts, W.P.M. 1995. Co-localized neuropeptides conopressin and Ala-Pro-Gly-Trp-NH2 have antagonistic effects on the vas deferens of *Lymnaea*. Neuroscience. 69(4): 1275-1287.

Voltzow, J. 1994. Gastropod: Prosobranchia. In: Microscopic Anatomy of Invertebrates, vol 5: Mollusca I. Wiley-Liss.Inc., pp 111-252.

Waldock, M.J. and Thain, J.E. 1983. Shell thickening in *Crassostrea gigas*: organotin antifouling or sediment induced. Marine Pollution Bulletin. 14: 411-415.

West, D.L. 1981. Reproductive biology of *Colus stimpsoni* (Prosobranchia: Buccinidae). IV. Oogenesis. Veliger. 24: 28-38.

WHO 2002. Report on Environmental Health. World Health Organization (WHO), Regional Office for the Eastern Mediterranean (EMRO), Regional Centre for Environmental Health Activities, CEHA, Amman, Jordan.

Zabala, S., Hermida, G.N. and Giménez, J. 2009. Ultrastructure of euspermatozoa and paraspermatozoa in the volutid snail *Adelomelon ancilla* (Mollusca: Caenogastropoda). Helgoland Marine Research. 63(3): 181-188.

http://www.fistenet.gov.vn. (accessed 26/1/2006).

APPENDICES

Appendix A

Tissue processing for paraffin sections (Bancroft and Gamble, 2002)

1. **Formulae for fixative solution**

Bouin's fluid

Saturated aqueous picric acid solution	75 ml
40% formaldehyde	25 ml
Glacial acetic acid	5 ml

2. **Tissue processing**

Fixation

Bouin's fluid	18-24 hours
(Transfer to 70% alcohol for washing out picric acid)	

Dehydration

70% ethanol	2 hours-overnight
95% ethanol	2 hours
Absolute ethanol	2 hours
Absolute ethanol	overnight

Clearing

Xylene	1 hour

Infiltration

Xylene: Wax_1	1 hour
Wax_1	1 hour
Wax_2	1 hour

Embedding Tissue is embedded in paraffin

Sectioning Cut at 5-6 µm using microtome

Appendix B

Staining methods for paraffin sections (Bancroft and Gamble, 2002)

1. **Preparation of solution**

Hariss's hematoxyline (Harris, 1900 cited by Bancroft and Gamble, 2002)

Hematoxyline	2.5 g
Absolute alcohol	25.0 g
Potassium alum	50.0 g
Distilled water	500 ml
Mercuric oxide	1.25 g
Glacial acetic acid	20 ml

The hematoxyline is dissolved in the absolute alcohol, and is then added to the alum, which has previously been dissolved in the warm distilled water in a 2-litre flask. The mixture is rapidly brought to the boil and the mercuric oxide is then slowly and carefully added. Plunging the flask into cold water or into a sink containing chopped ice rapidly cools the stain. When solution is cold, the acetic acid is added, and the stain is ready for immediate use.

Eosin

Stock solution (1% Alcoholic eosin)

Eosin Y	10.0 g
Distilled water	50.0 ml
95% alcohol	940.0 ml

Working solution (1% Alcoholic eosin)

Stock (1% Alcoholic eosin)	1 part
95% alcohol	1 part

2. **Staining processing**

Deparafinization section

Xylene	2 minutes (2 times)

Hydration

Absolute ethanol	2 minutes (2 times)
95% alcohol	2 minutes (2 times)
Running tap water	5 minutes
Staining	
Hematoxylin	6 minutes
1% acid alcohol (Differentiate)	5 seconds
Tap water	2 minutes
Saturated lithium carbonate (Blueing or neutralize)	30 seconds
Distilled water	1-2 minutes
Eosin	30 seconds-1 minute
95% ethanol	5-10 dips (2 times)
Dehydration	
Absolute alcohol	2 minutes (2 times)
Clearing	
Xylene	2 minutes (2-3 times)
Mounting with permount	

Appendix C

Tissue processing for transmission electron microscope (TEM) (Bancroft and Gamble, 2002)

1. Preparation of solution

1.1 *Phosphate buffer* (0.1 mol/l, pH 7.4)

Stock reagents

Solution A

Disodium hydrogen orthophosphate (Na_2HPO_4 anhydrous)	14.2 g
Distilled water	1.01

Solution B

Sodium dihydrogen phosphate ($NaH_2PO_4 2H_2O$)	15.6 g
Distilled water	1.01

Mix 40.5 ml of solution A with 9.5 ml of solution B. The pH should be checked and adjust if necessary, using 0.1 mol/l hydrochloric acid or 0.1 mol/l sodium hydroxide

1.2 *2.5% glutaraldehyde*

0.2 mol/L phosphate buffer, pH 7.4	50 ml
25% aqueous glutaraldehyde	12 ml
Distilled/deionized water	to 100 ml

Mix aqueous glutaraldehyde with buffer. Check the pH of the mixure and adjust if necessary to pH 7.4 and then add distilled water to make 100 ml.

2. Tissue processing

Fixation

2.5% glutaraldehyde	24 hours
Wash in 0.1 M phosphate buffer, pH 7.4	10 minutes (three times)
Post-fix in 1% OsO4 in phosphate buffer	2 h

Wash in 0.1 M phosphate buffer, pH 7.4	10 minutes (three times)
Dyhydration	
30% ethanol	30 minutes
50% ethanol	15 minutes
70% ethanol	15 minutes
75% ethanol	15 minutes
80% ethanol	15 minutes
85% ethanol	15 minutes
90% ethanol	15 minutes
50% ethanol	15 minutes
100% ethanol	15 minutes
Propylene oxide	30 minutes (2times)
Infiltration	
Propylene oxide: resin (2:1)	overnight
Propylene oxide: resin (1:2)	7 hours
Pure resin	overnight
Embedding	
Polymerize at 60 ºC for 24 hours	

3. Contrasting the ultra-thin section

Uranyl acetate:

3.1 Put a parafilm sheet on the bench, fix parafilm by pressing the edges to the bench's surface.

3.2 Place one small droplet of uranyle acetate solution (2%, light sensitive, radioactive) per grid onto parafilm.

3.3 Place grids onto drops (dull surface towards drop). Cover with petri dish and shade (cardboard box). Leave for 30 minutes.

3.4 Prepare three plastic beakers with distilled water. Wash grids subsequently in the three beakers.

3.5 Dry grids on filter paper.

Lead citrate:

3.6 Put a parafilm sheet on the bench, fix parafilm by pressing the edges to the bench's surface.

3.7 Place one small droplet of lead citrate solution (0.5%, CO_2 sensitive, toxic) per grid onto parafilm. Maximum five nets at one time.

3.8 Place two NaOH pellets on the edge of parafilm sheet to prevent carbonate precipitation.

3.9 Place grids onto drops (dull surface towards drop). Cover with petri dish and shade (cardboard box). Leave for 7-8 minutes.

3.10 Prepare three plastic beakers with distilled. Wash grids subsequently in the three beakers.

3.11 Dry grids on filter paper.

3.12 Let grids air dry for at least 15 minutes.

3.13 Grids are ready for TEM.

Appendix D

Tissue processing for immunohistochemistry (after fixation and tissue processing for paraffin sections)

1. Preparation of solutions

1.1 *DAB solution*

- added 1 drop of buffer stock solution into 2.5 ml of tab water, mixed
- added 2 drops of DAB, mixed
- added 1 drop of hydrogen peroxide, mixed
- added 1 drop of nickel, mixed

1.2 To prepare incubation medium (IM):

IM	for 2 ml	for 1 ml
10% serum	200 µl	100 µl
1% Triton x 100	20 µl	10 µl
In 1x PBS	1,796 µl	895 µl

2. Preparation of sections

2.1 Deparaffinized in xylene

Xylene I	10 minutes
Xylene II	10 minutes

2.2 Rehydrated in descending concentration of ethanol

Absolute alcohol I	10 minutes
Absolute alcohol II	10 minutes
95% alcohol	5 minutes
80% alcohol	5 minutes
70% alcohol	5 minutes

3. Rinsed 5 minutes in tab water

3. Immunohistochemistry

1. Washed sections in PBS (Phosphate Buffered Saline) 2 x 5 minutes
2. Pre-incubated in incubation medium (IM) (200 µl/slide) for 10 minutes.
3. Incubated in the primary antiserum: rabbit polyclonal anti-APGWamide (final serum dilution 1:500 diluted in IM) (200 µl/slide) for 1 hour at room temperature (RT) or over night at 4^{0} C (put a piece of parafilm over the slide to prevent it from drying out).
4. Washed 2 x 10 minutes in PBS.
5. Incubated in the secondary antibody: peroxidase-conjugated swine antirabbit (rabbit & HRP) (1:100 diluted in IM) (200 µl/slide) for 1 h at room temperature or overnight at 4^{0} C in the dark.
6. Washed 2 x 10 minutes in PBS
7. Visualized with DAB for 10 minutes.
8. Stopped reaction with tap water.
9. Dehydrated in the increasing concentration of ethanol

70% alcohol	2 minutes
80% alcohol	2 minutes
95% alcohol	2 minutes
Absolute alcohol	2 minutes

9. Cleared in xylene:

Xylene I	5 minutes
Xylene II	5 minutes

10. Mounted the slides with Entellan

VITAE

Name Mr. Chutchawan Muenpo

Student ID 4723001

Educational Attainment

Degree	Name of Institution	Year of Graduation
Bachelor of Science (Biology)	Prince of Songkla University	2003

Scholarship Awards during Enrollment

June/2004-May/2009 Royal Golden Jubilee (RGJ) PhD program. From Thailand Resarch Found (TRF), (Grant no. PHD/0076/2547)

Lists of Publications and Proceedings

Muenpo, **C**., Suwanjarat, J. and Klepal, W. Acute toxicity of tributyltin to the spotted babylon, *Babylonia areolata* (Gastropoda: Buccinidae). Proceeding of the 7th National Graduate Research Conference. Prince of Songkla University, Surat Thani campus, Surat Thani, April 4-5, 2007. pp. 96

Muenpo, **C**. and Suwanjarat, J. Reproductive cycle of the spotted babylon, *Babylonia areolata* (Gastropoda: Buccinidae) in the Gulf of Thailand. Proceeding of the RGJ – Ph.D. Congress VIII. Jomtien Palm Beach Resort Pattaya, Chonburi, April 20-22, 2007. pp. 251

Muenpo, **C**. and Suwanjarat, J. The morphological and histological expressions of TBT-induced imposex in *Babylonia areolata* (Gastropoda: Buccinidae). Proceeding of the RGJ Seminar Series LXIV: Science and Technology for the Sustainable Development. Faculty of Science, Prince of Songkla University, Hat Yai, Songkhla, September 4, 2009. pp. 11